Preclinical evaluation of a novel anti-leukemic mechanism

by

Sarah F. Zarabi

A thesis submitted in conformity with the requirements
for the degree of Doctor of Philosophy

Department of Medical Biophysics
University of Toronto

Preclinical evaluation of a novel anti-leukemic mechanism

Sarah F. Zarabi
Doctor of Philosophy
Department of Medical Biophysics
University of Toronto
2020

Abstract

Acute Myeloid Leukemia (AML) is a heterogeneous disease that is associated with a remarkably diverse group of genetic mutations that contribute to its biological complexity directly, or indirectly by triggering downstream cellular reactions. Given these complexities, identification of a single therapeutic strategy that can be effective against a wide range of AML subgroups remains challenging and very few effective novel antileukemic agents have been developed in the past 30 years. Consequently, the overall outcome of patients with AML remains poor. Despite aggressive chemotherapies, AML patients may not achieve remission even after two courses of induction (primary non-responders). Here, our retrospective data indicate that in primary non-responders with AML, remissions following a third induction course are uncommon and short-lived if not consolidated by stem cell transplant (SCT) . Thus, our data indicates that a 3rd induction should only be offered to primary non-responders with AML if an SCT strategy is in place. Collectively, this background highlights an urgent need for development of novel antileukemic strategies.

ClpP is a mitochondrial protease that is overexpressed in leukemic cells from approximately half of patients with AML. It degrades damaged or misfolded proteins inside mitochondria and has a central role in maintaining the integrity of mitochondrial metabolism by functioning as a protein quality control mediator. Herein, through genetic and chemical investigations, we demonstrate that ClpP activation results in prominent anti-leukemia and anti-lymphoma effects.

We identified a new class of antineoplastic compounds -imipridones- as potent ClpP activators. ClpP activation induces cell death in leukemia and lymphoma cells and stem cells and exerts antitumor effects in vivo whereas normal hematopoietic cells display resistance. In primary AML samples, sensitivity to ClpP activators correlates with pre-treatment ClpP expression level. Mechanistically, binding of imipridones to ClpP enhances proteolysis by enlarging the axial pores of the enzyme. ClpP activation impairs oxidative phosphorylation through reductions in respiratory chain complex subunits and abrogates mitochondrial morphology and function. The currently most potent ClpP activators, imipridones, are being evaluated in clinical trials. Our approach provides groundwork for further development of ClpP activators and represents a first-in-class therapeutic strategy for a subset of hematologic malignancies.

Acknowledgments

This dissertation would not have materialized without the encouragement, help, and guidance of countless people who have offered their unfailing support throughout my educational journey.

First and foremost, I am especially grateful to my supervisor, Dr. Aaron Schimmer, who made it possible for me to work on this project. Your vision, support, patience and encouragement was very much appreciated throughout this scientific endeavor. Thank you for being such a great role model and an excellent mentor. I am indebted to you more than you know.

I would also like to thank my program advisory committee members, Drs. David Hedley and Rodger Tiedemann for their insightful comments and hard questions. Your advice has only made this project better.

To our collaborators and especially our collogues at MD Anderson Cancer Centre. Thank you for all your hard work, dedication and scientific insight. Special thanks to Dr. Jo Ishizawa and Dr. Michael Andreeff for such a well-coordinated and educational collaborative experience. It has been a real pleasure working with you.

To members of Dr. Schimmer's lab. It has been an incredible experience working with you. Special thanks to Yulia Jitkova for her efforts in developing biochemical assays to investigate the activity of ClpP enzyme. I also would like to thank Rose Hurren, Marcela Gronda and Neil MacLean, and the graduate students and post-doctoral fellows of the Schimmer lab for teaching me many lab techniques, and assisting with the lab experiments. What a great team of enthusiastic scientists.

I owe a great debt of gratitude to my family. To my brother, Saeed, and my sister, Sahar, for the positive atmosphere they always created around me. To my parents, Masoud and Simin, who instilled in me a passion for science and a sense of responsibility. To my husband and beloved best friend, Nima, for his persistent confidence in me and for being such an amazing team player. I would have never made it here without your unwavering support and continued encouragement. Finally, to my little bundle of joy, Darian, whose arrival has changed my life forever. Thank you for being such a great inspiration.

Table of Contents

List of Tables

List of Figures

List of Appendices

List of Abbreviations

ADEPs	acyldepsipeptides
ANOVA	analysis of variance
AML	Acute Myeloid Leukemia
AMSA	amsacrine
APL	acute promyelocytic leukemia
Ara-C	cytarabine
ASXL	additional sex combs-like
ATP	adenosine triphosphate
BAK	Bcl-2 homologous antagonist killer protein
BAX	Bcl-2-associated X protein
BCL-2	B-cell lymphoma 2
BCL-XL	B-cell lymphoma-extra large
BioID	proximity-dependent biotin labeling
CBFB	core-binding factor beta
CD	cluster of differentiation
cDNA	complementary deoxyribonucleic acid
CEBPA	CCAAT/enhancer binding protein α
CETSA	cellular thermal shift assay
CSF1R	colony stimulating factor 1 receptor
ClpP	caseinolytic protease P
ClpX	caseinolytic protease X
CML	chronic myeloid leukemia
CR	complete remissions
CRi	complete remission with incomplete platelet recovery
CS	citrate synthase
DDX41	DEAD-box helicase 41
DFS	disease free survival
DMSO	dimethyl sulfoxide
DNA	deoxyribonucleic acid
DNMT3A	DNA methyltransferase 3 alpha
dsDNA	double-stranded DNA

DTT	dl-dithiothreitol
ECOG	Eastern Cooperative Oncology Group
EV	empty vector
EVI1	ecotropic virus integration site 1
FCCP	p-trifluoromethoxyphenylhydrazone
FCS	fetal calf serum
FDA	Food and Drug Administration
FLT3	FMS-like tyrosine kinase 3
GO	gemtuzumab ozogamicin
HiDAC	high-dose cytarabine
2-HG	2-hydroxyglutarate
IDH1	isocitrate dehydrogenase1
IDH2	isocitrate dehydrogenase2
IMDM	Iscove's Modified Dulbecco's Medium
IPTG	isopropyl-1-thio-B-D-galactopyranoside
ISR	integrated stress response
ITC	isothermal titration calorimetry
ITD	in-frame tandem duplications
IV	intravenous
αKG	α-ketoglutarate
KMT2A	Lysine methyltransferase 2a
LB	Luria-Bertrani Broth
LICs	leukemia-initiating cells
LSCs	leukemic stem cells
MAF	mutant allele frequency
MECOM	MDS1 and EVI1 complex
MDS	myelodysplastic syndromes
MHC	major histocompatibility complex
MKL1	megakaryoblastic leukemia 1
MLLT3	mixed lineage leukemia translocated to 3
MPN	myeloproliferative neoplasms
mtDNA	mitochondrial DNA
MTS	mitochondrial targeting sequence

mUPR	mitochondrial unfolded protein response
MYH11	myosin heavy chain 11
NAD^+	nicotinamide adenine dinucleotide coenzyme
NADH	nicotinamide adenine dinucleotide - hydrogen
NBM	normal bone marrow
NLN	neurolysin
NOX2	NADPH oxidase 2
NPM1	nucleophosmin
NRAS	neuroblastoma RAS viral oncogene homolog
NSG	NOD scid gamma mouse
NUP214	nucleoporin 214
O/E	overexpression
ONC-R	ONC201-resistant
OS	overall survival
OTC	ornithine transcarbamoylase
OXPHOS	oxidative phosphorylation
PARL	Presenilins-associated rhomboid-like protein
PDB	Protein Data Bank
PDGFR	platelet derived growth factor receptor
PFS	progression free survival
PITRM1	Pitrilysin metallopeptidase 1
RARA	retinoic acid receptor, alpha
RBM15	RNA Binding Motif Protein 15
RET	rearranged during transfection
RNA	ribonucleic acid
rRNA	ribosomal RNA
tRNA	transfer RNA
RNA-seq	RNA sequencing
ROS	reactive oxygen species
RUNX1	runt-related transcription factor 1
SCF	stem cell factor
SCID	severe combined immunodeficiency disease
SCT	stem cell transplantation

SDS-PAGE	sodium dodecyl sulphate-polyacrylamide gel electrophoresis
shRNA	short hairpin RNA
SMAC	second mitochondria-derived activator of caspases
SNV	single-nucleotide variant
SNP	single-nucleotide polymorphism
SOD	superoxide dismutase
TAM	transient abnormal myelopoiesis
TCGA	the Cancer Genome Atlas
TET2	Tet Methylcytosine Dioxygenase 2
TKD	Tyrosine Kinase Domain
TP53	tumor protein p53
TRAIL	Tumor Necrosis Factor-Alpha-Related Apoptosis-Inducing Ligand
TRE	tetracyclin responsive elements
VEGFR	vascular endothelial growth factor
WT	wild type

Chapter 1

1 Scientific background, goals, and objectives of the research projects

1.1 Literature review

1.1.1 Acute Myeloid Leukemia (AML)

Acute Myeloid Leukemia (AML) refers to a heterogenous group of hematologic malignancies that arise from clonal expansion of myeloid progenitor cells in the bone marrow and peripheral blood (I De Kouchkovsky et al., 2016). Large numbers of abnormal, immature myeloid cells (leukemic cells) accumulate in the bone marrow and blood and interfere with appropriate production and function of normal blood cells. Consequently, AML is associated with severe complications such as infection or bleeding. Left untreated, this process is generally rapidly lethal. The standard of care for treatment of AML include intensive induction chemotherapy followed by consolidative treatment strategies (chemotherapy or stem cell transplant). With these strategies, only 35-40% of adults younger than 60 years are cured from the disease and the prognosis is worse for those > 60 years old.

AML is a complex disease that is associated with a large number of cytogenetic abnormalities and molecular mutations that contribute to its biological heterogeneity (Döhner H et al. 2017). Due to these complexities the backbone of treatment regimens for AML remain mostly unchanged despite our increased understanding of AML biology in the past decades. Consequently, the overall prognosis of patients with AML remains poor (I De Kouchkovsky et al, 2016;).

1.1.2 AML pathobiology

AML arises from malignant expansion of hematopoietic precursor cells. These cells have undergone various genetic and/or epigenetic changes that do not disrupt their ability to proliferate but impair their capacity to maturate and differentiate into normal blood cells. The dysfunctional myeloid progenitors accumulate in the bone marrow and suppress the normal cells. The resultant multilineage cytopenia leads to complications and is eventually lethal in this disease (Cai SF et al., 2019).

1.1.2.1 Leukemic stem cells

Over the years, hematopathologists have noticed that leukemic cells of samples taken from different patients are morphologically heterogeneous. In addition to inter-patient heterogeneity, morphological diversity has also been observed among leukemic cells of an individual patient. These samples show that within the leukemia cell population cells are organized in a hierarchical system. A minor fraction of leukemia cells - leukemic stem cells (LSCs)- reside at the apex of this hierarchical pyramid and are capable of self-renewal and can also partially differentiate into bulk leukemic blasts that continue to proliferate but have lost their capacity to self-renew (Bonnet D et al., 1997). LSCs can initiate the disease when transplanted into immunodeficient animals. Self-renewal capacity of LSCs indicates that in order to achieve long term remissions in AML, LSCs should be eliminated. However, in addition to self-renewal capacity, LSCs demonstrate other properties such as relative quiescence, resistance to apoptosis, and increased drug efflux that render them relatively resistant to available cytotoxic therapies (Thomas D et al., 2017).

1.1.2.2 Genetic and epigenetic evolution in AML

Intra-individual heterogeneity of leukemic cells also arise from ongoing genetic and epigenetic evolution and clonal diversification that happen during the course of malignant transformation (Bullinger L et al., 2017).

Data from the Cancer Genome Atlas (TCGA) project reported an average of 13 coding mutations per AML case (Ley TJ et al., 2013). In addition, adult AML genomes contained a median of one somatic copy-number variant (eg, trisomies or monosomies) and an average of less than one gene fusion event. Somatic mutations in AML may impair differentiation processes and lead to accumulation of immature progenitors (e.g *RUNX1, CEBPA and RARA),* or may activate the signaling pathways that increase the proliferation rate and survival of the hematopoietic progenitors (e.g. *FLT3-ITD, KIT and NRAS*). A third group of somatic mutations in AML involves epigenetic modifiers such as DNMT3A, IDH1/2 and TET2. Mutations in epigenetic modifiers are commonly acquired early in the process of leukemic development and are present in the founding clone. These mutations have a prominent role in leukemogenesis by disrupting the epigenetic landscape. For example, it has been shown that *DNMT3A (*(Shlush L et al., 2014) and *IDH2* (Corces-Zimmerman MR et al., 2014) exist in pre-leukemic cells, can act as leukemia initiating mutations, and precede *NPM1c* and *FLT3*-ITD mutations. In addition, such mutations may persist after therapy, lead to clonal expansion during hematologic remission, and eventually lead to relapsed disease.

1.1.2.3 AML metabolism

Altered cellular metabolism is an important mechanism in cancer pathogenesis. More than 50 years ago, Warburg hypothesized that cancer cells undergo metabolic reprogramming to increase their aerobic glucose fermentation as a result of insufficient mitochondrial respiration. However, contrary to this conventional idea, functional mitochondrial respiration and oxidative phosphorylation are essential for survival of cancer cells. Today, it is believed that cancer cells ferment glucose while keeping up the mitochondrial respiration levels even in the presence of oxygen in order to meet their metabolic demands. As for many other cancers, studies have shown that mitochondrial oxidative phosphorylation (OXPHOS) and other metabolic pathways that are localized in mitochondria have important roles in progression and maintenance of AML (Kreitz J et al., 2019).

The mtDNA is transcribed and translated in the mitochondrial matrix. Thirteen mitochondrial proteins that are involved in oxidative phosphorylation are encoded by mtDNA. Proper translation of mtDNA is essential for appropriate function of this pathway in AML. For example, inhibition of the mitochondrial translation system by antimicrobial agent tigecycline

selectively inhibits the growth and viability of the leukemic blasts and stem cells compared to normal cells (Skrtic M et al., 2011). Among leukemic cells, LSCs are more dependent on mitochondrial oxidative phosphorylation than the bulk AML cells or normal hematopoietic stem cells, as they lack the ability to effectively upregulate their glycolytic system (Testa U et al., 2016). Finally, evasion of mitochondrial dependency has been proposed as a mechanism of drug resistance in AML. For example, primary AML samples that are resistant to chemotherapy adriyamycin express lesser amounts of a complex V subunit, ATP Synth-β (Song K et al., 2016). It has also been shown that leukemia cells that are resistant to mitochondrial translation inhibitor tigecycline upregulate their glycolysis via elevation of hypoxia inducible factor-1 expression (Jhas B et al., 2013). Collectively, these data suggest that increase reliance on mitochondrial oxidative phosphorylation is an important aspect of mitochondrial dependency in AML.

Other important mitochondrially localized metabolic pathways that are involved in AML progression include increased dependence on glutamine metabolism and increased fatty acid metabolism (Basak NP et al., 2015). These dependencies lead to evasion of apoptotic signals. In addition, α-ketoglutarate, a product of glutamine metabolism, participates in the Krebs cycle and also acts as a substrate for leukemia initiating IDH2 mutations to produce oncometabolite 2- hydroxyglutarate. In addition to their leukemia initiating roles, IDH2 mutations in AML increase the proliferation of leukemic cells and inhibit their differentiation (Kats LM et al., 2014).

1.1.2.4 The bone marrow microenvironment

Bone marrow is a soft tissue that is comprised of blood vessels and cells that are directly involved in hematopoiesis (hematopoietic cell population) and cells that support the function of the hematopoietic system (stromal cells). AML cells develop in the bone marrow. Leukemic cells disrupt normal hematopoietic progenitor cell niches in the bone marrow and ultimately manipulate and reshape the environment in a way that supports their survival and proliferation. These changes include alterations in expression of adhesion molecules, cell cycle regulators and pro-angiogenic factors of the stromal cells within bone marrow that ultimately induce pro-growth, anti-apoptotic and pro-invasive phenotypes in leukemic cells (Shafat MS et al., 2017).

Other major elements of the bone marrow microenvironment that favour leukemic growth include endothelial cells (provide a protective vascular network), fibroblasts (promote angiogenesis), and adipocytes (metabolic symbiosis). Finally, bone marrow stromal cells are capable of transferring their mitochondria to AML cells in a NOX2-dependent fashion via AML-derived tunneling nanotubes. The resultant increased mitochondrial respiration and adenosine triphosphate (ATP) generations in the AML cells promote their survival (Marlein CR et al., 2017).

1.1.3 AML epidemiology

AML is the most common acute leukemia in adults. It accounts for approximately 80% of leukemia cases in this age group (Yamamoto JF et al., 2008). The incidence is reported as 3 to 5 cases per 100,000 population in the United States and Europe. In adults, the median age at diagnosis is approximately 65 years. The incidence of AML increases with age and approximately 2 and 20 cases per 100,000 population have been reported for patients under or over 65 years, respectively. The incidence of AML is similar among patients with different ethnicities. The male:female ratio is approximately 5:3 (Siegel RL et al., 2017).

Several environmental factors including chemicals, radiation, tobacco, chemotherapy have been associate with development and progression of AML. Pre-existing genetic abnormalities such as trisomy 21, Fanconi anemia and familial mutations of *CEBPA*, *DDX41*, *RUNX1* have also been identified in AML. In some patients, evolution to AML is preceded by a preleukemic state that is characterized by presence of clonal hematopoiesis and may manifest as myelodysplastic syndrome, myeloproliferative neoplasms, paroxysmal nocturnal hemoglobinuria, and aplastic anemia (Shallis RM et al., 2019).

1.1.4 AML classification

Over the years, AML has been classified using several different classification systems. The World Health Organization system for AML classification is the most up-to-date modality (Shallis RM et al., 2019). This system is based upon a combination of morphology, immunophenotype, genetics, and clinical features and identifies six main AML subtypes:

- AML with recurrent genetic abnormalities that include the following subcategories:

    - AML with t(8;21)(q22;q22.1);RUNX1-RUNX1T1
    - AML with inv(16)(p13.1q22) or t(16;16)(p13.1;q22);CBFB-MYH11
    - APL with PML-RARA
    - AML with t(9;11)(p21.3;q23.3);MLLT3-KMT2A
    - AML with t(6;9)(p23;q34.1);DEK-NUP214
    - AML with inv(3)(q21.3q26.2) or t(3;3)(q21.3;q26.2); GATA2, MECOM
    - AML (megakaryoblastic) with t(1;22)(p13.3;q13.3);RBM15-MKL1
    - AML with mutated NPM1
    - AML with biallelic mutations of CEBPA
- AML with myelodysplasia-related features
- Therapy-related AML and MDS
- AML, not otherwise specified
- Myeloid sarcoma
- Myeloid proliferations related to Down syndrome
    - Transient abnormal myelopoiesis (TAM)
    - Myeloid leukemia associated with Down syndrome

1.1.5 Treatment of newly diagnosed AML

1.1.5.1 Induction

Standard therapies for acute myeloid leukemia include intensive chemotherapy and/or supportive care. Targeted therapies are added to the regimens where applicable. Among patients with AML, treatment approaches and outcomes differ between younger and older patients.

For younger adults (<60 years of age), the initial treatment of de novo AML include intensive induction chemotherapy with the goal to reduce total body leukemia cell population from approximately 10^{12} to below the cytologically detectable level of approximately 10^{9} cells (complete remission). A substantial burden of leukemia cells are still present at this point and will lead to relapse if left untreated. Thus, remissions should generally be consolidated with further chemotherapy or allogeneic stem cell transplant.

Standard dose cytarabine plus an anthracycline (7+3) is the most commonly used induction regimen for AML. In this protocol, a seven-day continuous intravenous (IV) infusion

of cytarabine (100 or 200 mg/m^2 per day) is given in combinations with a short infusion or bolus of an anthracycline on days 1 through 3. Daunorubicin is the most commonly used anthracycline in this regimen but other anthracyclines (eg, idarubicin) or synthetic anthracycline analogues (eg, mitoxantrone) have been used.

Clinical studies have compared standard dose cytarabine with high dose cytarabine (e.g. 1000 to 3000 mg/m2 intravenously over one to three hours every 12 hours for 8 to 12 doses) in combination with an anthracycline for newly diagnosed AML. In most of these trials, high dose cytarabine was associated with more toxicity and did not appear to improve the clinical outcome (Weick JK et al., 1996; Phillips GL et al., 1991). Similarly, addition of potentially non-cross-resistant drugs such as fludarabine, etoposide or clofarabine as a third agent to the 7 + 3 protocol does not appear to add significant clinical benefits (Estey EH et al., 2001; Bishop JF et al., 1990; Löwenberg B et al., 2017). However, addition of multi-targeted small molecule FLT3 inhibitor midostaurin to the 7 +3 protocol improves the event free and overall survivals in patients with FLT3 mutated AML (Stone RM et al., 2017). Gemtuzumab ozogamicin (GO) is another agents that has been successfully added to 7+3 regimen. GO is a recombinant, humanized anti-CD33 antibody. When added to the standard induction protocol, it improves the overall survival and decreases the risk of relapse but does not appear to increase the rate of complete remissions (CR) in CD33+AML (Hills RK et al. 2014). Other agents that have shown possible clinical benefits when added to standard induction regimens include cladribine (Holowiecki J et al., 2004) and the multikinase inhibitor, sorafenib (Röllig C et al., 2015).

1.1.5.2 Consolidative treatments

60-80 percent of adults with newly diagnosed AML will attain complete remission with induction chemotherapy. However, as stated above, significant leukemia burden (minimal residual disease) will be still present following intensive induction chemotherapy even after achieving complete remission. Thereby, without additional consolidative treatments, virtually all of these patients will relapse within a median of four to eight months. Thus, the goal of post remission therapies in AML is to eliminate the leukemia cells that survived the initial course of aggressive induction (but remain undetectable with standard diagnostic methods). Main consolidative approaches in AML include treatment with lower intensity chemotherapy

regimens (consolidation protocols) and/or allogeneic stem cell transplantation (Schlenk RF et al., 2019).

1.1.5.3 Lower intensity regimens

Elderly patients or patients with poor performance status or comorbidities who are not eligible for aggressive induction may receive lower intensity treatments with the goal to control (but not cure) the disease and minimize its complications. Lower intensity regimens that have shown superior progression free survival (PFS) and overall survival (OS) in this setting include hypomethylating agents (azacitidine and decitabine), and low dose cytarabine (Dombret H et al., 2015; Welch JS et al., 2016; Burnett AK et al., 2007). Other lower intensity agents that have been used in AML include the orally available inhibitor of BCL2, venetoclax (Wei AH et al., 2019), and a first-in-class oral inhibitor of the hedgehog pathway, Glasdegib (Norsworthy KJ et al., 2019). These agents have not proven to effectively control the disease as single agents but have been shown efficacy when combined with azacytidine, decitabine, or low dose cytarabine.

1.1.5.4 Supportive care

Transfusions with blood products such as red blood cells and platelets, and treatment of infectious complications with antibiotics as indicated are important aspects of supportive care in AML treatment. However, prospective and retrospective studies have shown that for elderly patients with AML and for patients with poor performance status, compared with supportive care alone, treatment of AML with lower intensity agents in addition to supportive measures is associated with improved survival, better symptom control, and a similar amount of remaining days spent in the hospital (Löwenberg B et al., 2009).

1.1.6 Treatment of relapsed AML

Reappearance of leukemia cells in the bone marrow, peripheral blood, or at extramedullary sites after attainment of CR is indicative of relapsed disease. Once relapse is confirmed the choice of therapy will depend on a number of patient related factors such as functional status, prior treatments, patient preference, and institutional approach.

Allogeneic stem cell transplant offers the highest chance of cure to patients with relapsed AML. The outcome is more favourable in patients who have achieved CR (Araki D et al., 2016).
Various protocols have been used for remission reinduction including high dose cytarabine (2 to 3 g/m2 every 12 hours for 8 to 12 doses), reinduction with cytarabine plus an anthracycline (eg. daunorubicin), or induction with mitoxantrone (10 to 12 mg/m2 per day) and etoposide (100 mg/m2 per day).These protocols have not been directly compared in clinical trials and at present, there is no consensus about the optimal induction regimen for relapsed AML (Brandwein JM et al., 2008).

Patients with targetable mutations such as *IDH1, IDH2 and FLT3* mutations may be amenable to treatment with targeted agents such as ivosidenib, enasidenib, or gilteritinib as bridging therapies to transplant. However, no studies have compared the outcome of targeted therapies alone versus intensive chemotherapies in this setting. Patients with highly unfavorable AML genotypes (eg, monosomal karyotype) are less likely to respond to standard therapies and are often considered for treatment with an investigational agent. Patients with poor performance status or comorbidities that are not eligible for SCT may receive lower intensity treatments, investigational therapies or palliation (Medeiros BC et al., 2018).

1.1.7 Treatment of primary refractory AML (primary non-responders)

Approximately 20 to 30 percent of young adult patients and up to 50 percent of older patients with newly diagnosed AML will fail to achieve CR with induction and reinduction chemotherapy and are classified as "primary non-responders". In most circumstances, treatment refractory AML has unfavorable cytogenetic and molecular features and/or is therapy related or associated with pre-existing MPN/MDS (Walter RB et al., 2015).
Management of AML with primary induction failure remains challenging and the prognosis of these patients remains poor. At present, there is no standard of care for treatment of primary refractory AML. Treatment options include salvage allogeneic stem cell transplantation (SCT), or subsequent courses of intensive chemotherapy, experimental therapies, or palliation. Treatment choice is often selected based upon the clinical circumstances and the availability of these therapeutic options (Dohner H et al., 2010).

SCT offers the highest chance of long-term remission for patients with high risk AML. However, the utility of SCT for patients with treatment refractory AML remains controversial (Duval M et al., 2010). In this clinical context, SCT is associated with higher rates of treatment related mortality and more post-transplant relapses occur. Alternatively, patients with primary refractory AML may undergo a third course of induction chemotherapy with the goal to achieve CR prior to SCT, or choose to receive lower intensity or experimental therapies in addition to supportive care with the main goal of controlling the disease burden and temporarily minimizing the complications (Roboz GJ et al., 2014).

1.1.8 AML prognosis

The response to treatment and overall outcome of patient with AML depends on a number of patient related and tumor related factors.

Of baseline patient characteristics, advanced age and poor functional status are the strongest predictors of adverse outcome (Estey EH et al., 2001). In older adults (>60 years of age), AML tends to be more biologically complex and is more resistant to treatments. Even among patients < 60 years of age, higher age is an adverse prognosticator. Major comorbidities such as advanced heart failure, renal insufficiency, diabetes or chronic infections are also associated with poor outcome and adversely affect patients performance status. Age at diagnosis and performance status have been used together to prognosticate AML. For example, retrospective analysis of outcome of 968 adults with newly diagnosed AML that were treated by the Southwest Oncology Group (SWOG) in prospective trials of induction therapy reported 30 day mortality rates of 5, 4, 9, and 21 percent for adults ≤65 years of age if they presented with an ECOG performance status of 0, 1, 2, or 3, respectively. Patients >65 years had rates of 13, 16, 35, and 60 percent, respectively (Appelbaum FR et al., 2006).

Other clinical factors that affect the outcome in AML include therapy related AML (prior exposure to cytotoxic agents or radiation therapy) and history of prior myelodysplasia or other hematologic disorders such as myeloproliferative neoplasms. AML in these settings is typically associated with complex cytogenetic abnormalities and molecular mutations, and is often refractory to treatment (Ossenkoppele G et al., 2019).

AML has also been classified into several prognostic groups using cytogenetic and/or molecular genetic features. For example, the classification system proposed by the European

Leukemia Network (Döhner H et al., 2016) categorizes AML into three prognostic groups based on the baseline cytogenetic and molecular findings:

1. Favourable risk AML
   - •t(8;21)(q22;q22.1); *RUNX1-RUNX1T1*
   - •inv(16)(p13.1;q22) or t(16;16)(p13.1;q22); *CBFB-MYH11*
   - •Mutated *NPM1* without *FLT3*-ITD or with low allelic ratio (<0.5) of *FLT3*-ITD
   - •Biallelic mutated *CEBPA*

2. Intermediate risk AML
   - •Mutated *NPM1* and high allelic ratio (>0.5) of *FLT3*-ITD
   - •Wild-type *NPM1* without *FLT3*-ITD or with low allelic ratio (<0.5) of *FLT3*-ITD (without adverse-risk genetic lesions)
   - •t(9;11)(p21.3;q23.3); *MLLT3-KMT2A*
   - •Cytogenetic abnormalities not classified as favorable or adverse

3. Adverse risk AML
   - •t(6;9)(p23;q34.1); *DEK-NUP214*
   - •t(v;11q23.3); *KMT2A* rearranged
   - •t(9;22)(q34.1;q11.2); *BCR-ABL1*
   - •inv(3)(q21.3;q26.2) or t(3;3)(q21.3;q26.2); *GATA2, MECOM (EVI1)*
   - •Monosomy 5 or del(5q); monosomy 7; monosomy 17/abn(17p)
   - •Complex karyotype, monosomal karyotype
   - •Wild-type *NPM1* and high allelic ratio (>0.5) of *FLT3*-ITD
   - •Mutant RUNX1, ASXL1, or TP53

These groups differ in rates of complete remission (CR), disease free survival (DFS) and overall survival (OS). Together with baseline patient characteristics, analyzing tumor related factors is an important part of evaluation of patients with newly diagnosed AML and can directly affect the choice of treatment (Leisch M et al., 2019).

1.1.9 Novel therapeutic strategies for AML

Despite remarkable advancements in development of novel antineoplastic agents for treatment of solid and hematological malignancies in the past decades, development of new therapeutic strategies for AML has shown a slow progress. Similar to other areas of cancer research, modern academic researchers and drug development programs in AML have focused on identifying new therapeutic targets for the disease. However, given the biological diversity and complexity of AML, identifying promising therapeutic strategies for this disease remains challenging and disease heterogeneity has posed a major obstacle for successful drug development in this field (Li S et al., 2916).

In recent years, however, owing to the breakthrough technologies in cancer research, our improved understanding of AML biology has led to development of several novel anti-leukemic agents that target specific molecular mutations. Notably, in 2017, for the first time since the year 2000, several new anti-leukemic drugs received regulatory approval in the US. This included a multikinase inhibitor, midostaurin (Kim ES et al., 2017), which is effective in AML with mutations in the FMS-like tyrosine kinase 3 (FLT3) gene, and two IDH inhibitors, ivosidenib (Sidaway P et al., 2018) and enasidenib (Kim ES et al., 2017), which are effective in a subset of AML with IDH1and IDH2 mutations, respectively.

1.1.9.1 Targeting molecular mutations in AML

1.1.9.1.1 FLT3 mutated AML

FLT3 encodes a receptor tyrosine kinase that is primarily expressed in hematopoietic precursors and promotes hematopoiesis under normal conditions. In-frame tandem duplications within exon 14 of FLT3 (FLT3-ITD mutations) are found in approximately 20% of cases of adult AML. These mutations lead to formation of hetero- and homodimers of the receptor tyrosine kinase in the absence of ligand. As a result, FLT3-ITD is constitutively active and promotes tyrosine kinase signaling. FLT3-ITD

mutations in AML are indicators of adverse prognosis. Other FLT3 mutations such as activating point mutations (e.g., Asp835) in the TKD of FLT3 have also been described but their prognostic significance remains unclear (Small D, 2016).

Several inhibitors of FLT3 have so far been identified and tested in clinical trials. For example, sorafenib is a multi- kinase inhibitors that inhibit FLT3 in addition to c-Kit, VEGFR, and PDGFR-α and -β. It inhibited FLT3 mutated AML in preclinical studies. In clinical trials, addition of sorafenib to standard chemotherapy has resulted in antileukemic efficacy but also increased treatment related toxicities (Röllig C et al., 2015). Midostaurin is another multikinase inhibitor that is active against FLT3 positive AML. In clinical studies, addition of midostaurin to induction and consolidation chemotherapies of newly diagnosed AML patients with FLT3 mutations followed by maintenance treatment with the drug for 12 months resulted in improved overall and event free survival. However, survival benefits were modest and rates of complete remission and allogeneic bone marrow transplantation were equivalent between arms (Stone RM et al., 2017).

Other available FLT3 inhibitors that are currently being tested in clinical trials include quizartinib (Zhou F et al., 2019) and gilteritinib (Bohl SR et al., 2019). These agents are highly potent and specific in inhibiting the FLT3 kinase (With the exceptions of inhibition of c-Kit, PDGFR-α, PDGFR-β, RET, and CSF1R with quizartinib that occurs at potencies at least 10-fold lower than for FLT3, and inhibition of AXL, a receptor tyrosin kinase, by gilteritinib at concentrations approximately 20-fold higher than that required for FLT3-ITD inhibition.) These agents have shown good clinical efficacy and tolerability and are capable of inducing remissions in patients with relapsed or refractory AML after allogeneic transplant (as single agents or in combination with chemotherapy) (Perl AE et al., 2019).

1.1.9.1.2 IDH1/IDH2 mutated AML

Isocitrate dehydrogenase 1 and 2 (IDH1 & IDH2) catalyze the interconversion of isocitrate and α-ketoglutarate (αKG) in the cytoplasm and mitochondria, respectively. Missense IDH1 & IDH2 mutations occur in less than 10 percent of adults with cytogenetically normal AML and result in neomorphic activity of these enzymes, catalyzing the NADPH-dependent reduction of αKG to R(")-2-hydroxyglutarate (2-HG) (Green CL et al., 2011; Xu W et al., 2011). Expression of R-2-HG in AML leads to depletion αKG and inhibits TET2 and other αKG-dependent enzymes. Consequently, IDH1 and IDH2 mutated AML cells display global DNA hypermethylation and a specific hypermethylation signature that is associated with impaired hematopoietic differentiation and increased stem/progenitor cell marker expression (Lu C et al., 2012).

Selective inhibitors of mutant IDH2 (AG-221, enasidenib) and IDH1 (AG-120, ivosidenib) have recently been tested in preclinical studies and clinical trials. In preclinical models, these agents reduced the levels of R-2-HG, restored the DNA methylation pattern and induced differentiation in leukemic cells (Golub D et al., 2019). In clinical studies, both agents induced complete remissions (CR rates of 23% for enasidenib and 24.7% for ivosidenib) in patients with relapsed or refractory AML with mutated IDH enzymes. These agents were recently approved by the U.S. Food and Drug Administration for treatment of AML in this setting and may offer an acceptable alternative to intensive chemotherapy (Sidaway P et al., 2018; Kim ES et al., 2017).

Other small molecule inhibitors of IDH enzymes are also being developed and tested in preclinical and clinical studies. Among these molecules, IDH305,a targeted inhibitor of the IDH1 R132 mutant protein has shown preclinical efficacy and has been advanced to a phase I study (Cho YS et al., 2017).

1.1.9.2 Immunotherapeutic strategies for AML

Cancer cells including AML blasts express specific stress proteins that are recognized by immune cells as target antigens. If not hidden by the neoplastic cells, these antigens recruit the immune cells and stimulate the immune system into attacking them. Thus, cancer cells can only progress if they are able to escape the immunosurveillance of the immune system. Over

the past years, immunotherapeutic strategies have emerged as novel targeted modalities in cancer treatment.

Susceptibility of AML cells to immune attack is signified by their immunological features and the possibility to eradicate leukemia cells by graft-versus-leukemia effect after allogeneic stem cell transplant. For example, expression of both major histocompatibility complex (MHC) classes I and II on AML cells makes them susceptible to T cell recognition and attack. In addition, AML blasts express co-stimulatory molecules such as CD80, CD86, and CD40 that are required for T cell stimulation. These intrinsic features have stimulated the exploration of a number of available immunotherapeutic approaches to target AML in recent years including monoclonal antibodies and antibody drug conjugates, bispecific T cell engaging antibodies, and adoptive cellular therapies (Felix S et al., 2017; Acheampong DO et al., 2018). However, given the clonal and genetic complexities of AML, design and application of immunotherapeutic strategies for AML remains challenging. Efforts are underway to identify ideal targets for immunotherapy in AML and to optimize the immunotherapeutic strategies.

1.1.9.3 Targeting deregulated pathways in AML

Pathways that regulate programmed cell death and other deregulated pathways downstream of molecular mutations in AML have also been explored as potential therapeutic targets in AML. For example, the BCL-2 family of proteins regulates mitochondria-mediated apoptosis. Antiapoptotic members of the BCL-2 family such as BCL-2, BCL-XL, BCL-2–like 2 (BCL-w) maintain the integrity of mitochondrial outer membrane and cell survival by preventing the activation of proapoptotic multi-domain effector proteins BAX and BAK and thereby regulating the release of proapoptotic factors such as cytochrome *c*, SMAC, and AIFs (Peña-Blanco A et al., 2018). These proteins are overexpressed in AML bulk and stem cell populations (Khan N et al., 2016). In preclinical models, inhibitors of BCL-2 have shown antileukemic activity as single agents and in combination with other antineoplastic agents (Leverson JD et al., 2017).

Several inhibitors of BCL-2 proteins have also been tested in clinical trials and demonstrated clinical response. For example, monotherapy with venetoclax, a specific inhibitor of BCL-2, was tested in a phase 2 open-label multicenter trial in patients with high-risk

relapsed/refractory AML and resulted in an overall response rate of 19% (Konopleva M et al., 2016). The outcome was more favourable in another study where venetoclax was combined with hypomethylating agents (azacytidine or decitabine) for patients 65 years or older with newly diagnosed AML in a phase 1 clinical trial, producing a CR/CRi rate of 61% (DiNardo CD et al., 2018). Further studies are underway to explore the clinical efficacy of BCL-2 inhibition in treatment of AML.

1.1.9.4 Targeting mitochondria in AML

AML cells and stem cells show decreased respiratory reserve capacity and are highly reliant on oxidative phosphorylation for their survival (Sriskanthadevan S et al., 2015). Targeting mitochondrial respiration by inhibiting the activity of respiratory chain enzymes, or through inhibition of other mitochondrial pathways such as mitochondrial translation (Skrtić M et al., 2011), mitochondrial DNA replication (Yehudai D et al., 2019), or mitochondrial proteases (Cole A et al., 2015) have been recently investigated in AML. For example, Skrtić et al showed that inhibition of mitochondrial translation by the antimicrobial tigecycline selectively targets AML cells in vitro and in vivo. Tigecycline was later tested in a phase I clinical trial in patients with relapsed and/or refractory AML (Reed GA et al., 2016). No clinical responses were observed in this trial. However, the drug was administered on a once daily dosing schedule and inhibition of mitochondrial protein translation was likely not sustained long enough to induce downstream cellular effects. Molina et al. recently demonstrated that IACS-010759, a small-molecule inhibitor of complex I of the mitochondrial electron transport chain, inhibits cell proliferation and induces apoptosis in preclinical models of AML (Molina JR et al., 2018). IACS-010759 is currently being evaluated in phase I clinical trials in patients with relapsed and/or refractory AML and solid tumors. Another group showed that in patients with AML, treatment with venetoclax in combination with azacitidine result in metabolic perturbations that lead to disruption of TCA cycle and inhibition of electron transport chain complex II (Pollyea DA et al., 2018). Consequently, leukemic stem cells were efficiently and selectively targeted.

Collectively, this background suggest an emerging role for targeting mitochondria as a novel therapeutic strategy in AML.

1.1.10 Identification of human mitochondrial protease, ClpP, as a therapeutic target for acute myeloid leukemia

In search for new therapeutic targets, Cole et al. recently performed an shRNA screen to determine whether knockdown of any of the members of the mitochondrial proteome will reduce viability of K562 leukemic cells (Cole et al., 2015). In this screen, 2422 shRNAs targeted 496 members of the mitochondrial proteome and of the top 25 targets, 4 were mitochondrial proteases (NLN, ClpP, PARL, and PITRM1) with 2 targeting ClpP ranking in the top 1% of all hits. Importantly, the group showed that genetic knockdown of ClpP reduced the growth and viability of several AML cell lines with high ClpP expression including K562, TEX, and OCI-AML2 and that ClpP knockout mice were viable and had normal hematopoiesis.

In primary AML samples, ClpP is equally expressed in stem cell and bulk populations and is over-expressed in approximately 45% of cases. ClpP over-expression occurs across the spectrum of cytogenetic and molecular mutations. ClpP expression positively correlates with expression of genes related to the mitochondrial unfolded protein response (Cole et al., 2015).

Using BioID-Mass Spectrometry (BioID-MS), it was shown that ClpP preferentially interacts with components of the respiratory chain or enzymes involved in mitochondrial metabolism (Cole et al., 2015). In view of the previously published data that demonstrated that AML cells have increased reliance on oxidative phosphorylation (Skrtić M et al., 2011; Lagadinou ED et al., 2013), the group hypothesized that ClpP inhibition reduces the growth and viability of AML cells by impairing the mitochondrial metabolism and oxidative phosphorylation. In support of this hypothesis, they observed that inhibition of the protease results in the accumulation of misfolded or degraded respiratory chain complex subunits and respiratory chain dysfunction in AML cells. Chemical or genetic inhibition of the protease impaired oxidative phosphorylation and selectively killed AML cells and stem cells over normal hematopoietic cells in vitro and in vivo (Cole et al., 2015) Collectively, these data suggest a mechanistic role for ClpP in

maintaining the integrity of mitochondrial metabolism and propose ClpP as a promising therapeutic target for AML.

1.1.11 ClpP Structure and function

Eukaryotic cells have two separate genomes; nuclear DNA and mitochondrial DNA. Mitochondrial DNA encodes two rRNAs, 22 t-RNAs and 13 of the 90 proteins in the mitochondrial respiratory chain. The remaining mitochondrial proteins are encoded by nuclear genes, translated in the cytoplasm and imported into the mitochondria. Mitochondria possess their own protein synthesis apparatus including mitochondrial ribosomes, initiation and elongation factors. In addition, mitochondria have protein degradation complexes that regulate their protein levels by eliminating excess and/or damaged proteins. To date, at least 15 proteases have been identified in different mitochondrial compartments, including caseinolytic protease P (ClpP) that is located in the mitochondrial matrix. (Corydon et al., 1998).

Human caseinolytic protease P (ClpP) is a mitochondrial serine protease complex that is structurally similar to the cytoplasmic/nuclear proteasome (Kang SG et al., 2014). It is encoded by a nuclear gene, translated in the cytoplasm and subsequently imported into the mitochondrial matrix. Inside the mitochondria, it is assembled into a double-ringed tetradecameric structure with a hollow chamber containing proteolytic active sites.

Each end of this barrel-shaped structure is capped by an AAA+ ATPase chaperone, ClpX that selects and unfolds the target proteins and allows for translocation of the substrate into the proteolytic chamber through the axial pores. The ClpP complex is thought to degrade damaged or misfolded proteins inside mitochondria (Kang SG et al., 2014).

The catalytic sites of ClpP are accessible only through the axial channels in each ring. Upon exposure to target proteins, ClpP undergoes a number of conformational changes

that result in transient enlargement of its axial pores. These structural arrangements facilitate passage of substrates and allow for efficient and targeted proteolysis. The barrel shape of the enzyme limits accessibility to its active sites and is thought to create a shield that protects unselected mitochondrial matrix proteins from being exposed to the catalytic sites (Kang SG et al., 2014).

Recently, our group demonstrated that mitochondrial ClpP is over-expressed in 45% of primary AML samples (Cole et al., 2015). ClpP is equally expressed in stem cell and bulk populations and over-expression occurs across the spectrum of cytogenetic and molecular mutations. ClpP expression is positively correlated with expression of genes related to the mitochondrial unfolded protein response (Cole et al., 2015). Functionally, ClpP maintains the integrity of oxidative phosphorylation as inhibition of the protease results in the accumulation of misfolded or degraded respiratory chain complex subunits and respiratory chain dysfunction in AML cells (Cole et al., 2015). Chemical or genetic inhibition of the protease leads to impaired oxidative phosphorylation and selectively kills AML cells and stem cells over normal hematopoietic cells in vitro and in vivo (Cole et al., 2015).

1.1.12 ClpP hyperactivation as a therapeutic strategy

While most attention has focused on the development of ClpP inhibitors, hyperactivation of ClpP is also an attractive novel therapeutic option. In 2005, Brötz-Oesterhelt et al. reported that naturally occurring antibiotics, acyldepsipeptides, ADEPs, hyperactivate ClpP (Brötz-Oesterhelt H et al, 2005). These compounds bind ClpP at its interface with ClpX and open the pore of the ClpP protease. Opening of the ClpP pore by ADEPs leads to deregulated ClpP activity and permits the protease to degrade full-length substrates without its regulatory subunit ClpX. ClpP activators are cytotoxic to a variety of microbial species including dormant bacteria that are responsible for chronic infections. Of note, systemic administration of ADEPS eradicated chronic infection in a mouse model of leukemia without toxicity. However, the anti-cancer activity of ClpP activators has not been previously reported and will be investigated in this proposal.

Hyperactivation of ClpP through structural rearrangements that lead to permanent enlargement of its axial pores may turn it into a promiscuous protease that is capable of degrading peptides and proteins without specificity inside the mitochondria. Consequently, the impaired mitochondrial proteostasis may activate the mitochondrial unfolded protein response (mUPR) and promote cell death. Alternatively, hyperactivated ClpP may retain substrate specificity, but become a more efficient protease with a faster rate of substrate degradation by facilitating passage of selective protein substrates through its chamber. This may in turn result in excessive degradation of the primary substrates of the enzyme including subunits of electron transport chain and other proteins that are involved in mitochondrial metabolism. As a result, hyperactivation of ClpP through enlargement of its axial pores may impair the integrity of mitochondrial metabolism and trigger apoptosis in AML cells that are highly reliant on oxidative phosphorylation. In keeping with this hypothesis, several studies have shown that activated bacterial ClpP has a selective proteolytic function that is guided by various tagging systems such as arginine phosphorylation (Trentini DB et al., 2016).

1.1.13 Genetically engineered constitutively active ClpP mutants provide insight into structural and enzymatic effects of ClpP hyperactivation

Recently, Ni et al designed and solved the crystal structure of a gain-of-function mutant of S. aureus ClpP which demonstrated increased proteolytic activity as a result of enlarged entrance pores (SaClpPY63A) (Ni T et al., 2016). By analyzing the crystal structure of this mutant, they identified Asn42 as a pivotal residue on S. aureus ClpP which possesses a unique side chain with three distinct conformational states that could be exploited to further expand the axial pores. Based on this information, they subsequently engineered a second gain-of-function mutant (SaClpPN42AY63A) with enlarged axial pores that showed enhanced proteolytic activity. As expected, expression of SaClpPN42AY63A severely compromised the growth of S. aureus and phenocopied treatment with ADEP antibiotics. Furthermore, by analyzing the structure and function of this genetically engineered SaClpP mutant, Ni et al were able to describe the molecular mechanisms by which ADEP antibiotics might activate S. aureus ClpP.

The genetic gain-of-function mutants of human mitochondrial ClpP, however, have not been previously reported. Similar to above mentioned investigations, hyperactive mitochondrial ClpP mutants can be used to study the impacts of mitochondrial ClpP hyperactivation in human cells in their native environments, and away from possible non-specific toxic effects of ClpP activating compounds. In living cells, these gain-of-function mitochondrial ClpP mutants will likely demonstrate an altered interactome map and their enhanced proteolytic activity will likely disrupt mitochondrial proteostasis and consequently impair mitochondrial metabolism and oxidative phosphorylation. As a result, expression (or overexpression) of these gain-of-funtion mitochondrial ClpP mutants may compromise the growth and viability of cell lines that are highly reliant on mitochondrial function.

1.1.14 Imipridone compounds as novel antineoplastic agents

ONC201 (Allen JE et al., 2016) and ONC212 (Wagner J et al., 2017) are orally active small molecules that belong to a family of chemical compounds known as imipridones. Imipridone compounds were recently discovered in a high throughput luciferase reporter screen that aimed to identify p53-independent inducers of apoptosis. These compounds demonstrates many ideal drug properties.

Owing to their three-ring heterocyclic core structure, ONC201 & ONC212 show good chemical stability, high water solubility at low pH and high lipophilicity at physiological pH. They also have low molecular weights, which enhance their oral bioavailability and promote their wide distribution throughout the body. ONC201 & ONC212 therefore display a favorable drug profile that is necessary for successful transitioning of a small compound to clinical studies. Thus, shortly after the selective anti-tumor activity of these compound was established, a number of preclinical studies were initiated to test their antineoplastic activity against a wide range of human cancers (Prabhu VV et al., 2016). In these studies, ONC201 & ONC212 demonstrated promising antineoplastic activity against a number of solid tumors and hematologic malignancies including breast (Greer YE et al., 2018), colorectal (Prabhu VV et al.,

2015), and prostate cancer (Prabhu VV et al., 2017) and multiple myeloma (Tu YS et al., 2017) and leukemia (Prabhu VV et al., 2018). Of note, in preclinical models of acute leukaemia (Kasumi-1, HL60), ONC 201 was associated with a time and dose-dependent decrease in cell viability for every cell line in the panel (Oncoceutics, 2017).

Consequently, several phase I and II clinical trials were launched to investigate the tolerability and the clinical antineoplastic effects of these compounds. So far, based on the interim results from the phase I trial of ONC 201 in patients with solid tumors (Stein MN et al., 2017), ONC201 has demonstrated a good safety profile and favorable pharmokinetics and treatment with ONC201 has been associated antineoplastic response in patients with advanced prostate and endometrial cancers.

Despite rapid advancement of the imirpidones compounds into clinical studies, the mechanism of action of these compounds is not entirely understood. Although ONC201 was originally discovered in a search for TRAIL inducing ligands, treatment of tumor cells with ONC201 results in only modest upregulation of TRAIL protein on the cell surface (Allen JE et al., 2015). Furthermore, the observed upregulation of TRAIL following treatment with ONC201 happens indirectly, through activation of Foxo3a (a regulator of TRAIL gene promoter) (Allen JE et al., 2013). Of note, Foxo3a is also involved in other cell signaling pathways including pathways that control mitochondrial metabolism and protect cells against oxidative stress by direct transcriptional control of expression of anti-oxidant genes such as superoxide dismutase (SOD2) (Nemoto S, et al., 2002; Jafari R, et al., 2014). It is therefore possible that the observed activation of Foxo3a (and the resultant mild upregulation of TRAIL) following treatment with ONC201 happen merely as a cellular response to stress, and that ONC201 exhibits its main antineoplastic effects through a different cellular mechanism such as disruption of mitochondrial metabolism.

Thus, despite their attractive antineoplastic efficacy and low toxicity, cellular mechanism of action of imipridones and their main target had remained largely unknown prior to the investigations that will be presented in this thesis.

1.2 Study aims and objectives

1.2.1 Part A: Investigating the survival outcome of primary non-responders with AML

We perform a retrospective chart review of patients with AML who did not achieve complete remission after treatment with induction and reinduction chemotherapy at Princess Margaret Cancer Centre. We assess their outcome following treatment with additional inductions, supportive/palliative care, or investigational treatments. Specifically, We assess rates of complete remission (CR), rates of relapse after attainment of CR, overall survival, and length of subsequent hospital stays with each treatment approach. Leukemic cells in primary non-responders with AML likely have features that render them resistant to chemotherapy. We therefore expect that rates of complete remission in this group of patients will be lower than rates of remission after induction or reinduction chemotherapy in newly diagnosed patients, and that the overall survival of these patients is poor.

1.2.2 Part B: Investigating ClpP hyperactivation as a novel therapeutic strategy in AML

Here, we hypothesize that hyperactivation of ClpP will lead to excessive degradation of the primary substrates of the enzymes that are mainly involved in energy metabolism. We speculate that the resultant disrupted mitochondrial function will be selectively cytotoxic to AML cells that are highly reliant on oxidative phosphorylation and mitochondrial energy production for their survival. To investigate this vulnerability, we use genetically engineered constitutively active ClpP mutants to assess the toxic effects of ClpP activation in living cells and in vivo. We also search for chemical compounds that can activate the protease. In our preliminary investigations, we identified imipridones as potent ClpP activators. We will confirm the ClpP activating effects of the compounds in cell free gel-based and fluorescence assays. We assess the binding of these compounds to purified recombinant ClpP using Isothermal Titration Calorimetry (ITC) and co-crytallography methods, and to endogenous protease in intact OCI-AML2 cells, using Cellular Thermal Shift Assays (CETSA). Using a proximity dependent biotinylation assay (BioID), we identify the potential interactors and putative substrates of hyperactivated ClpP. To further investigate the effects of ClpP

hyperactivation in leukemic cells, we measure the oxygen consumption rate, respiratory reserve capacity, and the enzymatic activity of the respiratory chain complexes in AML cells following treatment with imipridone compounds. We also test the effects of an inactivating ClpP mutation (D190A) on cellular resistance to the effects of imipridone. In addition, we investigate the cytotoxic effects of ClpP hyperactivation in AML cell lines and primary samples. We test whether ClpP hyperactivation kills AML cells and stem cells preferentially over normal hematopoietic cells and whether AML cells with the highest levels of ClpP are most sensitive. Finally, we test the preclinical efficacy and toxicity of ClpP hyperavtivation in xenograft models of leukemia. To date, no other group has investigated the utility of ClpP hyperactivation for treatment of leukemia or any other malignancy. Our approach represents a first-in-class therapeutic strategy for a subset of hematologic malignancies.

1.3 Summary

In summary, AML refers to a heterogenous group of hematologic malignancies that arise from malignant clonal hematopoiesis in the bone marrow and peripheral blood. AML results in abnormal function of hematopoietic cells, is associated with severe complications such as infection or bleeding, and is generally rapidly lethal if left untreated.

Biologically, a hierarchical system has been described within the leukemia cell population. A minor fraction of leukemia cells - leukemic stem cells (LSCs)- reside at the apex of this hierarchical pyramid. LSCs can initiate AML when transplanted into immunodeficient animals. These cells display self-renewal capacity and other properties such as relative quiescence, resistance to apoptosis, and increased drug efflux that render them relatively resistant to available cytotoxic therapies.

Genetically, AML cells are diverse and undergo ongoing genetic and epigenetic evolution during the course of malignant transformation. Somatic mutations in AML may impair differentiation processes and lead to accumulation of immature progenitors, may activate the signaling pathways that increase the proliferation rate and survival of the hematopoietic progenitors, or may involve epigenetic modifiers and thereby disrupt the epigenetic landscape of the leukemic cells. These mutations may also persist after therapy, lead to clonal expansion during hematologic remission, and eventually lead to relapsed disease.

Metabolically, AML cells display increased oxidative phosphorylation and poor respiratory reserve capacity compared to normal hematopoietic cells. Increased reliance of leukemic cells and stem cells on their mitochondrial function suggests that mitochondria can be potentially targeted as a therapeutic strategy against AML. For example, targeting mitochondrial respiration by inhibiting the activity of respiratory chain enzymes, or through inhibition of other mitochondrial pathways such as mitochondrial translation (Skrtić M et al., 2011), mitochondrial DNA replication (Yehudai D et al., 2019), or mitochondrial proteases (Cole A et al., 2015) have been recently investigated in AML.

Cole et al. (Cole A et al., 2015) recently described human mitochondrial caseinolytic protease P (ClpP) as a promising therapeutic target in AML. ClpP is a cylindrical protease that is thought to have a pivotal role in maintaining the integrity of mitochondrial respiration by functioning as a mitochondrial protein quality control mediator. Through a comprehensive body of investigations, the group demonstrated that ClpP inhibition is toxic to leukemic cells in vitro and in vivo, likely as a result of disruption of mitochondrial oxidative phosphorylation.

Herein, we first describe the clinical outcome of primary non responders with AML, paying specific attention to the rates of complete remission and overall survival of those who receive 3 or more inductions. We then investigate the preclinical efficacy of ClpP hyperactivation as a novel therapeutic strategy in AML. We hypothesize that hyperactivation of ClpP can be toxic to leukemic cells and stem cells through disruption of mitochondrial proteostasis, and consequently disruption of mitochondrial energy metabolism pathways. We use genetic and chemical tools to explore this possibility. A constitutively active S. aureus ClpP with point mutation was previously described. Through sequence homology, we induce a point mutation on human ClpP to mimic the structural changes that happen in S. aureus ClpP mutant. Using this constitutively active mutated ClpP, we study the toxic effects of ClpP hyperactivation in leukemia. We also search for chemical ClpP activators and identify imipridones as potent ClpP activators. We use these compounds to investigate ClpP hyperactivation as a first-in-class therapeutic strategy in AML.

1.4 References

Acheampong DO, Adokoh CK, Asante DB et al. Biomed Pharmacother. 2018 Jan;97:225-232.
Immunotherapy for acute myeloid leukemia (AML): a potent alternative therapy.

Allen JE, Krigsfeld G, Mayes PA et al. Sci Transl Med. 2013 Feb 6;5(171):171ra17.
Dual inactivation of Akt and ERK by TIC10 signals Foxo3a nuclear translocation, TRAIL geneinduction, and potent antitumor effects.

Allen JE, Krigsfeld G, Patel L et al. Mol Cancer. 2015 May 1;14:99.
Identification of TRAIL-inducing compounds highlights small molecule ONC201/TIC10 as a unique anti-cancer agent that activates the TRAIL pathway.

Allen JE, Kline CL, Prabhu VV et al. Oncotarget. 2016 Nov 8;7(45):74380-74392.
Discovery and clinical introduction of first-in-class imipridone ONC201.

Appelbaum FR, Gundacker H, Head DR et al. Blood. 2006;107(9):3481.
Age and acute myeloid leukemia.

Araki D, Wood BL, Othus M et al. J Clin Oncol. 2016;34(4):329-36.
Allogeneic Hematopoietic Cell Transplantation for Acute Myeloid Leukemia: Time to Move Toward a Minimal Residual Disease-Based Definition of Complete Remission?

Basak NP, Banerjee S. Mitochondrion. 2015 Mar;21:41-8.
Mitochondrial dependency in progression of acute myeloid leukemia.

Bishop JF, Lowenthal RM, Joshua D et al. Blood. 1990;75(1):27.
Etoposide in acute nonlymphocytic leukemia. Australian Leukemia Study Group.

Bohl SR, Bullinger L, Rücker FG. Int J Mol Sci. 2019 Apr 23;20(8).
New Targeted Agents in Acute Myeloid Leukemia: New Hope on the Rise.

Bonnet D, Dick JE. Nat Med. 1997 Jul;3(7):730-7.
Human acute myeloid leukemia is organized as a hierarchy that originates from a primitive hematopoietic cell.

Brandwein JM, Gupta V, Schuh AC et al. Am J Hematol. 2008;83(1):54-8.
Predictors of response to reinduction chemotherapy for patients with acute myeloid leukemia who do not achieve complete remission with frontline induction chemotherapy.

Brötz-Oesterhelt H, Beyer D, Kroll HP et al. Nat Med. 2005 Oct;11(10):1082-7.
Dysregulation of bacterial proteolytic machinery by a new class of antibiotics.

Bullinger L, Döhner K, Döhner H. J Clin Oncol. 2017 Mar 20;35(9):934-946.
Genomics of Acute Myeloid Leukemia Diagnosis and Pathways.

Burnett AK, Milligan D, Prentice AG et al. Cancer. 2007 Mar;109(6):1114-24.

A comparison of low-dose cytarabine and hydroxyurea with or without all-trans retinoic acid for acute myeloid leukemia and high-risk myelodysplastic syndrome in patients not considered fit for intensive treatment.

Cai SF, Levine RL. Semin Hematol. 2019 Apr;56(2):84-89.
Genetic and epigenetic determinants of AML pathogenesis.

Cho YS, Levell JR, Liu G et al. ACS Med Chem Lett. 2017 Sep 18;8(10):1116-1121.
Discovery and Evaluation of Clinical Candidate IDH305, a Brain Penetrant Mutant IDH1 Inhibitor.

Cole A, Wang Z, Coyaud E et al. Cancer Cell. 2015 Jun 8;27(6):864-76.
Inhibition of the Mitochondrial Protease ClpP as a Therapeutic Strategy for Human Acute Myeloid Leukemia.

Corces-Zimmerman MR, Hong WJ, Weissman IL et al. Proc Natl Acad Sci U S A. 2014 Feb 18; 111(7): 2548–2553.
Preleukemic mutations in human acute myeloid leukemia affect epigenetic regulators and persist in remission.

Corydon TJ, Bross P, Holst HU et al. Biochem J. 1998 Apr 1;331 (Pt 1):309-16.
A human homologue of Escherichia coli ClpP caseinolytic protease: recombinant expression, intracellular processing and subcellular localization.

De Kouchkovsky I, Abdul-Hay M. Blood Cancer J. 2016 Jul; 6(7): e441.
Acute myeloid leukemia: a comprehensive review and 2016 update.

DiNardo CD, Pratz KW, Letai A et al. Lancet Oncol. 2018 Feb;19(2):216-228.
Safety and preliminary efficacy of venetoclax with decitabine or azacitidinein elderly patients with previously untreated acute myeloid leukaemia: a non-randomised, open-label, phase 1b study.

Döhner H, Estey EH, Amadori S et al. Blood. 2010;115(3):453-74.
Diagnosis and management of acute myeloid leukemia in adults: recommendations from an international expert panel, on behalf of the European LeukemiaNet.

Döhner H, Estey E, Grimwade D et al. Blood. 2017 Jan 26;129(4):424-447.
Diagnosis and management of AML in adults: 2017 ELN recommendations from an international expert panel.

Döhner H, Estey E, Grimwade D et al. Blood. 2017;129(4):424.
Diagnosis and management of AML in adults: 2017 ELN recommendations from an international expert panel.

Dombret H, Seymour JF, Butrym A et al. Blood. 2015;126(3):291.
International phase 3 study of azacitidine vs conventional care regimens in older patients with newly diagnosed AML with>30% blasts.

Duval M, Klein JP, He W et al. J Clin Oncol. 2010;28(23):3730-8.

Hematopoietic stem-cell transplantation for acute leukemia in relapse or primary induction failure.

Estey EH. Cancer. 2001;92(5):1059.
Therapeutic options for acute myelogenous leukemia.

Estey EH, Thall PF, Cortes JE et al. Blood. 2001;98(13):3575.
Comparison of idarubicin + ara-C-, fludarabine + ara-C-, and topotecan + ara-C-based regimens in treatment of newly diagnosed acute myeloid leukemia, refractory anemia with excess blasts in transformation, or refractory anemia with excess blasts.

Golub D, Iyengar N, Dogra S et al. Front Oncol. 2019; 9: 417.
Mutant Isocitrate Dehydrogenase Inhibitors as Targeted Cancer Therapeutics.

Green CL, Evans CM, Zhao L et al. Blood. 2011;118(2):409.
The prognostic significance of IDH2 mutations in AML depends on the location of the mutation.

Greer YE, Porat-Shliom N, Nagashima K et al. Oncotarget. 2018 Apr 6;9(26):18454-18479.
ONC201 kills breast cancer cells in vitro by targeting mitochondria.

Hills RK, Castaigne S, Appelbaum FR et al. Lancet Oncol. 2014 Aug;15(9):986-96.
Addition of gemtuzumab ozogamicin to induction chemotherapy in adult patients with acute myeloid leukaemia: a meta-analysis of individual patient data from randomised controlled trials.

Holowiecki J, Grosicki S, Robak T et al. Leukemia. 2004;18(5):989.
Addition of cladribine to daunorubicin and cytarabine increases complete remission rate after a single course of induction treatment in acute myeloid leukemia. Multicenter, phase III study.

Jhas B, Sriskanthadevan S, Skrtic M et al. PLoS One. 2013;8(3):e58367.
Metabolic adaptation to chronic inhibition of mitochondrial protein synthesis in acute myeloid leukemia cells.

Kang SG, Maurizi MR, Thompson M et al. J Struct Biol. 2004 Dec;148(3):338-52.
Crystallography and mutagenesis point to an essential role for the N-terminus of human mitochondrial ClpP.

Kats LM, Reschke M, Taulli R et al. Cell Stem Cell. 2014 Mar 6;14(3):329-41.
Proto-oncogenic role of mutant IDH2 in leukemia initiation and maintenance.

Khan N, Hills RK, Knapper S et al. PLoS One. 2016 Sep 26;11(9):e0163291.
Normal Hematopoietic Progenitor Subsets Have Distinct Reactive Oxygen Species, BCL2 and Cell-Cycle Profiles That Are Decoupled from Maturation in Acute Myeloid Leukemia.

Kim ES. Drugs. 2017 Jul;77(11):1251-1259.
Midostaurin: First Global Approval.

Kim ES. Drugs. 2017 Oct;77(15):1705-1711.
Enasidenib: First Global Approval.

Konopleva M, Pollyea DA, Potluri J et al.Cancer Discov. 2016 Oct;6(10):1106-1117.
Efficacy and Biological Correlates of Response in a Phase II Study of Venetoclax Monotherapy in Patients with Acute Myelogenous Leukemia.

Kops GJ, Dansen TB, Polderman PE et al. Nature. 2002 Sep 19;419(6904):316-21.
Forkhead transcription factor FOXO3a protects quiescent cells from oxidative stress.

Kreitz J, Schönfeld C, Seibert M et al. Cells. 2019 Jul 31;8(8).
Metabolic Plasticity of Acute Myeloid Leukemia.

Lagadinou ED, Sach A, Callahan K et al. Cell Stem Cell. 2013 Mar 7; 12(3):329-41.
BCL-2 inhibition targets oxidative phosphorylation and selectively eradicates quiescent human leukemia stem cells.

Leisch M, Jansko B, Zaborsky N et al. Cancers (Basel). 2019 Feb 21;11(2).
Next Generation Sequencing in AML-On the Way to Becoming a New Standard for Treatment Initiation and/or Modulation?

Leverson JD, Sampath D, Souers AJ et al. Cancer Discov. 2017 Dec;7(12):1376-1393.
Found in Translation: How Preclinical Research Is Guiding the Clinical Development of the BCL2-Selective Inhibitor Venetoclax.

Ley TJ, Miller C, Ding L, et al. N Engl J Med 368:2059-2074, 2013
Cancer Genome Atlas Research Network: Genomic and epigenomic landscapes of adult de novo acute myeloid leukemia.

Li S, Mason CE, Melnick A. Curr Opin Genet Dev. 2016 Feb;36:100-6.
Genetic and epigenetic heterogeneity in acute myeloid leukemia.

Lichtenegger FL, Krupka C, Haubner S et al. J Hematol Oncol. 2017.
Recent developments in immunotherapy of acute myeloid leukemia.

Löwenberg B, Ossenkoppele GJ, van Putten W et al.N Engl J Med. 2009;361(13):1235.
High-dose daunorubicin in older patients with acute myeloid leukemia.

Löwenberg B, Pabst T, Maertens J et al. Blood. 2017;129(12):1636.
Therapeutic value of clofarabine in younger and middle-aged (18-65 years) adults with newly diagnosed AML.

Lu C, Ward PS, Kapoor GS et al. Nature. 2012 Feb 15;483(7390):474-8.
IDH mutation impairs histone demethylation and results in a block to cell differentiation.

Marlein CR, Zaitseva L, Piddock RE et al. Blood. 2017 Oct 5;130(14):1649-1660.
NADPH oxidase-2 derived superoxide drives mitochondrial transfer from bone marrow stromal cells to leukemic blasts.

Medeiros BC. Best Pract Res Clin Haematol. 2018 Dec;31(4):384-386.
Is there a standard of care for relapsed AML?

Molina JR, Sun Y, Protopopova M et al. Nat Med. 2018 Jul;24(7):1036-1046.
An inhibitor of oxidative phosphorylation exploits cancer vulnerability.

Nemoto S, Finkel T. Science. 2002 Mar 29;295(5564):2450-2.
Redox regulation of forkhead proteins through a p66shc-dependent signaling pathway.

Ni T, Ye F, Liu X et al. ACS Chem Biol. 2016 Jul 15;11(7):1964-72.
Characterization of Gain-of Function Mutant Provides New Insights into ClpP Structure.

Norsworthy KJ, By K, Subramaniam S et al., Clin Cancer Res. 2019 May 7.
FDA Approval Summary: Glasdegib for Newly Diagnosed Acute Myeloid Leukemia.

Oncoceutics. ONC 201. Adis Insight. 04 May 2017

Ossenkoppele G, Montesinos P. Crit Rev Oncol Hematol. 2019 Jun;138:6-13.
Challenges in the diagnosis and treatment of secondary acute myeloid leukemia.

Peña-Blanco A, García-Sáez AJ. FEBS J. 2018 Feb;285(3):416-431.
Bax, Bak and beyond - mitochondrial performance in apoptosis.

Perl AE. Blood. 2019 Jun 26. pii: blood.
Availability of FLT3 inhibitors--how do we use them?

Phillips GL, Reece DE, Shepherd JD et al. Blood. 1991;77(7):1429
High-dose cytarabine and daunorubicin induction and postremission chemotherapy for the treatment of acute myelogenous leukemia in adults.

Pollyea DA, Stevens BM, Jones CL et al. Nat Med. 2018 Dec;24(12):1859-1866.
Venetoclax with azacitidine disrupts energy metabolism and targets leukemia stem cells in patients with acute myeloid leukemia.

Prabhu VV, Allen JE, Dicker DT et al. Cancer Res. 2015 Apr 1;75(7):1423-32.
Small-Molecule ONC201/TIC10 Targets Chemotherapy-Resistant Colorectal Cancer Stem-like Cells in an Akt/Foxo3a/TRAIL-Dependent Manner.

Prabhu VV, Lulla AR, Madhukar NS et al. PLoS One. 2017 Aug 2;12(8):e0180541.
Cancer stem cell-related gene expression as a potential biomarker of response for first-in-class imipridone ONC201 in solid tumors.

Prabhu VV, Talekar MK, Lulla AR et al. Cell Cycle. 2018;17(4):468-478.
Single agent and synergistic combinatorial efficacy of first-in-class small molecule imipridone ONC201 in hematological malignancies.

Prabhu VV, Talekar MK, Lulla AR et al. Cell Cycle. 2018;17(4):468-478.
Single agent and synergistic combinatorial efficacy of first-in-class small molecule imipridone ONC201 in hematological malignancies.

Reed GA, Schiller GJ, Kambhampati S et al. Cancer Med. 2016 Nov;5(11):3031-3040.
A Phase 1 study of intravenous infusions of tigecycline in patients with acute myeloid leukemia.

Roboz GJ, Rosenblat T, Arellano M et al. J Clin Oncol. 2014;32(18):1919-26.
International randomized phase III study of elacytarabine versus investigator choice in patients with relapsed/refractory acute myeloid leukemia.

Röllig C, Serve H, Hüttmann A et al. Lancet Oncol. 2015 Dec;16(16):1691-9.
Addition of sorafenib versus placebo to standard therapy in patients aged 60 years or younger with newly diagnosed acute myeloid leukaemia (SORAML): a multicentre, phase 2, randomised controlled trial.

Röllig C, Serve H, Hüttmann A et al. Lancet Oncol. 2015 Dec;16(16):1691-9.
Addition of sorafenib versus placebo to standard therapy in patients aged 60 years or younger with newly diagnosed acute myeloid leukaemia (SORAML): a multicentre, phase 2, randomised controlled trial.

Schlenk RF, Jaramillo S, Müller-Tidow C. Semin Hematol. 2019 Apr;56(2):96-101.
What's new in consolidation therapy in AML?

Shafat MS, Gnaneswaran B, Bowles KM et al. Blood Rev. 2017 Sep;31(5):277-286.
The bone marrow microenvironment - Home of the leukemic blasts.

Shallis RM, Wang R, Davidoff A et al. Blood Rev. 2019 Jul;36:70-87.
Epidemiology of acute myeloid leukemia: Recent progress and enduring challenges.

Shallis RM, Wang R, Davidoff A et al. Blood Rev. 2019 Jul;36:70-87.
Epidemiology of acute myeloid leukemia: Recent progress and enduring challenges.

Shlush LI, Zandi S, Mitchell A et al. Nature. 2014 Feb 14; 506(7488): 328–333.
Identification of pre-leukemic hematopoietic stem cells in acute leukemia.

Sidaway P. Nat Rev Clin Oncol. 2018 Aug;15(8):472.
Ivosidenib effective in IDH1-mutant AML.

Siegel RL, Miller KD, Jemal A. CA Cancer J Clin. 2017;67(1):7
Cancer Statistics, 2017.

Skrtić M, Sriskanthadevan S, Jhas B et al. Cancer Cell. 2011 Nov 15;20(5):674-88.
Inhibition of mitochondrial translation as a therapeutic strategy for human acute myeloid leukemia.

Small D. Hematology Am Soc Hematol Educ Program. 2006:178-84.
FLT3 mutations: biology and treatment.

Song K, Li M, Xu X et al. Exp Hematol. 2016 Jul;44(7):540-60.
Resistance to chemotherapy is associated with altered glucose metabolism in acute myeloid leukemia.

Sriskanthadevan S, Jeyaraju DV, Chung TE et al. Blood. 2015 Mar 26;125(13):2120-30.
AML cells have low spare reserve capacity in their respiratory chain that renders them susceptible to oxidative metabolic stress.

Stein MN, Bertino JR, Kaufman HL et al. Clin Cancer Res. 2017 Aug 1;23(15):4163-4169.
First-in-Human Clinical Trial of Oral ONC201 in Patients with Refractory Solid Tumors.

Stone RM, Mandrekar SJ, Sanford BL et al. N Engl J Med. 2017;377(5):454.
Midostaurin plus Chemotherapy for Acute Myeloid Leukemia with a FLT3 Mutation.

Stone RM, Mandrekar SJ, Sanford BL et al. N Engl J Med. 2017;377(5):454.
Midostaurin plus Chemotherapy for Acute Myeloid Leukemia with a FLT3 Mutation.

Testa U, Labbaye C, Castelli G et al. Oncol Lett. 2016 Jul;12(1):334-342.
Oxidative stress and hypoxia in normal and leukemic stem cells.

Thomas D, Majeti R. Blood. 2017 Mar 23;129(12):1577-1585.
Biology and relevance of human acute myeloid leukemia stem cells.

Trentini DB, Suskiewicz MJ, Heuck A et al. Nature. 2016 Nov 3;539(7627):48-53.
Arginine phosphorylation marks proteins for degradation by a Clp protease.

Tu YS, He J, Liu H et al. Neoplasia. 2017 Oct;19(10):772-780.
The Imipridone ONC201 Induces Apoptosis and Overcomes Chemotherapy Resistance by Up-Regulation of Bim in Multiple Myeloma.

Wagner J, Kline CL, Ralff MD et al. Cell Cycle. 2017 Oct 2;16(19):1790-1799.
Preclinical evaluation of the imipridone family, analogs of clinical stage anti-cancer small molecule ONC201, reveals potent anti-cancer effects of ONC212.

Walter RB, Othus M, Burnett AK et al. Leukemia. 2015;29(2):312-20.
Resistance prediction in AML: analysis of 4601 patients from MRC/NCRI, HOVON/SAKK, SWOG and MD Anderson Cancer Center.

Wei AH, Strickland SA Jr, Hou JZ et al. J Clin Oncol. 2019;37(15):1277.
Venetoclax Combined With Low-Dose Cytarabine for Previously Untreated Patients With Acute Myeloid Leukemia: Results From a Phase Ib/II Study.

Weick JK, Kopecky KJ, Appelbaum FR et al. Blood. 1996;88(8):2841.
A randomized investigation of high-dose versus standard-dose cytosine arabinoside with daunorubicin in patients with previously untreated acute myeloid leukemia: a Southwest Oncology Group study.

Welch JS, Petti AA, Miller CA, et al. N Engl J Med. 2016;375(21):2023.
TP53 and Decitabine in Acute Myeloid Leukemia and Myelodysplastic Syndromes

Xu W, Yang H, Liu Y et al. Cancer Cell. 2011;19(1):17.
Oncometabolite 2-hydroxyglutarate is a competitive inhibitor ofα-ketoglutarate-dependent dioxygenases.

Yamamoto JF, Goodman MT. Cancer Causes Control. 2008;19(4):379.
Patterns of leukemia incidence in the United States by subtype and demographic characteristics, 1997-2002.

Yehudai D, Liyanage SU, Hurren R et al. Haematologica. 2019 May;104(5):963-972.
The thymidine dideoxynucleoside analog, alovudine, inhibits the mitochondrial DNA polymerase γ, impairs oxidative phosphorylation and promotes monocytic differentiation in acute myeloid leukemia.

Zhou F, Ge Z, Chen B. Drug Des Devel Ther. 2019 Apr 8;13:1117-1125.
Quizartinib (AC220): a promising option for acute myeloid leukemia.

Chapter 2

2 Remissions after third induction chemotherapy for primary non-responders with acute myeloid leukemia (AML) are uncommon and short-lived

The work presented in this chapter has been previously published.

Sara Farshchi Zarabi , Steven Chan, Vikas Gupta, Dina Khalaf, Andrzej Lutynski, Mark D. Minden, Amr Rostom, Anna Rydlewski, Andre C. Schuh, Hassan Sibai, Karen W. L. Yee and Aaron D. Schimmer.

Princess Margaret Cancer Centre, Toronto, Ontario, Canada

LEUKEMIA & LYMPHOMA, 2018
VOL. 59, NO. 1, 237–240

2.1 Abstract

The outcome of adult patients with AML who are primary non-responders to two courses of induction chemotherapy is poor. However, the utility of a 3rd induction for a select subgroup of these patients is uncertain. Here, we performed a retrospective chart review to investigate the response rates and survival after a 3rd course of induction chemotherapy for primary non-responders with AML.

Between May 1999 and March 2015, 95 patients with AML were identified as primary non-responders to induction and reinduction chemotherapy at Princess Margaret Cancer Centre. Median age was 58.3 years [range: 20-76.6]. 48 (51%) were male. 2% had favorable, 38% intermediate, and 46% adverse cytogenetics. 14 patients received a 3rd induction, while the

others received supportive/palliative care ± low-dose chemotherapy (56 pts), or a non-induction clinical trial (25 pts).

Three out of 14 patients (21%) who received a third induction achieved complete remission (CR). None of the 11 other patients responded to the 3rd induction and none had prolonged aplasia. 1 of 14 (7%) died during 3rd induction. For patients who survived the immediate post induction period and were discharged from hospital the median overall survival from the start of the 2nd induction did not differ between patients who did and did not receive a 3rd induction (278 days [range: 97-1304] vs 181.5 days [range: 47-1855] respectively (p= 0.09))

In summary, remissions after 3rd inductions for primary non-responders are uncommon, and short-lived, suggesting that 3rd inductions should be considered with caution and only when an SCT strategy is in place.

2.2 Introduction

Approximately 20-30% of adult patients with acute myeloid leukemia (AML) will not achieve complete remission (CR) with induction and reinduction chemotherapy and are classified as "primary non-responders" (Walter et al, 2015). Currently, there is no widely accepted standard of care for management of AML with primary induction failure and the prognosis of these patients remains poor. Based on the clinical circumstances and the availability of therapeutic options, these patients may undergo salvage allogeneic stem cell transplantation (SCT), or receive subsequent courses of intensive chemotherapy, experimental therapies, or palliation (Dohner et al, 2010)

SCT offers the highest chance of long-term remission for patients with high risk AML. However, the utility of SCT for patients who have not attained CR is controversial (Araki et al 2016; Duval et al, 2010; Gupta et al,2011). When provided to patients who are not in CR, SCT is associated with higher rate of treatment related mortality and more frequent post-transplant relapses. Thus, a third course of induction chemotherapy is sometimes offered to primary non-responders with AML with the goal to induce CR prior to SCT (Roboz et al, 2014)

The overall response rate to reinduction chemotherapy among patients who do not achieve remission after the first course of induction chemotherapy with cytarabine (Ara-C) and daunorubicin ("7+3") is approximately 53%. However, remissions are brief if not consolidated with SCT (Brandwein et al, 2008). To our knowledge, the rate of CR for primary non-responders with AML who receive a third induction has not been reported in the literature. It remains uncertain whether a third induction course will result in durable CRs for patients with primary induction failure and whether attainment of CR with the third induction course prior to SCT will result in superior survival outcome compared to less intensive therapies.

In this retrospective chart review we investigated the outcome of primary non-responders with AML who underwent a third course of induction chemotherapy or received non-induction therapies and/or palliative care at Princess Margaret Cancer Centre.

2.3 Methods

We retrospectively reviewed the survival outcome of all adult patients with AML who did not achieve CR with induction and reinduction chemotherapy at Princess Margaret Cancer Centre between May 1999 and March 2015.

2.3.1 Definitions

"Induction" course was defined as the first course of intensive chemotherapy aimed to induce CR. Patient who did not achieve CR following the induction course underwent "reinduction" therapy (a 2nd course of intensive chemotherapy). A "third induction" was offered to patients who did not achieve CR with reinduction if they were eligible for (and agreeable to undergo) further intensive chemotherapy. Response to treatment following each line of intensive chemotherapy was assessed by evaluation of peripheral blood counts and a bone marrow aspiration examination on day 28 post completion of the chemotherapy course, if clinically indicated. Failure to achieve CR was defined based on the Revised Recommendations of the International Working Group for response criteria in AML as evidence of persistent AML in blood or bone marrow (>5% blasts) for patients who survived at least 7 days after completion of the final dose of each line of intensive chemotherapy (Cheson et al, 2003). Overall survival (OS) following each induction course was defined as the time from the start of the induction until the date of last follow-up or of death from any cause. Cytogenetic risk groups were defined according to the European Leukemia Net prognostic system (Mrozek et al, 2012).

2.3.2 Data collection process

After obtaining Institutional Research Ethics Board approval, we used the Princess Margaret Leukemia Database to retrieve the baseline demographic data of the AML patients who were classified as "non-responders" following their first and second course of induction chemotherapy between May 1999 and March 2015. We referred to the individual patient records to confirm the diagnosis, remission status and outcomes following each course of induction chemotherapy. Patients with acute promyelocytic leukemia (APL) and chronic myeloid leukemia (CML) in blast crises were excluded from the analysis.

2.3.3 Treatment protocols

Induction and re-induction protocols consisted of standard "7+3" regimen (cytarabine 100 (age <60) or 200 (age ≥60) mg/m^2 as a 7-day continuous intravenous infusion combined with daunorubicin 60 mg/m^2 IV bolus daily for 3 days (or amsacrine 100 mg/m^2 IV daily for 5 days for patients with LVEF 40 – 49%)), Nove-HiDAC (mitoxantrone 10 mg/m^2 IV daily from Days 1–5, etoposide 100 mg/m^2 IV daily Days 1–5, followed by cytarabine 1.5 (age <60) or 1 (age≥60) g/m^2 IV over 3 hours every 12 hours, Days 6–7), Flag-Ida (fludarabine 30 mg/m^2 on days 2 through 6, cytarabine 2 grams/m^2 on days 2 through 6, G-CSF on days 1 through 7, and idarubicin 8 mg/m^2 daily on days 4 through 6), or combinations of 7+3 or Nove-HiDAC regimens with investigational agents. 1 patient received induction chemotherapy with combination of clofarabine and cytarabine and 1 patient received induction with FLAG regimen (fludarabine plus cytarabine) and both received this therapy at an outside institution prior to transfer to the Princess Margaret for subsequent therapy. No patients received the same regimen for both induction and re-induction.

The third induction protocols consisted of standard chemotherapeutic regimens (7+3, Nove-HiDAC, Flag-Ida, amsacrine plus cytarabine or combinations of novel agents with induction chemotherapeutics (induction clinical trials). For patients who achieved CR following the 3rd induction, consolidation protocols consisted of AraC 3 g/m2 iv q12 h for 6 doses on days 1, 3, 5 and daunorubicin 45 mg/m2 /d for 2 days for patients aged < 60 years. SCT was offered to

patients aged <65 years who achieved CR following the third induction, if a matched donor was available and the patient's general medical status did not signify a contraindication to transplant.

Patients who were enrolled in non-induction clinical trials received treatment with non-induction novel regimens in addition to supportive/palliative care. Patients in the supportive/palliative care ± low-dose chemotherapy group received intravenous hydration, transfusion support, and treatment with oral and/or intravenous antibiotics, if clinically indicated. In addition, low dose chemotherapy was provided to this group of patients as a palliative measure.

2.3.4 Statistical analysis

Stata version 11.1 was used for all analyses. Baseline demographic and disease related characteristics were expressed by mean (standard deviation) or median (range) for continuous variables and ratios (in percentages) for categorical variables. The differences in baseline characteristics, AML subgroups, and cytogenetic and molecular risk stratifications between those who did or did not receive a third induction were evaluated by Fisher exact test for categorical variables and Wilcoxon rank-sum test for continuous variables. Kaplan-Meier method was used to estimate the survival functions. Mantel Cox log rank test was used to compare the survival curves. Two sided tests were used for all statistical analyses. P values <0.05 were considered statistically significant.

2.4 Results

2.4.1 Baseline characteristics

Between May 1999 and March 2015, 95 patients with AML did not achieve CR following induction and reinduction chemotherapy at the Princess Margaret Cancer Centre and were

identified as primary non-responders. Median age was 58.3 years [range: 20-76.6]. 48 (50%) were male. 60%had de novo AML, 23% had AML secondary to MDS or MPN and 17% had therapy related AML. 46% of these patients had an adverse cytogenetic risk profile, 38% had intermediate (normal karyotype 20%), and 2% had favorable cytogenetics Of the 95 primary non-responders with AML, 14 patients received a third course of induction chemotherapy while the other 81 patients received supportive/palliative care ± low-dose chemotherapy or were enrolled in non-induction clinical trials. Table 2-1 describes the baseline characteristics of the primary non-responders with AML based on the treatment categories. The induction and reinduction regimens are described in detail in the method section. The median time between induction and reinduction was 41 days [range: 14-229]. The third induction was started a median of 53 days [range36-126] from the start of the second induction. Compared with patients who did not receive further inductions, a greater proportion of those who received a third induction had de novo AML (93% vs 59% P value 0.02). There were no other statistically significant differences in baseline characteristics between the two groups.

Table 2-1: Baseline characteristics of the primary non responders with AML.

	All patients	2 inductions	≥3 inductions	P value
N	95	81	14	
Age, median (range)	58.3 (20-76.6)	58.6 (20.0-76.6)	53.9 (20.2-70.7)	
Gender, n (%)				
• **Male**	48 (51)	42 (52)	6 (43)	0.58
• **Female**	47 (49)	39 (48)	8 (57)	
Cytogenetic and molecular risk stratification, n (%)				
• **Adverse**	44 (46)	40 (49)	4 (29)	0.25
• **Intermediate**	36 (38)	29 (36)	7(50)	0.38
• **Normal**	19 (20)	15 (19)	4 (29)	0.47
• **Favorable**	2 (2)	1 (1)	1 (7)	0.27
• **Missing**	13 (14)	11 (14)	2 (14)	1.0
AML subgroups, n (%):				
• **de novo AML**	61 (64)	48(59)	13 (93)	0.02
• **Secondary to MDS or MPN**	22 (23)	21 (26)	1 (7)	0.18
• **Secondary to prior chemotherapy**	16 (17)	16 (20)	0 (0)	1.0
Initial induction chemotherapy, n (%)				
• **7 + 3**	86 (91)	74 (91)	12 (86)	0.62
• **Flag-ida**	2 (2)	2 (3)	0 (0)	1.0
• **Nove-HiDAC**	1 (1)	1 (1)	0 (0)	1.0
• **7+3 variant***	2(2)	2 (3)	0 (0)	1.0
• **Nove variant***	2 (2)	1 (1)	1 (7)	0.27
• **FLAG**	1 (1)	1 (1)	0 (0)	1.0
• **ARA-C + mitoxantrone**	1 (1)	0 (0)	1 (7)	0.15
Second line induction chemotherapy, n (%)				
• **7 + 3**	3 (3)	1(1)	2 (14)	0.06
• **Flag-ida**	7 (7)	6 (7)	1 (7)	1.0
• **Nove-HiDAC**	55 (58)	49 (60)	6 (42)	0.25
• **7+3 variant***	2 (2)	2 (3)	0 (0)	1.0
• **Nove variant***	27 (28)	22 (27)	5 (36)	0.53
• **clofarabine + cytarabine**	1 (1)	1 (1)	0 (0)	1.0
Time (days) between first and second induction, median (range)	41(14-229)	42 (14-229)	39.5 (22-72)	0.18

2.4.2 Subsequent treatments

For the 14 patients who received a third induction, the induction protocols consisted of standard chemotherapeutic regimens for 8 patients (Flag-Ida using high dose Ara-C as a continuous infusion (n=1), AMSA+HiDAC (n=2), Daunorubicin+ HiDAC (n=1), and Nove-HiDAC (n=4)) and combinations of novel agents with induction chemotherapeutics (induction clinical trials) for 6 patients. Table 2-2 describes the baseline characteristics of the 14 patients who received a 3rd induction and the chemotheraputic regimens used for each induction course. The cytogenetic and molecular analysis of the bone marrow samples of these patients are described in table 2-3. For the 81 primary non responders who did not receive a third induction, subsequent treatments included supportive/palliative care ± low-dose chemotherapy for 56 patients and therapy with novel agents in the context of non-induction clinical trials (in addition to supportive/palliative care ± low-dose chemotherapy) for 25 patients.

Table 2-2. Baseline characteristics and treatment course of the 14 patients who received a 3rd induction

ID	Age	Gender	Cytogenetics	Secondary AML	1st induction	2nd induction	3rd induction	%blast post 2nd induction	%blast post 3rd induction	Outcome	Vital status
1	20	F	High risk	N	7+3	Nove-HiDAC	ARA-C + amsacrine	10	<5	CR post 3rd induction . No SCT due to ongoing infection. Relapsed 2.3 m post CR	Deceased
2	68	F	Intermediate	N	Mitoxantrone +ARA-C	7+3	Nove-HiDAC	20	<5	CR post 3rd induction. Ineligible for SCT due to age. Relapsed 4.7 m post CR	Deceased
3	32	M	High risk	N	7+3	Nove-HiDAC + valproic acid	Flag-ida	90	<5	CR post 3rd induction. SCT 2.8 m following CR. Remains alive 4.6 yrs post CR	Alive
4	35	M	High risk	N	7+3	Nove-HiDAC	ARA-C + amsacrine	20	50	No response	Deceased
5	59	M	Intermediate	N	7+3	Nove-HiDAC	7 + 3 +AEG35156	60	NA	No response	Deceased
6	24	F	Intermediate	N	7+3	Nove-HiDAC	Nove-HiDAC	10	45	No response	Deceased
7	61	F	High risk	N	7+3	Flag-Ida	Nove-HiDAC	40	28	No response	Alive
8	64	F	NA	N	7+3	ARA-C + amsacrine	Nove-HiDAC	NA	50	No response	Deceased
9	40	M	Intermediate	N	7+3	Nove-HiDAC	7 + 3 +AEG35156	10	80	No response	Deceased
10	52	F	Intermediate	N	7+3	Nove-HiDAC + Imatinib	7+3	NA	NA	No response	Deceased
11	34	M	High risk	N	7+3 + Gemtuzumab	Nove-HiDAC + valproic acid	7 + 3 +AEG35156	50	65	No response	Deceased
12	63	F	NA	N	7+3	Nove-HiDAC + Nilotinib	ARA-C + R05045337	78	22	No response	Deceased
13	71	F	Intermediate	N	7+3	Nove +Azacitidine	ARA-C + R05045337	90	83	No response	Deceased
14	56	M	Favorable	Y (prior MDS)	7+3	Nove-HiDAC + valproic acid	ARA-C + ABD-869	60	NA	No response	Deceased

Table 2-3. Cytogenetic and molecular analysis of bone marrow samples of the 14 patients who received 3rd induction.

ID	Cytogenetics	Molecular
1	46,XX,del(5)(q31),t(11;12)(p13;p13)[4]/45,idem, -13[5]/46,XX[1]	NA
2	46,XX[20]	NA
3	45,X,-Y,add(12)(q22) or dup(12)(q21q23)[20], 15q22(PMLx2),17q12(RARAx2)[4]	NA
4	45,XY,inv(3)(q21q26.2),-7[20]	NA
5	46,XY	FLT3 wild type
6	46,XX	NA
7	45,XX,t(3;3)(q21;q26.2),-7[10]/46,XX[1]	NA
8	NA	NA
9	46,XY[20]	NA
10	47,XX,+8[14]	FLT3-ITD mutation (intermediate level); NPM1 wild type; no FLT3TKD mutation
11	45,XY,inv(3)(q21q26.1),del(5)(q22q35),-7[19]/46,XY[1]	NA
12	Result by G-banding: unsuccessful. Result by interphase FISH: negative for monosomy 7 / 7q deletion; no result for 5q probe set	NPM1 and FLT3 wild type
13	46,XX,t(1;14)(q21;q11.2)[20]	FLT3-ITD mutation (low level); FLT3 TKD point mutation, NPM1 wild type
14	46,XY[20]	NPM1 mutation; FLT3 wild type.

2.4.3 Treatment outcomes

From the first day of the second induction regimen, the median OS for all primary non-responders with AML (n=95) was 170 days [range: 20-1855]. 19 patients died in hospital during the admission for the second induction. The median OS after the start of the second induction for this group of patients that died during their admission for second induction was 64 days [range 20-190]. 3 patients died within the first 30 days following the second induction.

For all patients who did not receive a third induction (n=81) the median OS following the start of the second induction was 145 days [range: 20-1855]. For all patients who survived the immediate post induction period and were discharged from the hospital following completion of the second induction (n=76), the median OS from the start of the 2nd induction did not differ between those who did and did not receive a 3rd induction (278 days [range: 97-1304] vs 181.5 days [range: 47-1855] respectively (p= 0.09)) (Figure 2-1a). In the third induction group 93% of patients had de novo AML whereas 59% of patients who did not receive a third induction had de novo AML (p=0.02). Comparison of patients with de novo AML showed no significant difference in the median OS from the start of 2nd induction between those who did and did not receive a 3rd induction (191 days [range: 67-1855] vs 280 days [97-1304] respectively (p=0.24) (Figure 2-1b). Among all patients who did not receive a third induction 4 patients had a prior diagnosis of CMML (with AML transformation); no patient with prior CMML received a third induction. After excluding CMML patients from the survival analysis, there was no statistically significant difference in the OS from the start of the second induction between those who did or did not receive a third induction (278 days [range: 97-1304] vs 181.5 days [range: 66-1855] respectively (p=0.12)) (Figure 2-1c). For the 14 patients who received a third induction the median OS from the start of the 3rd induction was 206 days [range 45-1263].

Three patients (21%) achieved CR following the third induction. One patient with de novo AML and intermediate cytogenetic risk profile achieved CR after a third course of induction chemotherapy with FLAG-Ida where Ara-C was given as a continuous infusion. This patient underwent allogeneic stem cell transplant 3.7 months after the third induction and remains

alive 4.6 years post CR; therapy prior to the third induction included 7+3 and NOVE/HiDAC. The bone marrow blast count was 92% and 90% after the first and second inductions, respectively. The third induction course for the other 2 patients consisted of Nove-HiDAC and AMSA+HiDAC chemotherapy, where the Ara-C was given as continuous infusion. These two patients had previously not achieved CR following induction with NOVE-HiDAC and 7+3 regimens and re-induction with 7+3 and NOVE-HiDAC regimens, respectively. These patients were not eligible for SCT due to institutional age criteria (>65 y/o) (first patient) and presence of active infection (second patient). They received consolidation therapy with combinations of Ara-C plus daunorubicin (first patient) and Ara-c plus amsacrine (second patient) starting on days 42 and 57 following completion of their third induction course, respectively. They presented with relapsed disease 2.3 and 4.7 months post CR. Following relapse, their course of therapy included supportive care and administration of palliative intent low-dose chemotherapy. OS following relapse was 104 and 107 days for these two patients.

None of the 11 other patients achieved remission following the 3rd induction; interestingly none had prolonged aplasia with the regimens used. 1 of 14 (7%) died during the first 30 days after the start of the 3rd induction. For 3 patients, the marrow blast count after the 3rd induction was not available as a bone marrow aspirate was not performed. The failure of the 3rd induction in these patients was determined by increasing number of blasts in peripheral blood (n=2) and infiltration of soft tissue with leukemic cells (n=1). 1 patient who did not achieve remission with the 3rd induction received a 4th induction. This patient previously did not achieve CR following induction with 7 + 3 plus gemtuzumab (clinical trial regimen), re-induction with NOVE/HiDAC, and third induction with a combination regimen that consisted of Ara-C, Idaurubicin, and AEG35156 (clinical trial), and received a fourth induction with Ara-C plus m-Amsa and died 32 days after initiation of this protocol.

Among the 83 patients who did not receive a 3rd induction, 1 patient achieved CR on a phase 1 clinical trial (MDM2 inhibitor). He successfully underwent SCT and remains in CR 3.6 years post SCT. This patient had previously not achieved CR following induction with standard 7+3 regimen and re-induction with NOVE-HIDAC + nilotinib and had received clinical trials with elesclomol and elacytarabine.

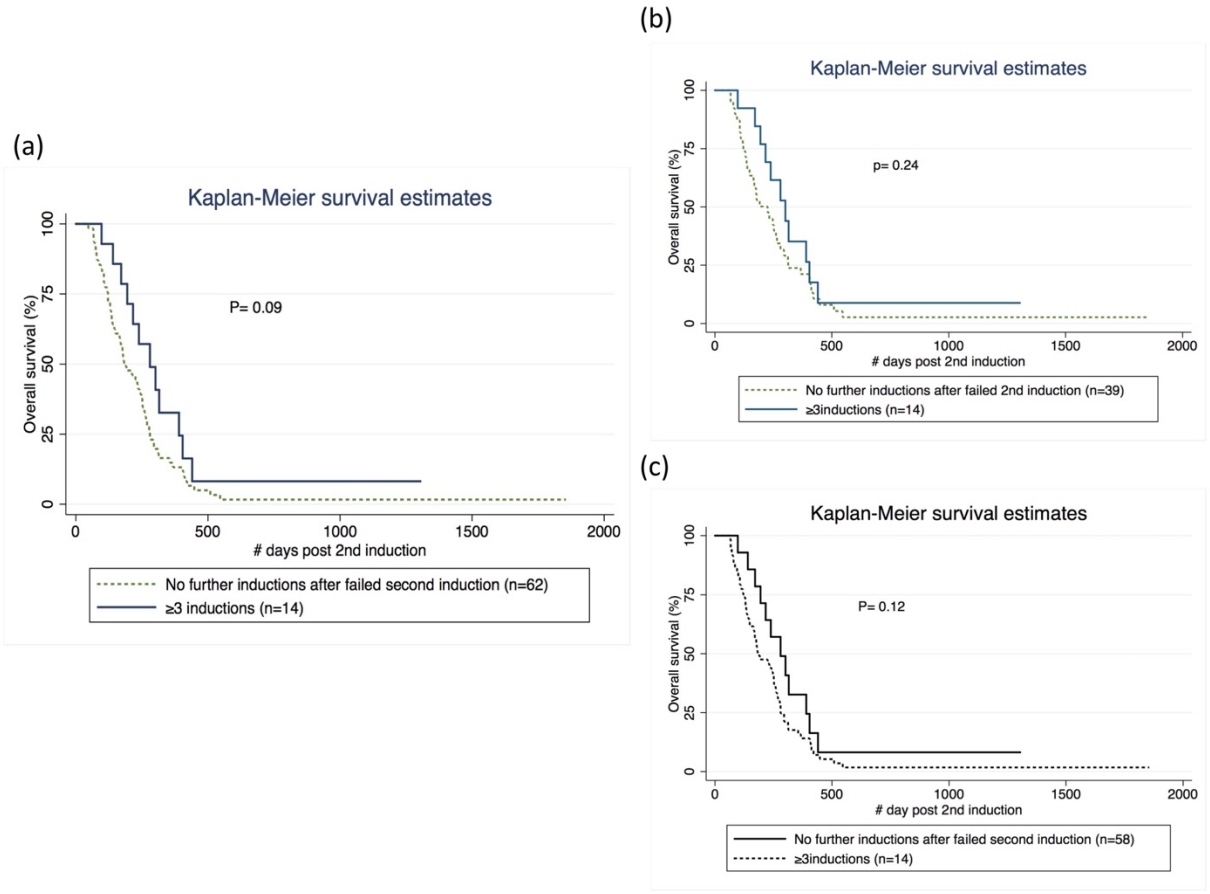

Figure 2-1. Overall survival (*calculated from the second induction*) for primary non-responders with AML based on the treatment categories.

(a) All primary non-responders. (b) Patients with de novo AML. (c) Survival analysis after excluding patients with prior CMML.
All patients in this analysis had survived the immediate post induction period and were successfully discharged from the hospital following the second induction.
Dashed line: received supportive/palliative care ± low dose chemotherapy or were enrolled in non-induction clinical trials. Solid line: received further inductions.

2.4.4 Length of hospital stay

As per institutional protocol, patients were discharged from the hospital after completion of the second induction once they were medically stable, and prior to administration of further therapies. Median length of hospital stay during the admissions for the second and third inductions were 36 (9-108) and 34.5 (6-72) days respectively ($p = 0.47$). Median cumulative length of subsequent hospital admissions to the Princess Margaret Cancer Centre following discharge after the second induction was longer for patients who received a 3rd induction compared with those who did not. (60 days [range: 27-136] vs. 9 days [range: 0-128], $p<0.0001$)). Our retrospective chart review did not capture the frequency of clinic visits or admissions to local hospitals.

2.4.5 Discussion

Our data suggests that compared with palliative options a third induction course alone does not significantly improve the overall survival of primary non-responders with AML, and might be associated with longer duration of hospital stay. Thus a 3rd induction course, if offered to unselected primary non-responding AML patients who are not eligible for curative therapies, may have a negative impact on the quality of life without providing additional clinical benefit. A third induction course, however, was associated with 21% rate of CR and therefore might be a reasonable therapeutic option for otherwise eligible primary non-responding AML patients prior to SCT.

SCT with or without preceding attempts to achieve CR with further inductions has been suggested as a curative strategy for primary non-responders with AML (Araki et al, 2016; Fung et al, 2003). However, the mortality rate related to the procedure is higher and the post-transplant relapses are more frequent for patients who are not in CR (Araki et al, 2016). In addition, based on the institutional policy, SCT might not be an available therapeutic option for primary non-responding AML patients who have not achieved CR.

In our retrospective cohort, 3 out of 14 (21%) primary non-responders with AML achieved CR following the third course of induction chemotherapy. Of these patients, only 1 patient was eligible for SCT and remains alive 4.6 years post CR. The other 2 patients were not eligible for SCT and received consolidation therapy following the third induction. The CR duration for these 2 patients were short (2.3 and 4.7 months). These findings suggest that for primary non-responders who achieve CR with a third induction, the CR duration is short if the induction therapy is not followed by SCT. This observation highlights the importance of rapid SCT in patients who achieve CR following a third induction.

In a retrospective analysis of survival outcome of patients with AML who did not achieve CR with their first line induction chemotherapy, Brandwein et al reported an overall response rate of approximately 50% with reinduction (Brandwein et al, 2008). The median relapse free survival following the second induction for patients who achieved CR but did not undergo

SCT was 9.1 months in that study. The relapse free survival was even shorter (6.8 months) for patients with high-risk cytogenetics. Higher percentage of bone marrow blast count and poor risk cytogenetics were identified as predictors of adverse response to the second induction.

A limitation of our study is our small sample size for the subgroup of patients who received a 3rd induction. While 3/11 of patients in our study achieved CR with a third induction, a larger sample size would be required to have improved confidence in this rate and to identify variables that predicted CR after a third induction. Further studies examining the molecular mutation profile and gene expression in the leukemic blasts from these patients might be helpful to understand the subset of patients who might benefit from this therapeutic strategy and the agents most likely to produce response.

In summary, our data indicate that for primary non-responders with AML rates of remission following a third course of induction chemotherapy are low and durations of remission are brief. Overall, for this group of patients, survival outcomes do not differ between those who do and do not receive a third induction. As such, in the setting of primary induction failure, third inductions should only be considered in highly selected cases and in patients with who are eligible for SCT. A reasonable approach might be to consider a third induction only in selected cases where a well-defined and rapid SCT strategy is in place.

2.5 References

Araki D, Wood BL, Othus M, Radich JP, Halpern AB, Zhou Y, et al. Allogeneic Hematopoietic Cell Transplantation for Acute Myeloid Leukemia: Time to Move Toward a Minimal Residual Disease-Based Definition of Complete Remission? J Clin Oncol. 2016;34(4):329-36.

Brandwein JM, Gupta V, Schuh AC, Schimmer AD, Yee K, Xu W, et al. Predictors of response to reinduction chemotherapy for patients with acute myeloid leukemia who do not achieve complete remission with frontline induction chemotherapy. Am J Hematol. 2008;83(1):54-8.

Cheson BD, Bennett JM, Kopecky KJ, Buchner T, Willman CL, Estey EH, et al. Revised recommendations of the International Working Group for Diagnosis, Standardization of Response Criteria, Treatment Outcomes, and Reporting Standards for Therapeutic Trials in Acute Myeloid Leukemia. J Clin Oncol. 2003;21(24):4642-9.

Dohner H, Estey EH, Amadori S, Appelbaum FR, Buchner T, Burnett AK, et al. Diagnosis and management of acute myeloid leukemia in adults: recommendations from an international expert panel, on behalf of the European LeukemiaNet. Blood. 2010;115(3):453-74.

Duval M, Klein JP, He W, Cahn JY, Cairo M, Camitta BM, et al. Hematopoietic stem-cell transplantation for acute leukemia in relapse or primary induction failure. J Clin Oncol. 2010;28(23):3730-8.

Fung HC, Stein A, Slovak M, O'Donnell M R, Snyder DS, Cohen S, et al. A long-term follow-up report on allogeneic stem cell transplantation for patients with primary refractory acute myelogenous leukemia: impact of cytogenetic characteristics on transplantation outcome. Biol Blood Marrow Transplant. 2003;9(12):766-71.

Gupta V, Tallman MS, Weisdorf DJ. Allogeneic hematopoietic cell transplantation for adults with acute myeloid leukemia: myths, controversies, and unknowns. Blood. 2011;117(8):2307-18.

Mrozek K, Marcucci G, Nicolet D, Maharry KS, Becker H, Whitman SP, et al. Prognostic significance of the European LeukemiaNet standardized system for reporting cytogenetic and molecular alterations in adults with acute myeloid leukemia. J Clin Oncol. 2012;30(36):4515-23.

Roboz GJ, Rosenblat T, Arellano M, Gobbi M, Altman JK, Montesinos P, et al. International randomized phase III study of elacytarabine versus investigator choice in patients with relapsed/refractory acute myeloid leukemia. J Clin Oncol. 2014;32(18):1919-26.

Walter RB, Othus M, Burnett AK, Lowenberg B, Kantarjian HM, Ossenkoppele GJ, et al. Resistance prediction in AML: analysis of 4601 patients from MRC/NCRI, HOVON/SAKK, SWOG and MD Anderson Cancer Center. Leukemia. 2015;29(2):312-20.

Chapter 3

3 Mitochondrial ClpP-mediated proteolysis induces selective cancer cell lethality

The work presented in this chapter has been previously published.

Jo Ishizawa [*], Sarah F. Zarabi[*], R. Eric Davis, Ondrej Halgas Takenobu Nii, Yulia Jitkova, Ran Zhao, Jonathan St-Germain, Lauren E. Heese, Grace Egan, Vivian R. Ruvolo, Samir H. Barghout, Yuki Nishida, Rose Hurren, Wencai Ma, Marcela Gronda, Todd Link, Keith Wong, Mark Mabanglo, Kensuke Kojima, Gautam Borthakur, Neil MacLean, John Man Chun Ma, Andrew B. Leber, Mark D. Minden, Walid Houry, Hagop Kantarjian, Martin Stogniew, Brian Raught, Emil F. Pai, Aaron D. Schimmer[#], Michael Andreeff[#] (* These authors contributed equally. # Co-corresponding authors)

Cancer Cell. 2019 May 13;35(5):721-737

Acknowledgements and Contributions

J.I., S.F.Z, A.D.S, and M.A. designed the study, analyzed results and wrote the manuscript: R.E.D., W.M. and J.M.C.M. analyzed RNA-seq data: O.H. and E.F.P. designed and performed crystallography, modeling, ITC and gel filtration experiments; analyzed results and wrote the manuscript: J.S.T, analyzed data and wrote the manuscript: R.Z., Y.J, L.E.H., J.S.T., V.R.R., T.N., G.E., S.H.B, Y.N., R.H., M.G., K.W., M.M., K.K., N.M., and A.B.L. performed experiments and analyzed data: T.L, G.B. and H.K. did study design, data analysis and interpretation: M.D.M. provided critical reagents and supervised research: W.H. and B.R. supervised research and wrote the manuscript. M.S. designed the ONC212 chemical structure.

We thank Ronald A. DePinho for reviewing the manuscript; Rodrigo Jacamo, Teresa McQueen and Venkata Lokesh Battula for support in establishing some of the engineered cell lines; Xiaoming Wang, Hong Mu, Huaxian Ma, Bing Carter, Qi Zhang, Lina Han, Marina Konopleva for assisting in in vivo studies; Jairo Matthews, Gheath Al-Atrash and Steven Kornblau for primary sample and data collection; and Wolfgang Oster at Oncoceutics for providing imipridones. Part of the experiments were performed at the Sequencing and Microarray Facility, High Resolution Electron Microscopy Facility, and Flow Cytometry & Cellular Imaging Facility at MD Anderson, supported by the CCSG grant NIH P30CA016672. This work was supported by Leukemia and Lymphoma Society, Canadian Institutes of Health Research, MaRS Innovation, The Ontario Institute for Cancer Research with funding provided by the Ontario Ministry of Research and Innovation, The Princess Margaret Cancer Centre Foundation, and the Ministry of Long Term Health and Planning in the Province of Ontario, the Barbara Baker Chair in Leukemia and Related Diseases (to A.D.S.); Haas Chair in Genetics, NIH Leukemia SPORE grant P50CA100632 and the University of Texas MD Anderson Cancer Center Support Grant CA016672, MDS/AML Moon Shot (to M.A.); and NIH Leukemia SPORE Career Enhancement Programs (to J.I.). We are most grateful to Shaun Labiuk, Canadian Light Source, for the collection of diffraction data. *Parts of the research described in this paper were performed using beamline 08ID-1 at the Canadian Light Source, which is supported by the Canada Foundation for Innovation, the Natural Sciences and Engineering Research Council of Canada, the University of Saskatchewan, the Government of Saskatchewan, Western Economic Diversification Canada, the National Research Council Canada, and the Canadian Institutes of Health Research.* E.F.P. thanks the Canada Research Chairs program for support.

3.1 Abstract

The mitochondrial caseinolytic protease P (ClpP) plays a central role in mitochondrial protein quality control by degrading misfolded proteins. Using genetic and chemical approaches, we showed that hyperactivation of the protease selectively kills cancer cells, independently of p53 status, by selective degradation of its respiratory chain protein substrates and disrupts mitochondrial structure and function, while it does not affect non-malignant cells. We identified first-in-class antineoplastic compounds -imipridones- as potent hyperactivators of ClpP. Through biochemical studies and crystallography, we show that imipridones bind ClpP

non-covalently and induce proteolysis by diverse structural changes. Our findings suggest a general concept of inducing cancer cell lethality through activation of mitochondrial proteolysis. Imipridones are presently in clinical trials.

Keywords

Mitochondrial ClpP, cancer, acute myeloid leukemia, lymphoma, imipridone, oxidative phosphorylation, respiratory chain complex, mitochondrial proteolysis

Significance

Activation of bacterial ClpP is cytotoxic to gram positive cocci, but the effects of mitochondrial ClpP activation on human cancers are not well understood. We demonstrate that activating ClpP could be a therapeutic strategy for human cancers with increased ClpP, irrespectively of p53 mutational status. We also identified imipridones as potent allosteric agonists of human ClpP through extensive biochemical analyses. Through co-crystallography, we defined the precise 3D conformational changes that occur upon hyperactivating ClpP with impiridones. We also determined that ClpP hyperactivation increases mitochondrial proteolysis and leads to mitochondrial dysfunction. Thus, these data support the clinical development of imipridones, and other ClpP activators for human cancers with increased ClpP expression.

3.2 Introduction

Eukaryotic cells have two separate genomes; nuclear DNA and mitochondrial DNA. Mitochondrial DNA encodes two rRNAs, 22 t-RNAs and 13 of the 90 proteins in the mitochondrial respiratory chain. The remaining mitochondrial proteins are encoded by nuclear genes, translated in the cytoplasm and imported into the mitochondria. Mitochondria possess their own protein synthesis apparatus including mitochondrial ribosomes, initiation and elongation factors. In addition, mitochondria have protein degradation complexes that regulate their protein levels by eliminating excess and/or damaged proteins. To date, at least 15 proteases have been identified in different mitochondrial compartments, including caseinolytic protease P (ClpP) that is located in the mitochondrial matrix. ClpP is an oligomeric serine protease that is similar to the cytoplasmic/nuclear proteasome (Corydon et al., 1998).

After import into the mitochondria, ClpP is assembled into a double-ringed tetradecameric structure with a hollow chamber containing proteolytic active sites. The tetradecameric structure is capped at each end by an AAA ATPase chaperone, ClpX (de Sagarra et al., 1999).

The function of the ClpXP complex in mitochondria is not fully understood, but insights have been gained from its bacterial homologue that shares structural homology. Bacteria lack a ubiquitin-dependent proteolytic system and instead eliminate intracellular proteins with a family of proteases including the bacterial ClpXP complex. In bacteria, ClpX recognizes and unfolds native substrates and feeds them into the barrel of the ClpP protease for degradation. The bacterial ClpXP complex is responsible for degrading excess proteins including those whose translation stands on ribosomes.

Recently, we demonstrated that mitochondrial ClpP is over-expressed in 45% of primary AML samples (Cole et al., 2015). ClpP is equally expressed in stem cell and bulk populations and over-expression occurs across the spectrum of cytogenetic and molecular mutations. ClpP expression is positively correlated with expression of genes related to the mitochondrial unfolded protein response (Cole et al., 2015). Functionally, ClpP maintains the integrity of oxidative phosphorylation as inhibition of the protease results in the accumulation of misfolded or degraded respiratory chain complex subunits and respiratory chain dysfunction in AML cells (Cole et al., 2015). Chemical or genetic inhibition of the protease leads to impaired oxidative phosphorylation and selectively kills AML cells and stem cells over normal hematopoietic cells in vitro and in vivo (Cole et al., 2015).

In bacteria, naturally occurring antibiotics, acyldepsipeptides (ADEPs), hyperactivate ClpP by binding the protease at its interface with ClpX and opening the pore of the ClpP protease complex(Brotz-Oesterhelt et al., 2005). When activated by ADEPs, ClpP can degrade full-length substrates without its regulatory subunit ClpX. Indeed, these ClpP activators are cytotoxic to a variety of microbial species including dormant bacteria that are responsible for resistant chronic infections (Brotz-Oesterhelt et al., 2005; Conlon et al., 2013). Thus, the activity of ClpP needs to be tightly regulated to maintain cellular homeostasis. While ClpP activators have been studied in bacteria, the effects of hyperactivating mitochondrial ClpP in malignancies have not been systematically investigated. Through a chemical screen for ClpP activators, we identified imipridones (ONC201 and ONC212) as potent ClpP activators. Using these compounds as well as constitutively active ClpP mutants, we interrogated the biological and therapeutic effects of mitochondrial ClpP hyperactivation.

3.3 Methods

3.3.1 Experimental Models and Subject Details

3.3.1.1 Mice

For all the animal studies in the present study, the study protocols were approved by the Institutional Animal Care and Use Committee (IACUC) at the Princess Margaret Cancer Centre and MD Anderson Cancer Center.

Two million Z138 cells transfected with the wild-type or D190A mutant *CLPP*-over-expressing vector and labeled with luciferase were injected to individual NSG mice (n = 7 per treatment group, all female). After confirming engraftment measured by in vivo bioluminescence imaging on d 9 post-transplantation, ONC212 (50mg/kg/d) or vehicle (water) is administered by oral gavage every other day until the mice got moribund. Tumor burden measured by luminescence was followed weekly until d 31. Independently, two million Z138 cells transfected with tetracycline-inducible Y118A mutant ClpP were labeled with luciferase and injected to individual NSG mice (n = 10 per treatment group, all male). After confirming engraftment measured by in vivo bioluminescence imaging on day 5 post-transplantation, the mice were treated with or without tetracycline (2 mg/mL) in drinking water until moribund. One million OCI-AML2 cells were injected to individual SCID mice (n = 10 per treatment group, all male). Five days after injection, mice were treated with ONC201 twice daily with ONC201 by oral gavage (100 mg/kg) for 13 days. Engraftment experiments using patient-derived xenograft AML cells were performed as previously reported (Ishizawa et al., 2016). Primary AML cells were transplanted into female 6-week-old NSG mice, and leukemia cells were harvested from secondarily transplanted mice. Leukemic cells were treated with or without 250 nM of ONC212 for 36 hr, then 0.7 million trypan blue–negative cells were injected via tail vein into each of 7 NSG mice per treatment group. The mice in each group were monitored for survival.

3.3.1.2 Bacterial Cell Culture

For the expression and purification of human mitochondrial ClpP protein *E. coli* SG1146 carrying pETSUMO2-CLPP(-MTS) were grown aerobically in Luria-Bertrani Broth (LB; 10g/L tryptone, 5g/L yeast extract, 10g/L NaCl) supplemented with 50µg/mL kanamycin at 37°C with shaking at 180rpm.

3.3.2 Method details

3.3.2.1 Protein purification and crystallization

Human ClpP was expressed and purified as described previously (Kang et al., 2004)(Kimber et al., 2010; Wong et al., 2018). Wild type and mutant (Y118A and D190A) human ClpP (without mitochondrial targeting sequences) were cloned into pETSUMO2 expression vectors and expressed in *E. coli* SG1146 (Kimber et al., 2010). To induce protein expression, bacteria, after reaching OD_{600} ~ 0.6, were treated with 1mM isopropyl-1-thio-B-D-galactopyranoside (IPTG) for 4 h at 37^{o}C, harvested by centrifugation, and disrupted in lysis buffer (25mM Tris-HCl (pH 7.5), 0.5 M NaCl, 10 mM imidazole, 10% glycerol) by Emulsiflex C5(4 passes; Avestin, Ottawa, Canada). Following cell lysis, the insoluble material was removed by centrifugation (26,892 x g (Sorvall rotor SS-34) for 30 min) and the supernatant was passed through a 5 mL Ni sepharose high-performance (GE) column pre-equilibrated with lysis buffer. The protein was eluted with 400mM imidazole, diluted with 25mL of dialysis buffer (25mM Tris-HCl (pH 7.5), 0.1 M NaCl, 10% glycerol), mixed with SUMO protease (1:100 ; Lee et al., 2008), and dialyzed overnight at 4 ^{o}C with light stirring into 4L of dialysis buffer using SnakeSkin 10K dialysis membrane (ThermoScientific, Waltham, MA). The dialyzed material was then passed through a second 5 mL Ni-column (ThermoScientific, Waltham, MA) and the flow-through solution containing untagged ClpP was collected. All collected fractions were analyzed by SDS-PAGE.

For crystallography, protein was concentrated using Amicon Ultra-15 30K concentrator (Sigma-Aldrich), and further purified using an anion exchange 5mL QSepharoseHP HiTrap (Amersham Biosciences, Little Chalfont, UK) column with a linear gradient from 100 mM to 1M NaCl in 20mM Tris-HCl (pH 7.5). Protein eluted at about 200 mM NaCl concentration.

It was then pre-concentrated using Amicon Ultra-15 30K concentrators and dialyzed at 4°C overnight into 25 mM Bis-Tris, pH 6.5, containing 3 mM DTT. ClpP was then further concentrated to a final concentration of 12 mg/mL. ONC201, solubilized in 100% DMSO, was added to the concentrated protein to bring the final concentration of the compound to 2.5 mM with a DMSO concentration of 5%.

The ClpP-ONC201 complex was crystallized at 4°C by the hanging drop vapor diffusion method. 2 µL of protein-drug solution were mixed with 2 µL of reservoir solution. Wells containing reservoir solutions of 500 µL of 5% (w/v) PEG 4,000, 100 mM KCl, and 100 mM NaAc (pH 5.2) produced crystals of 100-200 µm in all three dimensions. Crystals appeared in 2-3 weeks and were harvested into reservoir solution containing 5% (w/v) PEG 4,000, 100 mM KCl, and 100 mM NaAc (pH 5.2), 2.5 mM ONC201, and 5% DMSO; 20% glycerol was added for cryo-protection. Crystals in standard cryo-loops were flash-frozen in liquid nitrogen.

3.3.2.2 Collection and processing of diffraction data

Diffraction data were obtained at beamline 08ID-1 of the Canadian Light Source (Saskatoon, Canada) at 100 K and recorded with the help of a Pilatus3 S 6M detector (Dectris, Switzerland). The wavelength was 0.97949 Å and 2500 images were collected with a 0.1° oscillation range and 0.2 s exposures. Crystal to detector distance was 392.6 mm. Data were indexed, integrated, and scaled using the XDS (Kabsch, 2010) and CCP4 (Winn et al., 2011) software packages. The protein complex crystallized in space group C2 with one ClpP heptamer ring in the asymmetric unit (ASU), as had previously

been seen for the closed conformation of human mitochondrial ClpP (PDB-ID:1TG6)(Kang et al., 2004).

3.3.2.3 Structure solution and refinement

The crystal structure of the ClpP-ONC201 complex was solved by molecular replacement using the PHENIX software package (Adams et al., 2010; McCoy et al., 2007). The same software was applied for refinement and validation and the package COOT (Emsley and Cowtan, 2004; Emsley et al., 2010) for model building. Starting phases for structure determination were calculated using the activated ClpP heptamer structure with waters removed as the search model (PDB: 6BBA; Wong et al., 2018). Riding hydrogens were used during the last several rounds of refinement (Afonine and Adams, 2012) to optimize the geometry but were not included in the final deposited coordinate file. See **Supplemental Data 2** for data reduction and refinement statistics. PyMol v1.3 software was used to generate structure figures (DeLano, 2002). Coordinates and structure factors of the ClpP-ONC201 complex structure have been deposited into the RCSB - Protein Data Bank with Accession No. 6DL7.

3.3.2.4 Chemical screen

Assay buffer consisted of 25 mM HEPES pH 7.4, 5 mM $MgCl_2$, 5 mM KCl, 0.03% Tween 20, 10% glycerol, 16 mM creatine phosphate, 13 U/ml creatine kinase, and 3 mM ATP. 1.0 μM human ClpP (Cole et al., 2015) was dissolved in the assay buffer using Biomek FX robotic liquid handler (Beckman Coulter Life Sciences, Indianapolis, IN) and mixed with 0.625 mM and 1.25 mM-concentrations of each compounds in 384-well plates using Beckman Multimek 96/384 liquid handling system (Beckman Coulter Life Sciences, Indianapolis, IN) at 0.2 μL per well (final concentrations 4.15 and 8.3 μM, respectively) and incubated at 37C for 10 min. Fluorescent tagged- substrates, FITC-casein (4.0 μM) was then added to each well and fluorescence was measured at

485/535 nm every 5 min for 70 min at 37°C using PHERAstar microplate reader (BMG LABTECH, Ortenberg, Germany)

3.3.2.5 ClpP enzymatic assays

Assay buffer consisted of 25 mM HEPES pH 7.5, 5 mM $MgCl_2$, 5 mM KCl, 0.03% Tween 20, 10% glycerol, 16 mM creatine phosphate,13 U/ml creatine kinase, and 3 mM ATP for FITC-Casein assay, 100mM KCl, 5 % glycerol, 10mM MgCl2, 20mM Triton X-100, and 50mM TRIS pH 8 for AC-WLA-AMC assay, 50 mM Tris, pH 8 , 300 mM KCl, and 15% glycerol for Ac-Phe-hArg-Leu-ACC assay, 50 mM Hepes, pH 7.5 with 5 mM ATP, 0.03% Tween 20, 15 mM MgCl2 , 100 mM KCl and 5% Glycerol for FAPHMALVPV (Clptide) assay, and 25 mM Tris, pH 7.5 with 150 mM NaCl for MCA-Pro-Leu-Gly-Pro-D-Lys assay (Gersch et al., 2016).

For fluorescence assays, 0.7 μM (for FITC-casein, AC-WLA-AMC, and Ac-Phe-hArg-Leu-ACC assays) or 7.0 μM (for FAPHMALVPV and MCA-Pro-Leu-Gly-Pro-D-Lys assays) human ClpP was dissolved in the assay buffer, incubated at 37°C for 10 min, and mixed with increasing concentrations of ONC201, ONC201 isomer, and ONC212 (0-100 μM) in 96 well plates at 50 μL per well in triplicate. Fluorescent tagged-substrates, FITC-casein (4.5 μM) or AC-WLA-AMC (15mM) (Wong et al., 2018), Ac-Phe-hArg-Leu-ACC (100 μM), FAPHMALVPV (50 μM) and MCA-Pro-Leu-Gly-Pro-D-Lys (25 μM) were then added to each well and fluorescence was measured at 485/535 nm for FITC casein assay, at 360/440 nm for AC-WLA-AMC assay, at 380/440 nm for Ac-Phe-hArg-Leu-ACC assay, at 320/420 nm for FAPHMALVPV (Clptide) assay, and at 320/405 nm for MCA-Pro-Leu-Gly-Pro-D-Lys assay every 30 s for 90 min at 37°C using a monochromator microplate reader (Clariostar BMG LABTECH, Ortenberg, Germany). Hill coefficient was determined using Origin7, Pharmacology – Dose-response curve with log (compound concentration) as the independent variable.

For gel-based assays, 1.5 μM ClpP, alone and in combination with 4.5 μM ClpX, was mixed with 22 μM unlabeled bovine α-casein and treated with 0.2 and 6.3 μM

concentrations of ONC201 and ONC212 in FITC-casein assay buffer (See above). The mixture was incubated at 37°C for 3 h, loaded on 12% SDS-PAGE, run at 120V, and stained with Coomassie Blue.

3.3.2.6 Isothermal titration calorimetry (ITC)

ITC binding measurements were performed using the MicroCal VP-ITC system (Malvern, Malvern, UK). Aliquots of purified wild type and D190A ClpP were dialyzed separately overnight at 4°C with light stirring into 20 mM Tris.HCl, 5% DMSO, pH 7.65(at room temperature) using SnakeSkin 10K dialysis membrane (ThermoFisher, Waltham, MA). The VP-ITC cell was filled with 20 µM ClpP (WT or D190A; ClpP monomer concentration) and 100 µM ONC201 was used in the syringe. The following setup was used: Injection volume: 281.55 µL, Cell volume: 1.4551 mL, Spacing time between injections: 240 s, 27 injections: 10 µL over 20 s each; 1st 2 µL over 4 s, filter period – 2 s, steering speed – 307, temperature – 25°C, reference power – 15 µCal/s. In the reversed experiment 500µM WT ClpP in the syringe was titrated into 50µM ONC201 solution; same instrument setup was used for these experiments. Control experiments were carried out to account for dilution effects upon ligand into protein and protein into ligand titration. Data were analyzed with Origin7 MicroCal Analysis software.

3.3.2.7 Gel filtration

0.4mg of WT or D190A ClpP in 400µL (with or without ONC201 in 1:1 molar ratio – ClpP monomer to ONC201 ratio; in running buffer) was loaded onto the analytical size exclusion column Superdex 200 10/300 GL (Amersham Biosciences, Little Chalfont, UK) and run at room temperature at 0.5mL/min in the running buffer (20mM TrisHCl, 100mM NaCl, pH7.5).

3.3.2.8 Cell culture

OCI-AML2 cells were grown in Iscove's Modified Dulbecco's Medium (IMDM) with 10% FBS. OCI-AML3, HCT116, OC316 and SUM159 cells were cultured in RPMI medium with 10% FBS. TEX cells(Warner et al., 2005) were provided by Dr. John Dick (Ontario Cancer Institute, Toronto, Canada) and grown in IMDM supplemented with 15% FCS, 2 mM L-glutamine, 20 ng/ml stem cell factor (SCF), and 2 ng/ml IL-3 (R&D Systems, Minneapolis, MN). Z138 cells were cultured in RPMI with 20% FBS. T-REx HEK293 cells were grown in DMEM with 10% FBS.

ClpP -/- and ClpP / T-REx HEK293 cells were a gift from Dr. Aleksandra Trifunovic's lab (CECAD Research Center, University of Cologne, Germany). All the other cell lines were purchased from Leibniz-Institut Deutsche Sammlung von Mikroorganismen und Zellkulturen (DSMZ, Braunschweig, Germany) or the American Type Culture Collection (ATCC, Manassas, VA).100units/mL penicillin and 100ug/mL streptomycin was added to the media for all cells lines. All cells were cultured at 37ºC and 5% CO2. The authenticity of the cell lines was confirmed by DNA fingerprinting with the short tandem repeat method, using a PowerPlex 16 HS System (Promega, Madison, WI) within 6 m before the experiments.

3.3.2.9 Primary cells

Bulk AML cells from AML patients and peripheral blood stem cells from healthy G-CSF-treated stem cell donors were isolated by Ficoll density centrifugation and apheresis, respectively. Isolated cells were maintained in IMDM supplemented with 10% FBS, or Myelocult H5100 (Stemcell Technologies, Vancouver, BC) , supplemented with 100 ng/mL SCF, 10 ng/mL FLT3-L, 20 ng/mL IL-7, 10 ng/mL IL-3, 20 ng/mL IL-6, 20 ng/mL G-CSF, 20 ng/mL GM-CSF. Cells were supplemented with 100 μg/ml penicillin, and 100 U/ml streptomycin, at 37°C and 5% CO2 in humidified atmosphere. The University Health Network (Toronto, ON) and MD Anderson Cancer Center (Houston, Texas) institutional review boards approved the collection and use of

human tissue for this study. All samples were obtained from consenting patients.

3.3.2.10 Cell viability assays

For Alamar-Blue assays, cells (1 x 10^4 / well) were plated in 96-well plates (final volume of 100 µL/well), and treated with increasing concentrations of ONC201 and ONC212 (0 to 100µM). After a 72-hr period of incubation at 37ºC, 10µL of Alamar Blue was added to the culture medium and the mixture was incubated for an additional 2 h at 37ºC. Cytotoxicity was measured using spectrophotometry of fluorescence at excitation 560 nm & emission 590 nm (SpectraMax M3, Molecular Devices, San Jose, CA). For apoptosis analysis, annexin V and PI binding assays were performed to assess apoptosis as described previously(Ishizawa et al., 2016). Cells (1.5 x 10^5 / well for AML cells in 24-well plates and 0.8 x 10^5 for HCT116 cells in 12-well plates) were plated and treated with ONC201 and ONC212. Annexin V and PI were stained after 72 hr incubation. Annexin V- and PI-negative cells were counted as live cells.

3.3.2.11 Cellular thermal shift assay (CETSA)

CETSA was conducted as previously described(Jafari et al., 2014). OCI-AML2 cells were treated with increasing concentrations of ONC201 or ONC212 for 30 min at 37°C. Cells were then washed and re-suspended in PBS containing proteinase inhibitors and heated to 67°C for 3 min using a thermal cycler (SimpliAmp, Applied Biosystems). This temperature was experimentally derived by heating cells pretreated with the drug for 1 h at different temperatures to determine the optimal thermal shift of the protein. Following this step, cells were lysed by 4 freeze-thaw cycles with vortexing and pure cell lysates were collected after centrifugation at 16,000g for 30 min at 4ºC.

In wash-off experiments, ONC201 (10 µM) treated cells were washed in PBS, pelleted and re-suspended in fresh media and incubated for increasing time intervals starting from 15-75 min at 37°C. After this, cells were again washed and re-suspended in PBS

containing proteinase inhibitors, heated to 67°C for 3 min, and cell lysates were collected as described above.

3.3.2.12 RNA-sequencing

Barcoded, Illumina compatible, strand-specific total RNA libraries were prepared using the TruSeq Stranded Total RNA Sample Preparation Kit (Illumina, San Diego, CA). Briefly 1µg of DNase I treated total RNA was depleted of cytoplasmic and mitochondrial ribosomal RNA (rRNA) using Ribo-Zero Gold (Illumina). After purification, the RNA was fragmented using divalent cations and double stranded cDNA was synthesized using random primers. The ends of the resulting double stranded cDNA fragments were repaired, 5′-phosphorylated, 3'-A tailed and Illumina-specific indexed adapters were ligated. The products were purified and enriched by 11 cycles of PCR to create the final cDNA library. The libraries were quantified using the Qubit dsDNA HS Assay Kit (ThermoFisher) and assessed for size distribution using the Fragment Analyzer (Advanced Analytical, Ankeny, IA), then multiplexed 4 libraries per pool. Library pools were quantified by qPCR and sequenced, one pool per lane, on the Illumina HiSeq4000 sequencer using the 75 bp paired end format. For each sample, TopHat was used to align reads from FASTQ files to the reference genome (hg19) and generate BAM files. These were then used as input to rnaseqmut, which identifies genomic nucleotide positions at which a minimum number and proportion of reads have a variant sequence, i.e., indels or single-nucleotide variants (SNVs). There was no filtering to exclude known single-nucleotide polymorphisms (SNPs). For each SNV identified in either or both of the parental or ONC201-resistant samples of Z138 cells, rnaseqmut provided the number of reads (forward and backward) with a WT nucleotide in that position, and the number of reads with the SNV in that position, for each sample. If the total number of reads at that position exceeded a minimum number of total reads (20), Fisher's exact test was used to compare the difference in the mutant allele frequency (MAF) in parental vs. resistant cells. SNVs meeting the criteria for minimum read number and Fisher test-significant MAF difference in either direction (i.e., higher in either the drug-naïve or resistant cells) were further characterized by ANNOVAR (Wang et al., 2010) as to whether they were intergenic, intronic, in the 5' or 3' UTR, or

within exons, and if the latter, whether they were synonymous (silent), nonsynonymous (NSV), or involved the gain or loss of a stop codon. All raw data have been deposited at the Sequence Read Archive (SRA), accession ID# SUB4176298.

3.3.2.13 Site directed mutagenesis

All point mutations were induced using Phusion High Fidelity DNA polymerase or QuikChange II site directed mutagenesis kit (Agilent Technologies, Santa Clara, CA) using the manufacture's protocol (New England Biolabs, Ipswich, MA). The primers used were as follows:

Y118A*CLPP* fwd: 5' gagagcaacaagaagcccatccacatggccatcaacagccctggtggtgtggtgacc 3'

Y118A*CLPP* rev: 5'ggtcaccacaccaccagggctgttgatggccatgtggatgggcttcttgttgctctc 3'

D190A*CLPP* fwd: 5'ggccaagccacagccattgccatccagg 3'

D190A*CLPP* rev: 5' cctggatggcaatggctgtggcttggcc 3'

For *in vitro* experiments, mutant genes without mitochondrial targeting sequence (MTS) were fused in frame with N-terminal His6-SUMO-2 tags in pETSUMO2 expression vectors. For experiments involving mammalian cells lines, full length mutant genes (with MTS) were cloned into an expression vector with a C-terminal VA-tag (StrepIII-His6-TEV-TEV-3xFLAG). All mutations were confirmed by sequencing.

3.3.2.14 Immunoblot analysis

Cells were lysed at a density of 1 x 10^6 /50 µL (for AML cells) or 1 x 10^6 /100 µL (for HCT116 cells) in protein lysis buffer (0.25 M Tris-HCl, 2% sodium dodecylsulfate, 4% β-mercaptoethanol, 10% glycerol, 0.02% bromophenol blue). Protein lysates for Oxphos cocktail antibodies were incubated for 30 min at room temperature, otherwise, at 95°C for 5 min for denaturing (antibodies used are listed below). Immunoblot analysis was performed as reported previously(Ishizawa et al., 2016). Briefly, an equal amount of protein lysate was loaded onto a 10-12% SDS-PAGE gel (Bio-Rad), and quantitated using the Odyssey imaging system (LI-COR Biotechnology, Lincoln, NE). Antibodies used: total OXPHOS rodent WB antibody cocktail, anti-SDHA, anti-SDHB, anti-NDUFA12, anti-ClpP, anti-ATF4, anti-eIF2α, anti-phospho-eIF2a (S51) , anti-ClpP, anti-CQCRC2, anti-CS, anti-NDUFB8, anti-β-actin, and anti-GAPDH.

3.3.2.15 Proximity-dependent biotin labeling (BioID)

Wild-type and Y118A mutant *CLPP* sequences were PCR amplified and fused in-frame with a mutant *E. coli* biotin conjugating enzyme, BirA R118G (or BirA*), in a pcDNA5 FRT/TO plasmid under a CMV promoter positively regulated by tetracycline. For each construct, in-frame fusion was confirmed by Sanger Sequencing. The plasmids were then transfected into T-REx 293 cells using PolyJet (3ul) (SignaGen, Rockville, MD). Stable cells expressing the tetracycline-regulated, BirA*-tagged WT or constitutively active mutant ClpP proteins were selected using hygromycin B (200 µg/mL). Cell pools expressing the BirA* epitope tag alone, or BirA* fused to the unrelated mitochondrial enzyme ornithine transcarbamoylase (OTC) were used as negative controls.

At approximately 60% confluence, cells were treated with 1 µg/ml tetracycline and 50 µM biotin in addition to 0.6µM ONC201 or vehicle control for 48h. Cells were scraped in their media, pooled and washed twice in 25 ml cold PBS, pelleted by centrifugation at 1000 × g for 5 min at 4°C, and lysed in ice-cold modified RIPA buffer for 1. Pure cell lysates were then incubated with RIPA-equilibrated streptavidin-sepharose beads

(GE Healthcare, Little Chalfont, UK) in an end-over-end rotator for 2 h at 4°C. Beads were washed seven times with 1 mL of 50 mM ammonium bicarbonate (pH 8.0) and the biotinylated proteins were digested with trypsin. Two separate biological replicates (starting from the cloning phase) were generated for wild-type ClpP (treated and untreated) and each mutant. Samples containing the peptide fragments were analyzed by mass spectrometry.

3.3.2.16 Mass spectrometry analysis

High performance liquid chromatography was conducted using a 2-cm pre-column (Acclaim PepMap™ 100; 75 µm ID; 3 µm, 100 Å C18; ThermoFisher Scientific, Waltham, MA) and a 50-cm analytical column (Acclaim® PepMap RSLC, 75 µm ID; 2 µm, 100 Å C18; ThermoFisher Scientific, Waltham, MA), applying a 120-min reversed-phase gradient (225nl/min, 5-40% CH_3CN in 0.1% HCOOH) on an EASY-nLC1000 pump (ThermoFisher Scientific, Waltham, MA) in-line with a Q-Exactive HF mass spectrometer (ThermoFisher Scientific, Waltham, MA). A parent ion MS scan was performed at a resolution of 60,000 (FWHM at 200 *m/z*), followed by up to 20 MS/MS scans (15,000 FWHM resolution, minimum ion count of 1000 for activation) of the most intense MS scan ions using higher energy collision induced dissociation (HCD) fragmentation.

Dynamic exclusion was activated such that MS/MS of the same *m*/*z* (within a range of 10 ppm; exclusion list size = 500) detected twice within 5 sec was excluded from analysis for 15 sec. For protein identification, Thermo .RAW files were converted to the .mzML format using Proteowizard(Kessner et al., 2008), then searched using X!Tandem(Craig and Beavis, 2004) and Comet(Eng et al., 2013) against the Human RefSeq Version 45 database (containing 36113 entries). Search parameters specified a parent ion mass tolerance of 10 ppm, and an MS/MS fragment ion tolerance of 0.4 Da, with up to 2 missed cleavages allowed for trypsin. Variable modifications of +16@M and W, +32@M and W, +42@N-terminus, and +1@N and Q were allowed. Proteins identified with an iProphet cut-off of 0.9 (corresponding to ≤1% FDR) and at least two

unique peptides were analyzed with SAINT Express v.3.6. Control runs (18 runs from cells expressing the FlagBirA* epitope tag only) were collapsed to the two highest spectral counts for each prey, and high confidence interactors were defined as those with BFDR≤0.01. All raw mass spectrometry files have been deposited at the MassIVE archive (massive.ucsd.edu), accession ID# MSV000082381.

3.3.2.17 Network analysis

ClpP interaction data were imported into Cytoscape 3.6.0, and proteins grouped according to previously reported physical interaction and functional data.

3.3.2.18 Lentiviral infection and ClpP over-expression

A lentiviral wild-type or D190A mutant ClpP-over-expressing vector was generated by amplifying the cDNA by using primers *CLPP* cDNA fwd and *CLPP* cDNA rev (listed below) from Z138 cells and inserting it by InFusion cloning (TaKaRa Bio USA, Mountain View, CA) between the EcoR1 and BamH1 sites of pCDH-EF1a-MCS-BGH-PGK-GFP-T2A-Puro (Systems Biosciences, Palo Alto, CA) by using primers InFusion *CLPP* fwd and InFusion *CLPP* rev (listed below). We then derived *CLPP* D190A from the wild type vector using paired primers (*CLPP* mut D190A fwd and *CLPP* mut D190A rev) (listed below) with a QuikChange II site directed mutagenesis kit (Agilent Technologies, Santa Clara, CA). We followed the manufacturer's method except that used Stbl3 cells (ThermoFisher, Waltham, MA) in lieu of XL10-Gold. We identified the correct clones by Sanger sequence analysis. The sequences of all primers used to construct plasmids are listed below.

CLPP cDNA fwd 5'- ACTGAATTCGCCACCATGTGGCCCGGAATATTGGT-3'

CLPP cDNA rev 5'- ATCGGATCCTCTCAGGTGCTAGCTGGGAC-3'

InFusion *CLPP* fwd 5'-
TAGAGCTAGCGAATTGCCACCATGTGGCCCGGAATATT-3'

InFusion *CLPP* rev 5'-CGGCGGCCGCGGATCTCAGGTGCTAGCTGGGACAG-3'

CLPP mut D190A fwd 5'-GGGCCAAGCCACAGCCATTGCCATCCAGGCAG-3'

CLPP mut D190A rev 5'-CTGCCTGGATGGCAATGGCTGTGGCTTGGCCC-3'

*CLPP*1 890 rev seq: 5'-GGCTCATCCTCACCGTCCTG-3'

*CLPP*1 540 rev seq: 5'-GATGTACTGCATCGTGTCGT-3'

A tetracycline-inducible system based on two lentiviral vectors was developed as we previously described (Frolova et al., 2012). The first lentiviral vector (pCD510-rtTA) was generated by excising the reverse tetracycline-controlled transactivator (rtTA) coding sequence from pSLIK-Venus-TmiR-Luc (ATCC ID: MBA-239) with BamHI and BstBI and cloning the resulting fragment into NotI and BstBI restriction sites of pCD510-B1 (SystemBio). Thus, pCD510-rtTA expresses rtTA under the CMV promoter and Puromycin selection marker under a second promoter EF-1. To generate the second vector (pCD550A1-TRE), we replaced the original EF1 promoter by an inducible promoter composed of six tetracyclin responsive elements (TRE) followed by the minimal CMV promoter. cDNA sequence of wild-type or Y118A mutant *CLPP* was inserted under the control of a tetracycline inducible promoter (TRE) followed by the minimal CMV promoter and CopGFP, as selection marker, under the control of the EF-1 promoter. For lentiviral infections, HEK293T cells (ATCC, Manassas, VA) were co-transfected with pMD2.G and psPAX2 (kind gifts of Didier Trono, plasmids 12259 and 12260, respectively, Addgene Inc., Cambridge, MA) along with the lentiviral vectors using JetPrime transfection reagent (VWR, Radnor, PA) according to the manufacturer's protocol. The transfection medium was replaced after 6 h with fresh DMEM medium with 10% FBS and 24 h later the viral supernatants were collected and

concentrated by using Centricon Plus-70 filter units (Sigma-Aldrich). OCI-AML3, Z138 and HCT116 cells were infected overnight with viral supernatants supplemented with 8 μg/ml of Polybrene (Sigma-Aldrich). Seventy-two h after infection stably transduced cells were selected by FACS resulting in a homogeneous population of GFP-labeled cells.

3.3.2.19 Measurement of oxygen consumption rate

Oxygen consumption was measured using a Seahorse XF96 analyzer (Seahorse Bioscience, North Billerica, MA). Cells were treated with increasing concentrations of ONC201 or vehicle control (DMSO) in their growth medium for 72 h at 37°C, resuspended in XF Assay medium supplemented with 2.0 g/l glucose and 100 mM pyruvate, and seeded at 1 x 10^5 cells/well in XF96 plates. Cells were then equilibrated to the un-buffered medium for 60 min at 37 ºC in a CO_2-free incubator and transferred to the XF96 analyzer. To measure the spare reserve capacity of mitochondrial respiratory chains, cells were treated with 2 μM oligomycin and 0.25 μM carbonyl cyanide *p*-trifluoromethoxyphenylhydrazone (FCCP) in succession.

3.3.2.20 Respiratory chain complexes activity

Enzymatic activities of respiratory chain complexes were measured as previously described(Sriskanthadevan et al., 2015). NADH-dependent activity of complex I was determined using Complex I Enzyme Activity Microplate Assay Kit in whole cell lysates following oxidation of NADH to NAD^+ and simultaneous reduction of the provided dye. Complex II (succinate dehydrogenase) activity was measured in 2 ug isolated mitochondria in 20 mM sodium succinate-supplemented 100 mM HEPES, pH 7.4 containing 1 mg/mL bovine serum albumin, 20 uM rotenone, and 2mM KCN by monitoring malonate-sensitive reduction of 170 uM 2,6-dichloroindophenol when coupled to complex II-catalyzed reduction of 50 uM decylubiquinone (Skrtic et al., 2011). Complex IV activity was measured by KCN-sensitive oxidation of 2 mg/mL

ferrocytochrome *c* in 3 ug isolated mitochondria treated with 1 mg/mL dodecyl-D-maltoside in 25 mM Tris buffer, pH 7.0 supplemented with 125 mM KCl. Ferrocytochrome c was obtained by reduction of 40 mg/mL ferricytochrome c with 0.5 M L-ascorbic acid (Skrtic et al., 2011).

3.3.2.21 Mitochondrial ROS measurement

To measure reactive oxygen species level in mitochondrial, cells were treated with ONC201 (0-2.5 μM) for 72 h at 37 ºC, stained with MitoSox (Molecular Probes/Life Technologies, Eugene, OR), and incubated in the dark for 30 min at 37 ºC and 5% CO2 in humidified atmosphere. Cells were then centrifuged to remove the dye and resuspended in binding buffer containing annexin V-FITC (BioVision, Milpitas, CA). Following this step, annexin V negative cells were identified and analyzed by flow cytometry in a Canto II 96 well cytometer (Fortessa system, Becton Dickinson, San Jose, CA). Positive control samples were treated with 50 μM antimycin A (Sigma-Aldrich) at 37 ºC 5 h before staining with MitoSox.

3.3.2.22 Quantification and statistical analysis

Statistical analyses were performed using the two-tailed Student's *t* test, One-way ANOVA or Mann-Whitney test by the Prism (version 7.0; GraphPad Software) statistical software programs. The Kaplan-Meier method was used to generate survival curves, and log-rank test was used for comparison of the two groups. P values less than 0.05 were considered statistically significant (*P<0.05, **P < 0.01, ***P < 0.001, ****P < 0.0001). Unless otherwise indicated, values are expressed as the mean ± SD calculated by performing three independent experiments.

3.3.2.23 Data and software availability

The structure of the human mitochondrial ClpP in complex with ONC201 was deposited into the RCSB - Protein Data Bank (PDB) under the accession number 6DL7.

3.4 Results

3.4.1 Activation of mitochondrial ClpP induces anti-tumor effects in in vitro and in vivo

Activation of ClpP is cytotoxic to bacteria (Brotz-Oesterhelt et al., 2005; Conlon et al., 2013), so we tested the anti-cancer effects of ClpP activation by generating a constitutively active ClpP mutant by engineering a point mutation (Y118A) in human ClpP. We selected this site as it is homologous to the Y63A mutation in *S. aureus* ClpP (**Figure 3-1A**). The Y63A ClpP mutation in *S. aureus* enlarges the entrance pores of the bacterial enzyme causing hyperactivation of the protease (Ni et al., 2016). We purified recombinant Y118A ClpP and tested its enzymatic activity. Compared to wild-type (WT) ClpP, Y118A ClpP demonstrated increased cleavage of its fluorogenic protein substrate FITC-casein in a cell-free enzymatic assay (Leung et al., 2011) (**Figure 3-1B**).

To evaluate the effects of this mutation in tumor cells, OCI-AML3 and Z138 cells were transduced with tetracycline-inducible WT or mutant ClpP (Y118A) via lentiviral infection and then treated with tetracycline to induce the expression. Induction of the constitutively active ClpP mutant, but not WT ClpP, induced apoptosis in a dose-dependent manner (**Figure 3-1C**). The genetic activation of ClpP also exerted in vivo anti-tumor effects, consistent with its pro-apoptotic activity. Z138 cells with a tetracycline-inducible mutant ClpP (Y118A) were injected intravenously into NSG mice. Mice were then treated with tetracycline or vehicle. The tetracycline-treated group survived significantly longer than the untreated group (median survival: 48 vs 40 days, $p < 0.0001$) (**Figure 3-1D**).

As an alternative strategy to test the antitumor effects of ClpP activation, we next used Acyldepsipeptide 1 (ADEP1). ADEP antibiotics are known activators of bacterial ClpP that bind the protease outside of its active site at the ClpX interface and open the ClpP axial pore. We tested the effects of ADEP1 on mitochondrial ClpP and demonstrated that it activated the mitochondrial protease and promoted ClpP cleavage of FITC casein (EC_{50} 21.33 uM [95 % CI 20.12-22.61]) (**Figure 3-1E**). We then treated OCI-AML2 cells with this compound and demonstrated that it reduced the growth and viability of these cells with an IC_{50} of 50 uM [95% CI 48.4-51.6] (**Figure 3-1F**).

Thus, our data indicates that genetic or pharmacologic activation of mitochondrial ClpP could induce lethality in tumor cells in vitro and in vivo.

A

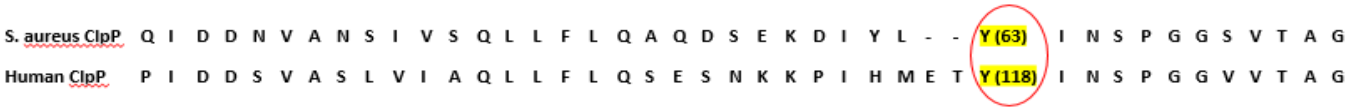
S. aureus ClpP Q I D D N V A N S I V S Q L L F L Q A Q D S E K D I Y L - - Y (63) I N S P G G S V T A G
Human ClpP P I D D S V A S L V I A Q L L F L Q S E S N K K P I H M E T Y (118) I N S P G G V V T A G

B

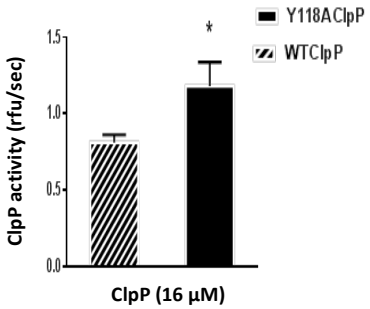
Y118AClpP
WTClpP
ClpP activity (rfu/sec)
1.5
1.0
0.5
0.0
*
ClpP (16 µM)

C

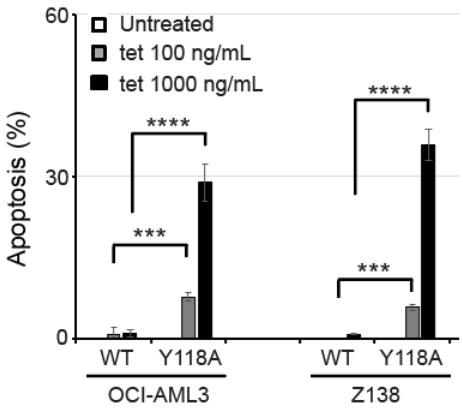
Untreated
tet 100 ng/mL
tet 1000 ng/mL
Apoptosis (%)
60
30
0
****
***
****
***
WT
Y118A
WT
Y118A
OCI-AML3
Z138

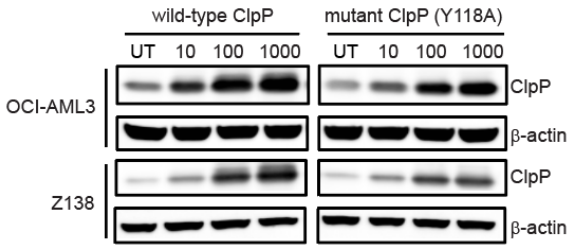
wild-type ClpP
mutant ClpP (Y118A)
UT 10 100 1000
UT 10 100 1000
OCI-AML3
ClpP
β-actin
Z138
ClpP
β-actin

D

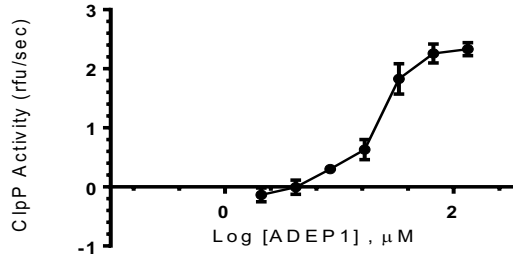
ClpP Activity (rfu/sec)
3
2
1
0
-1
0
2
Log [ADEP1], µM

E

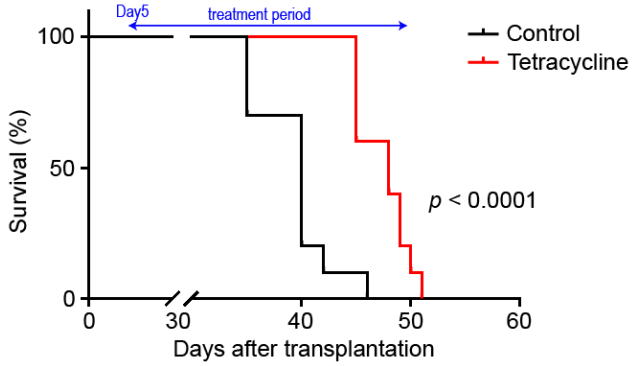
Day5
treatment period
Control
Tetracycline
Survival (%)
100
50
0
p < 0.0001
0
30
40
50
60
Days after transplantation

F

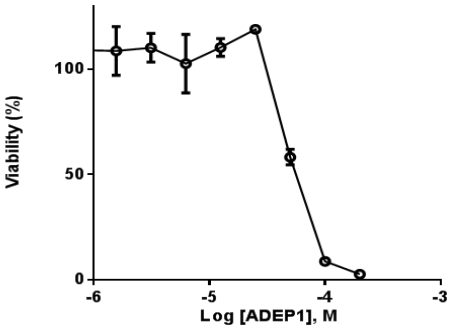

Figure 3-1. Mitochondrial ClpP activation induces anti-tumor effects in in vitro and in vivo.

(A) Sequence alignment of S. aureus and human ClpP.

(B) FITC-casein degradation kinetics of WT ClpP and Y118A ClpP mutants.

(C) Tetracycline-inducible over-expression of wild-type or constitutively active Y118A mutant ClpP in OCI-AML3 and Z138 cells. Cells were treated with tetracycline at indicated concentrations for 144 hr. Data represent percent mean ± SD apoptotic (annexin V-positive) cells (top). ***P < 0.001, ****P < 0.0001. ClpP protein levels were examined by immunoblot analysis (bottom).

(D) Survivals of xenograft mice using Z138 cells with tetracycline-inducible Y118A mutant ClpP over-expression. The mice (n = 10 each) were treated with or without tetracycline (2 mg/mL in drinking water).

(E) Effects of ADEP1 on degradation of FITC-casein by recombinant WT ClpP. Mean ± SD

(F) Effects of ADEP1 on viability of OCI-AML2 cells measured by alamar blue assay after a 72-hr period of exposure to the drug. Mean ± SD

3.4.2 The imipridones ONC201 and ONC212 potently activate mitochondrial ClpP

To find a more potent pharmacologic way to activate human ClpP, we sought to identify other small molecule ClpP activators. Accordingly, we conducted a chemical screen of an in-house library of 747 molecules focused on on-patent and off-patent drugs approved for clinical use or in clinical trial for malignant and non-malignant indications. We screened this library to identify molecules that increased ClpP-mediated cleavage of its fluorogenic protein substrate FITC-casein using a cell-free enzymatic assay (Leung et al., 2011). Under basal conditions, ClpP could not cleave full length proteins without its chaperone ClpX. However, through this screen, we found that the imipridone ONC201 activated the protease and facilitated ClpP-mediated cleavage of FITC-casein in the absence of ClpX (**Figure 3-2A**). ONC201 (**Figure 3-2B**) is a drug with the preclinical efficacy in solid tumors and hematologic malignancies in vitro and in vivo(Allen et al., 2016; Allen et al., 2013; Ishizawa et al., 2016; Kline et al., 2016; Tu et al., 2017). The drug is currently being evaluated in clinical trials in a diverse spectrum of cancers (Arrillaga-Romany et al., 2017; Kline et al., 2016; Stein et al., 2017). Its more potent derivative, ONC212 (**Figure 3-2B**), is in preclinical evaluation (Lev et al., 2017). Of note, molecular targets of impirpridones that physically bind the drugs and are functionally important for its cytotoxicity have not been identified.

We confirmed that ONC201 activated ClpP without requiring ClpX and induced cleavage of FITC-casein as well as the fluorogenic peptides, AC-WLA-AMC, Ac-Phe-hArg-Leu-ACC, and FAPHMALVPC (Clptide) with EC50's of 0.85 μM, 1.67 μM, 0.82 μM, and 3.23 μM, respectively, where the EC50 represents the concentration of the drug that drives half maximal response (**Figure 3-2C-E)**. We also tested the effects of the structurally related imipridones, ONC201 inactive isomer (its inactive analog) and ONC212, and the bacterial ClpP activator ADEP1, on ClpP activity. ONC212 increased ClpP-mediated cleavage of FITC-casein and AC-WLA-AMC, Ac-Phe-hArg-Leu-ACC, and FAPHMALVPC (Clptide) with EC50's of 0.46μM, 0.18 μM, 0.37 μM, and 3.37 μM respectively (**Figure 3-2C-E**). ADEP1 was a less potent ClpP activator compared to ONC201 and ONC212 (**Figure 3-2E**) and the inactive isomer of ONC201 did not

increase ClpP mediated cleavage of its substrates (**Figure 3-2 E,F**). FITC-casein data showed clear positive cooperativity (Gersch et al., 2015) with Hill coefficient of 1.98 ± 0.16 for ONC201 and 4.98 ± 0.47 for ONC212. Notably, the activities of imipridones were greater than the activation achieved by the Y118A mutation in ClpP (**Figure 3-1B, Figure 3-2 E**). We also tested another fluorogenic peptide, a non-ClpP substrate, MCA-Pro-Leu-Gly-Pro-D-Lys (DNP)-OH peptide, which was not cleaved after activating ClpP with imipridones or ADEP1 (**Figure 3-2 E**). Of note, pre-incubation of ClpP with ONC201 and ONC212, did not increase the ability of the compounds to activate ClpP, suggesting a reversible (non-covalent) mode of activation (**Figure 3-2G**). As the imipridones were much more potent ClpP activators compared to ADEP1 (**Figure 3-1E, Figure 3-2H**), we focused subsequent studies on these compounds.

To confirm the results of the fluorogenic assays, we tested the effects of ONC201 and ONC212 in a gel-based assay that measures the degradation of α-casein by ClpP **(Figure 3-2I)**. The addition of ONC201 and ONC212 activated ClpP and induced cleavage of α-casein without the need for ClpX.

We then showed that ONC201 directly interacted with the recombinant protease using isothermal titration calorimetry (ITC) by adding increasing amounts of ONC201 to a solution of ClpP (**Figure 3-2J**), and in another setting, titrating ClpP into a solution of ONC201 (**Figure 3-2K,L**) (Gersch et al., 2015). We also confirmed direct interaction of ONC201 with ClpP by gel filtration (**Figure 3-2M**), where we observed a clear shift towards higher molecular weight. As human mitochondrial ClpP was shown, unlike bacterial ClpPs, to exist as heptamer in the absence of ClpX (Kang et al., 2005) even at concentrations > 3mg/mL, ONC201 binding to the protease clearly shifted the equilibrium from the 7-mer to the 14-mer of ClpP.

Thus, taken together, we identified ONC201 and its analogue, ONC212, as ClpP ligands that bind and hyperactivate this mitochondrial protease.

A

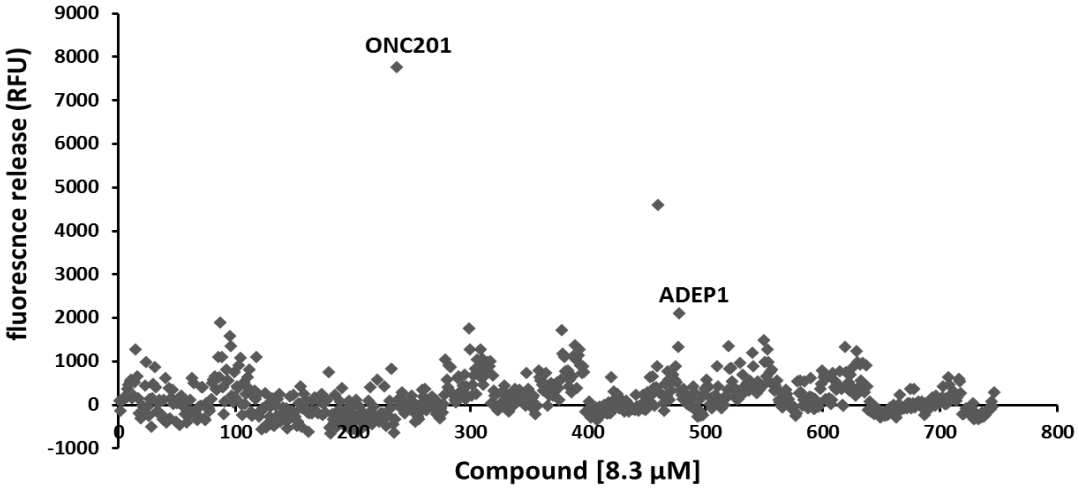
fluorescnce release (RFU)
ONC201
ADEP1
Compound [8.3 µM]

B


ONC201
ONC212

C

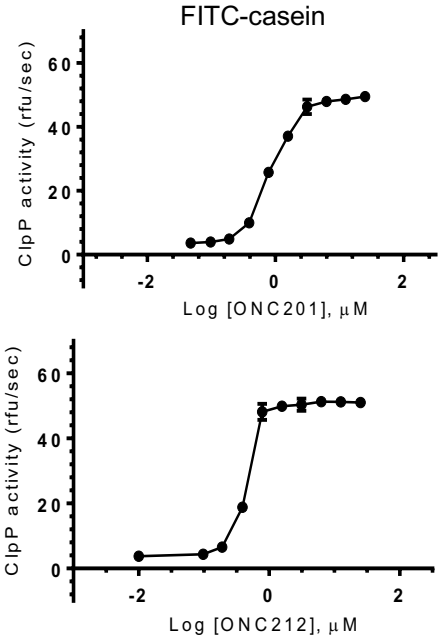
FITC-casein
ClpP activity (rfu/sec)
Log [ONC201], µM
Log [ONC212], µM

D

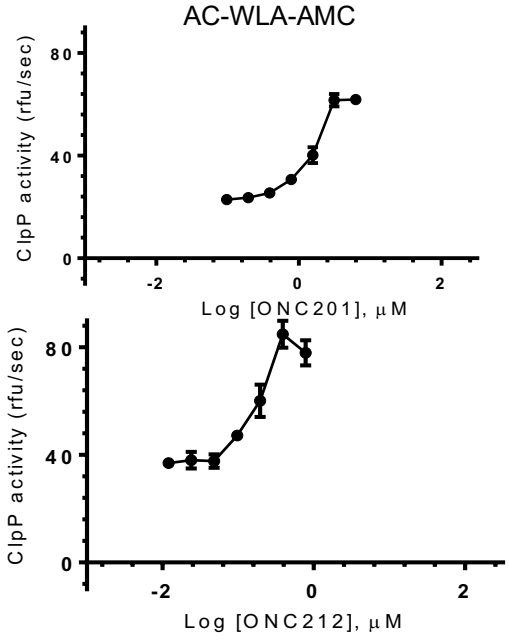
AC-WLA-AMC
ClpP activity (rfu/sec)
Log [ONC201], µM
Log [ONC212], µM

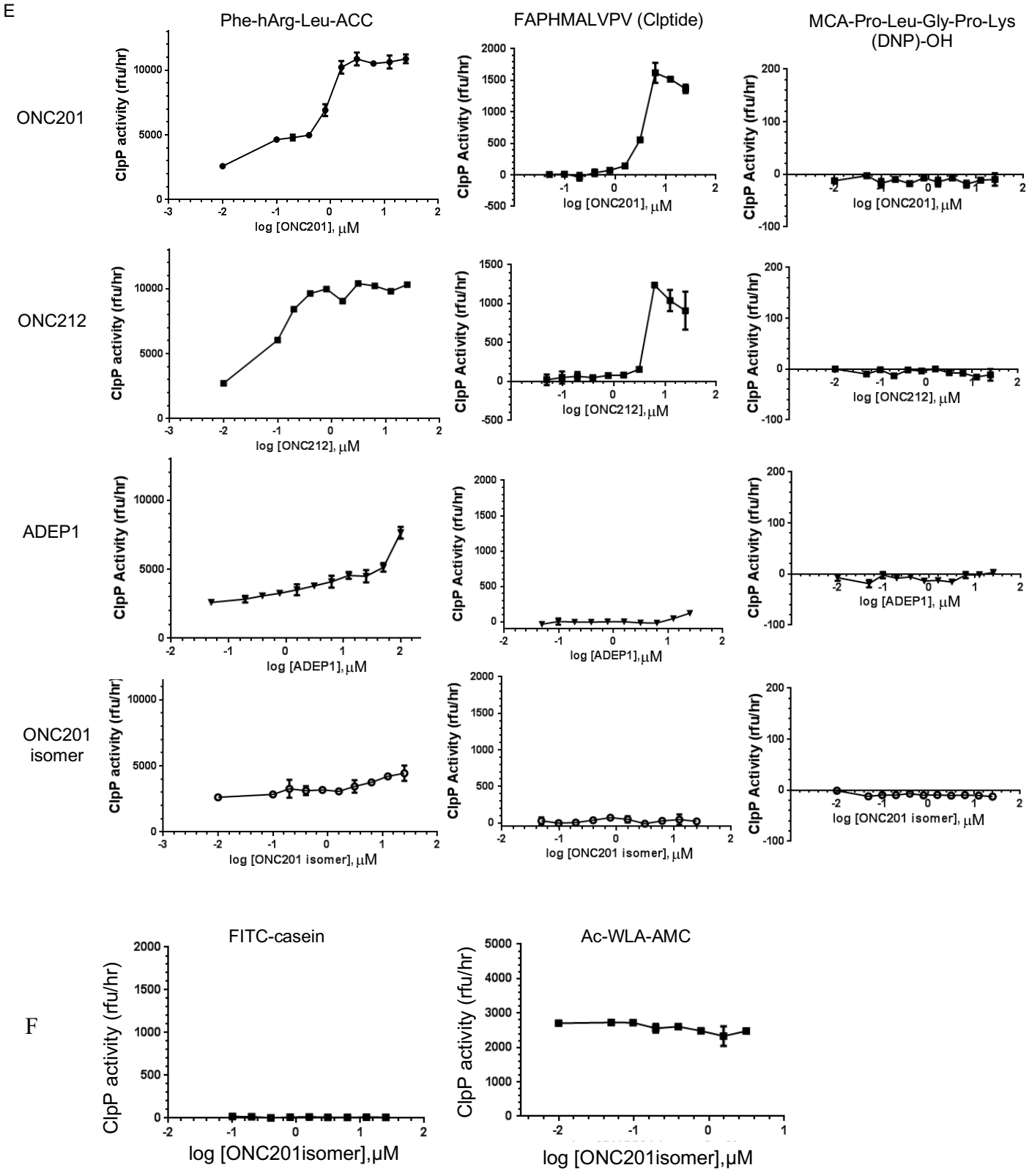
E
Phe-hArg-Leu-ACC
FAPHMALVPV (Clptide)
MCA-Pro-Leu-Gly-Pro-Lys (DNP)-OH
ONC201
ONC212
ADEP1
ONC201 isomer
ClpP activity (rfu/hr)
ClpP Activity (rfu/hr)
log [ONC201], μM
log [ONC212], μM
log [ADEP1], μM
log [ONC201 isomer], μM
F
FITC-casein
Ac-WLA-AMC
log [ONC201isomer],μM

G

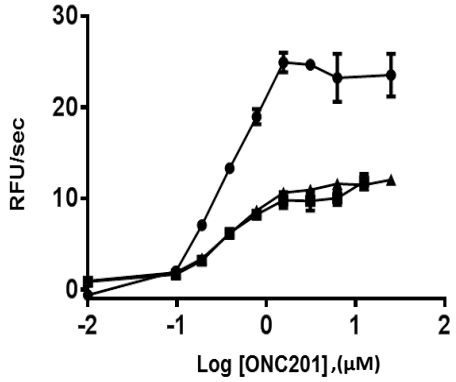
30
20
10
0
RFU/sec
-2
-1
0
1
2
Log [ONC201],(μM)

H

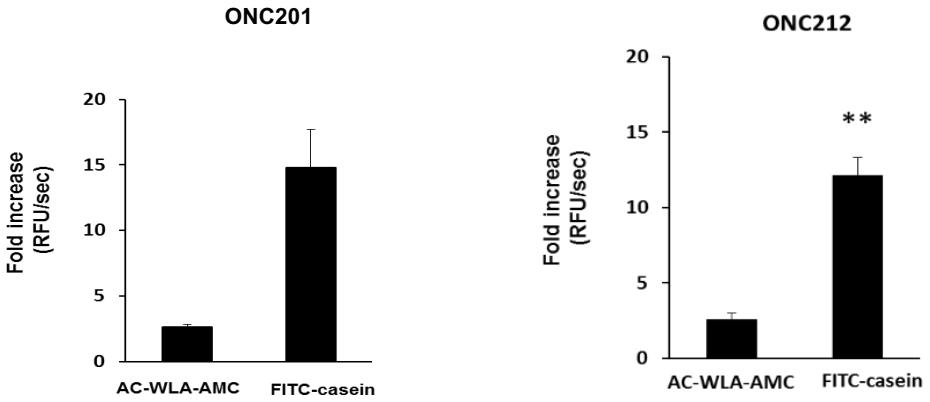
ONC201
Fold increase (RFU/sec)
20
15
10
5
0
AC-WLA-AMC
FITC-casein
ONC212
Fold increase (RFU/sec)
**
20
15
10
5
0
AC-WLA-AMC
FITC-casein

I

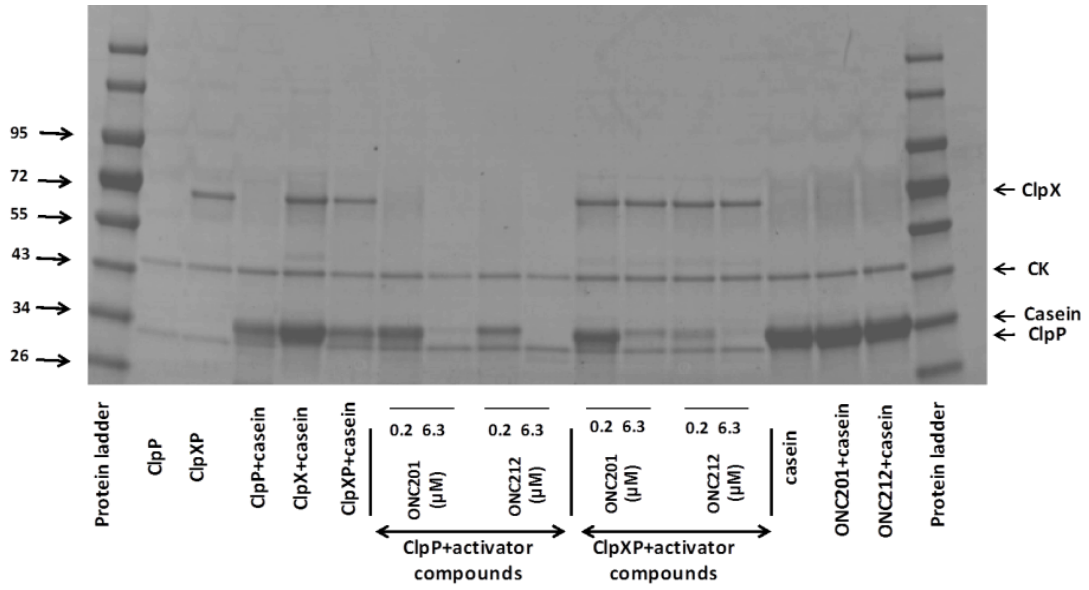
95
72
55
43
34
26
ClpX
CK
Casein
ClpP
Protein ladder
ClpP
ClpXP
ClpP+casein
ClpX+casein
ClpXP+casein
0.2 6.3
ONC201 (μM)
0.2 6.3
ONC212 (μM)
0.2 6.3
ONC201 (μM)
0.2 6.3
ONC212 (μM)
casein
ONC201+casein
ONC212+casein
Protein ladder
ClpP+activator compounds
ClpXP+activator compounds

J

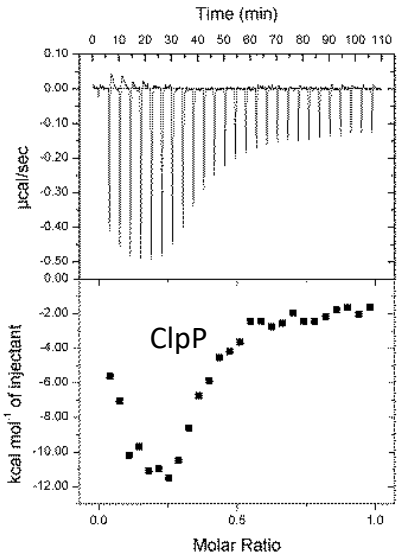
Time (min)
µcal/sec
kcal mol-1 of injectant
ClpP
Molar Ratio

K

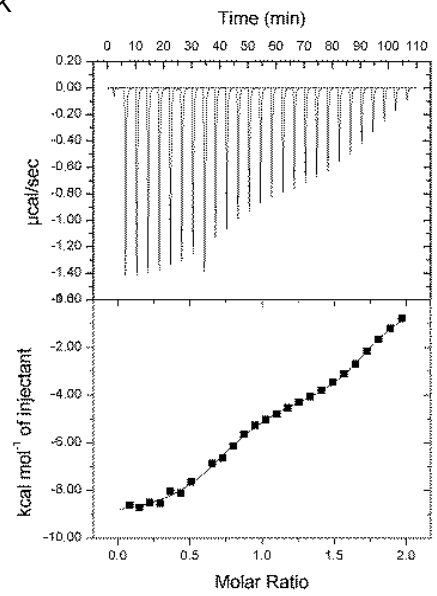
Time (min)
µcal/sec
kcal mol-1 of injectant
Molar Ratio

L

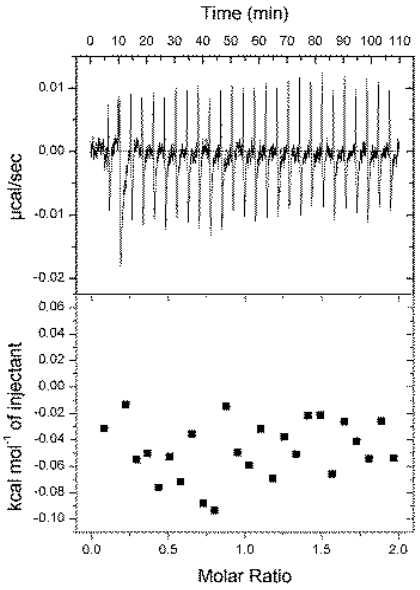
Time (min)
µcal/sec
kcal mol-1 of injectant
Molar Ratio

M

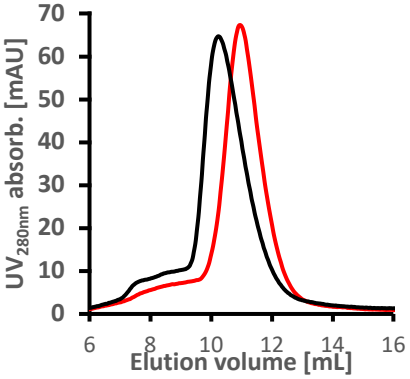
UV280nm absorb. [mAU]
Elution volume [mL]

Figure 3-2. The imipridones ONC201 and ONC212 activate mitochondrial ClpP.

(A) A chemical library of 747 molecules was screened for their effects on degradation rate of fluorogenic substrate FITC-casein by recombinant WT ClpP.
(B) Chemical structures of ONC201 and ONC212.
(C & D) Effects of ONC201 and ONC212 on degradation of fluorogenic substrates (AC-WLA-AMC (C) and FITC-casein (D) by recombinant WT ClpP. Mean ± SD.
(E) Effects of ONC201, ONC212, ADEP1 and ONC201 inactive isomer on degradation of fluorogenic substrates (Phe-hArg-Leu-ACC, Clptide, and MCA-Pro-Leu-Gly-Pro-Lys (DNP)-OH) by WT ClpP. Error bars represent mean ± SD for triplicate experiments.
(F) Effects of ONC201 inactive isomer on degradation of FITC-casein (left) and Ac-WLA-AMC (right) by recombinant WT ClpP. Mean ± SD.
(G) Effect of pre-incubation of WT ClpP with ONC201 (0-60min) on degradation rate of FITC-casein. Mean ± SD.
(H) Effects of ONC201 and ONC212 on degradation of fluorogenic substrates (AC-WLA-AMC and FITC-casein) by WT ClpP. Error bars represent mean ± SD for triplicate experiments
(I) Degradation of α-casein by purified recombinant WT ClpP and ClpXP complexes treated for 3 h with ONC201, ONC212 or vehicle control (DMSO) in FITC-casein assay buffer detected on SDS-PAGE.
(J) Isothermal calorimetry binding experiment showed nonstandard behaviour when 100μM ONC201 was titrated into 20μM ClpP (concentration of ClpP monomer).
(K) Binding of ClpP to ONC201 measured by isothermal calorimetry. 500μM WT ClpP titrated into 50μM ONC201.
(L) Control – buffer titrated into 50μM drug.

(M) Gel filtration showed shift to higher molecular weight species when ClpP was run with ONC201 (1:1). Black = 14-mer; Red = 7-mer

3.4.3 ONC201 binds ClpP non-covalently at the interface with ClpX

To identify the precise molecular interaction between ONC201 and the ClpP protein we co-crystallized human ClpP protease with the drug and determined the structure of the protein-drug complex at 2 Å resolution (PDB-ID: 6DL7).

Seven ONC201 molecules are clearly visible in the electron density map(**Figure 3-3A-D**). They occupy hydrophobic pockets between each of the seven subunits. Direct interactions between protein residues and the ONC201 activator involve extensive hydrophobic contacts and a hydrogen bond to the hydroxyl group of Tyr-118 (2.8 Å). In addition, the oxo-group of ONC201 forms water-mediated hydrogen bonds with the side chain nitrogen of Gln-107 and the carbonyl oxygen of Leu-104. The phenyl ring of the drug is positioned between Tyr-138 and Tyr-118, engaging in π-stacking interactions.

The binding of ONC201 leads to the axial entrance pore opening up, increasing its radius from 12 Å, as seen in an apparently closed conformation of human mitochondrial ClpP (Kang et al., 2004), to 17 Å (**Figure 3-3E, top**), doubling the pore size. The ClpP 14-mer assumes a more compact form and its height decreases from 93 Å to 88 Å (**Figure 3-3E, middle**). In addition to opening the entrance pore, the N-terminal residues show increased dynamics, as evidenced by the significantly higher temperature factors of this region (**Figure 3-3E, bottom**). Electron density corresponding to the first seven N-terminal residues is very weak and residues 64-73 lack any discernable density. The C-terminal residues following Pro-248 are also not visible in the electron density map. ONC201 binding induces further structural changes around the active site region at the heptamer-heptamer interface. In the human apo-ClpP structure (Kang et al., 2004), this region is well defined. In the ClpP-ONC201 complex, residues 178-193, encompassing the end of strand β6, all of strand β7 and the first third of helix α5, undergo a large conformational change and show increased dynamics with the region around residues 183-187 again not visible in electron density maps (**Figure 3-3E, bottom**). This change directly impacts the placement of the catalytic triad residues (i.e., Ser-153, His-178, and Asp-227) in the active site. The ring of His-178 separates from

Ser-153 by more than 5 Å while rotating by about 70°. Asp-227 moves in the same direction but only by 2.8 Å (**Figure 3-3D**). It is worth noting that in the ONC201 complex the catalytic aspartates from subunits that are neighbors in the tetradecameric ring, across from each other at the heptamer-heptamer interface, approach each other rather closely (4.6 Å) whereas they are separated by ca. 17 Å in the ligand-free structure. In addition, it is now Ser-181, which is the closest interacting side chain, not anymore the postulated catalytic Ser-153. The side chain hydroxyl of Ser-181 interacts closely (3.2 Å) with the carboxylate of Asp-227 in the neighboring subunit. The conformational changes induced by ONC201 binding also include the opening of channel-like pores in the central region of the "side wall" of the protease, similar to the ones described previously for the bacterial enzyme and represent potential escape routes for peptide products (Sprangers et al., 2005) (**Figure 3-3F**).

Thus, ONC201 binds ClpP non-covalently outside the active site, and activates the protease by stabilizing the ClpP 14-mer, enlarging the axial pore of the enzyme, and inducing structural changes in the residues surrounding and including the catalytic triad.

In ONC212 the 4-(2-methylbenzyl) group present in ONC201 is replaced by a 4-(4-trifluoromethylbenzyl) substituent. In the crystal structure of the ClpP-ONC201 complex, the ortho-methyl group of ONC201 points toward the bulk solvent. Its removal should only be of minor influence on its binding energy. In proteins, fluorophilic environments include peptide bonds, especially in hydrophobic surroundings, engaging in C-F···H-N, C-F···C=O and C-F···H-C_α multipolar interactions. Positively charged side chains of arginine residues also provide opportunities for binding enhancement (Müller et al., 2007).

When modeled based on the ONC201 site and subjected to two cycles of MD refinement (Adams et al., 2010), the para-trifluoromethyl substituent of ONC212 sticks into an extension of a generally apolar binding pocket of ClpP, which accepts the benzyl ring to which the CF_3-group is connected (**Figure 3-3G**). There are no strong clashes with protein residues and atomic movements observed are all distinctly smaller than 1 Å. The peptide bonds of Ile 75, Leu 79, Ala 101, and Phe 105 are in potential binding

distance. In addition, the side chains of Arg 78 and Arg 81 are both close enough to be able to swing around and interact with the CF_3-substituent. Arg 78, which forms a salt bridge with Glu 82, could easily be displaced in this interaction by Arg 81, especially as all three residues are on the protein surface and in contact with bulk solvent. We conclude that the highly electronegative trifluoromethyl substituent likely enhances ONC212's potency by providing more opportunities for multipolar bonds and an improved structural complementarity to ClpP.

A

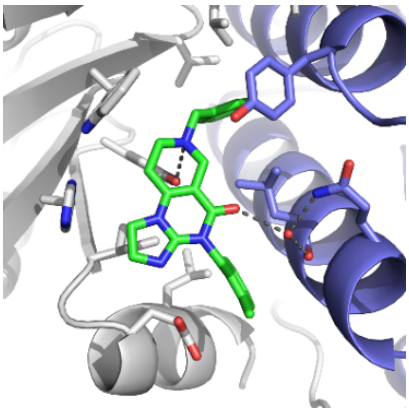

B

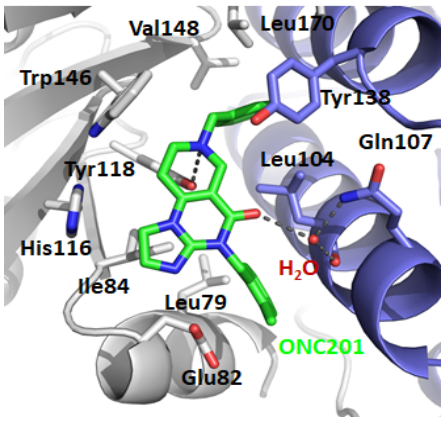
Val148
Leu170
Trp146
Tyr138
Gln107
Tyr118
Leu104
His116
H_2O
Ile84
Leu79
ONC201
Glu82

C

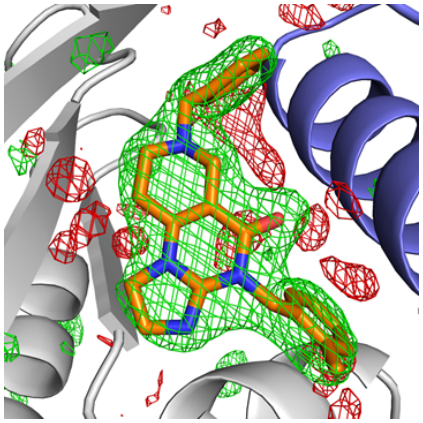

D

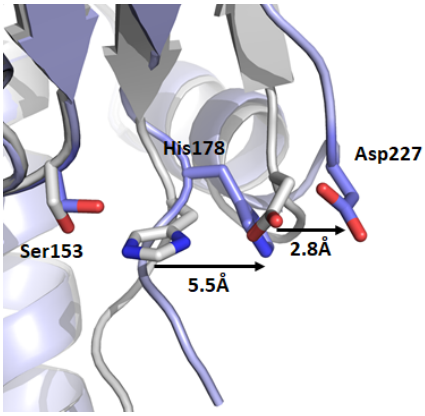
His178
Asp227
Ser153
2.8Å
5.5Å

E

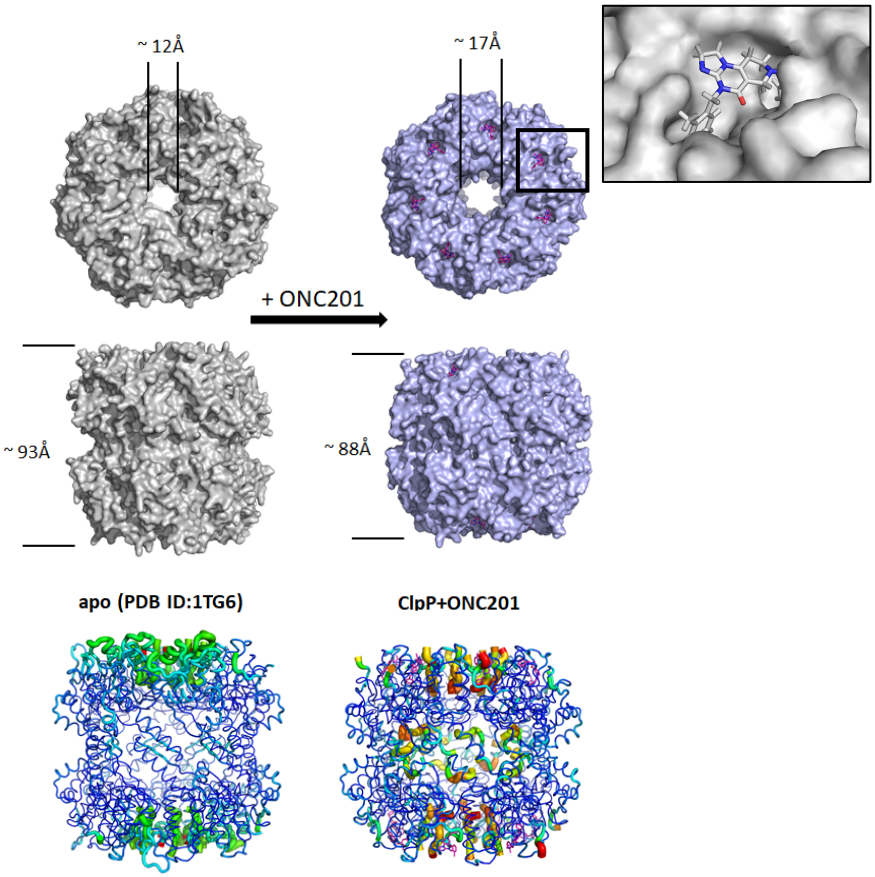
~ 12Å
~ 17Å
+ ONC201
~ 93Å
~ 88Å
apo (PDB ID:1TG6)
ClpP+ONC201

F

ONC201-ClpP

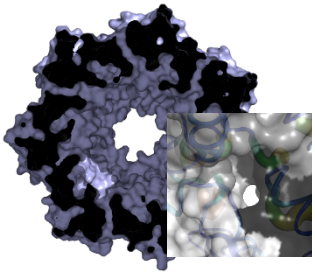

G

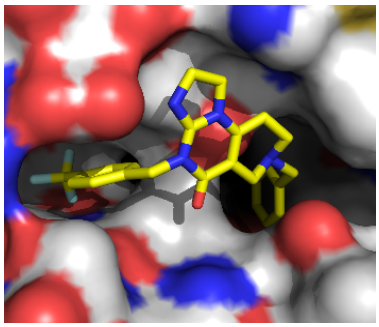

ONC212-ClpP

Figure 3-3. The imipridones bind to ClpP and are cytotoxic to leukemia and lymphoma cells.

(A) ONC201 binds in the hydrophobic pocket between two subunits (left, hydrogen bonds are indicated by dashed lines; water molecule mediating hydrogen bonding in red sphere).
(B) ONC201 binds in the hydrophobic pocket between two subunits (gray and blue, hydrogen bonds are indicated by dashed lines; water molecule mediating hydrogen bonding in red sphere).
(C) ONC201 fits well into the positive mFo-DFc difference density (green). Map calculated by omitting ONC201 molecules from the structure and contoured at 3σ (ClpP chain A – gray, chain G – violet; negative difference density in red).
(D) Catalytic triad rearranges itself upon ONC201 binding to ClpP – both His178 and Asp227 move away from Ser153 (apo - grey; ONC201 bound - violet).
(E) Binding of ONC201 (magenta) to ClpP opens up the axial pore and induces protein compaction (top and front view; apo-grey PDB ID:1TG6; with ONC201 blue). Bottom row: ONC201 binding increases dynamics of the N-termini (pore region) and the heptamer interface as evidenced by temperature factor variation (B-factors; low to high – blue to red).
(F) ONC201 binding to ClpP induces pores in the heptamer interface (cross-section through the assembled ClpP tetradecamer; position of pores indicated by black triangles). Closeup of the pore (inset) between chains C (bottom left), D (bottom right) and symmetry-related chain K (top). Protein chains are indicated by ribbon colored based on residue B-factors (blue to red – low to high; protein surface in shades of gray).
(G) Model of ONC212-binding to ClpP. ONC212 clamps into two surface depressions at the interface of two human ClpP subunits. The trifluoromethyl substituent extends deeply and fits well into the pocket that in the crystal structure of the ONC201 complex accommodates its 4-(2-methylbenzyl) group. The ligand is displayed as sticks and the surrounding protein is shown in surface representation. Color coding is: carbon in yellow (ligand) and white (protein), nitrogen in dark blue, oxygen in red, fluorine in light blue.

3.4.4 Imipridones bind ClpP in cells

Given the ability of ONC201 and ONC212 to activate ClpP in the cell-free assays above, we tested whether they could bind ClpP in cells using Cellular Thermal Shift Assay (CETSA). CETSA evaluates ligand-induced changes in melting temperature (Tm) of target proteins in cells to determine the binding affinity of ligands towards their targets (Jafari et al., 2014). Both ONC201 and ONC212 bound endogenous ClpP in OCI-AML2 at concentrations associated with activation of the protease in the enzymatic assays. (**Figure 3-4A(I&II),B**). We then tested the reversibility of binding of ONC201 to ClpP in OCI-AML2 cells by washing ONC201-treated cells in PBS and re-incubating them in fresh media prior to CETSA **(Figure 3-4A(III))**. ClpP thermal stability rapidly decreased following removal of drug from the media, consistent with non-covalent binding observed in the crystal structures.

A

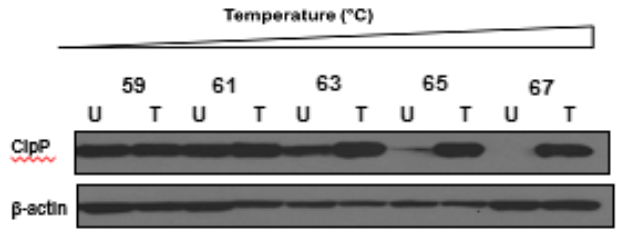
Temperature (°C)
59
61
63
65
67
U T U T U T U T U T
ClpP
β-actin

B

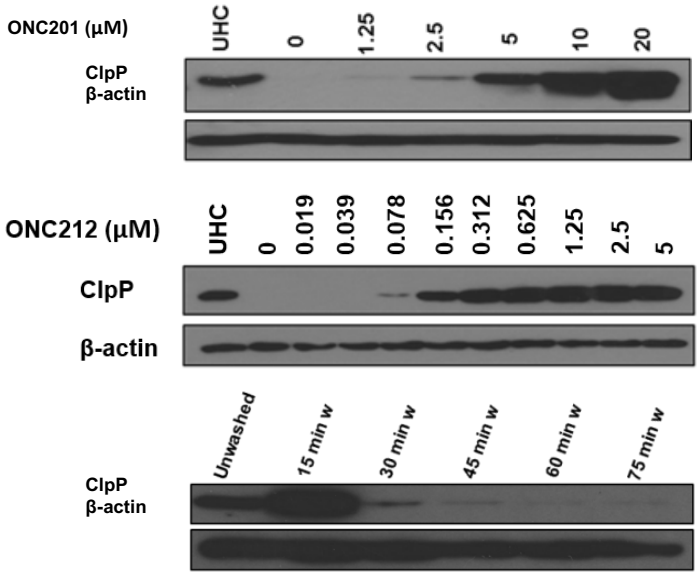
ONC201 (μM)
UHC
0
1.25
2.5
5
10
20
ClpP
β-actin
ONC212 (μM)
UHC
0
0.019
0.039
0.078
0.156
0.312
0.625
1.25
2.5
5
ClpP
β-actin
Unwashed
15 min w
30 min w
45 min w
60 min w
75 min w
ClpP
β-actin

Figure 3-4. Imipridones bind ClpP in living cells.

(A) Effect of treatment with 10 uM ONC201 on thermal stability of endogenous ClpP in OCI-AML2 cells tested by CETSA. U: untreated control; T: treated with 10 uM ONC201. Intact cells were treated with ONC201 for 30 min and heated (59-67°C) for 3min prior to collection of cell lysates for immunoblotting.

(B) Concentration-dependent effects of treatment with ONC201 (I) and ONC212 (II) on thermal stability of endogenous ClpP in OCI-AML2 cells assessed using cellular thermal shift assays (CETSA). UHC: unheated control. OCI-AML2 cells were treated with increasing concentrations of ONC201 or ONC212 for 30 min, washed and re-suspended in PBS containing proteinase inhibitors, and heated to 67°C for 3 min prior to collection of cell lysates for immunoblotting. (III) Effect of removal of ONC201 from media on thermal stability of endogenous ClpP in intact OCI-AML2 cells. ONC201 (10 μM) treated cells were washed with PBS and re-incubated in fresh medium for up to 75 min prior to CETSA. w=wash

3.4.5 ClpP activation by imipridones ONC201 and ONC212 kills malignant cells through a ClpP-dependent mechanism

We further evaluated the effects of hyperactivating ClpP on the growth and viability of leukemia and lymphoma cells. We treated OCI-AML2, OCI-AML3, TEX leukemia cells and Z138 lymphoma cells as well as HCT-116 (colon), HeLa (cervical), OC316 (ovarian) and SUM159 (breast) cells with increasing concentrations of ONC201 and ONC212. Both ONC201 and ONC212 reduced the growth and viability of the tested cells with IC50 values in the low micromolar (ONC201) or nanomolar range (ONC212) (**Figure 3-5A,B)**. We confirmed cell death and apoptosis induction by the compounds using the Annexin V/PI assay (**Figure 3-5A,C**). Reductions in growth and viability by the imipridones matched their ability to bind ClpP by CETSA and activate the enzyme in the enzymatic assays. We further assessed the effects of ClpP activation on primary AML and normal hematopoietic cells. ONC201 and ONC212 induced apoptosis in primary AML patient samples, including those with high risk cytogenetics and molecular mutations (**Figure 3-5D, Table 3-1**). Notably, we recently reported profound efficacy of ONC201 in *TP53* mutant tumors (Ishizawa et al., 2016; Kline et al., 2016), an observation of potential clinical significance.

To assess whether activation of ClpP is functionally important for cell death induced by imipridones, we treated *CLPP* / and *CLPP* $^{-/-}$ T-REx HEK293 cells with increasing concentrations of ONC201, ONC201 inactive isomer, and ONC212. ONC201 and ONC212 reduced the growth and viability of wild type cells, but *CLPP* $^{-/-}$ T-REx HEK293 cells that lack the protease were resistant to ONC201 and ONC212 **(Figure 3-5E).** ONC201 isomer did not significantly decrease the growth and viability of *CLPP* / or *CLPP* $^{-/-}$ T-REx HEK293, and ONC201-sensitive or ONC201-resistant Z138 cells (**Figure 3-5F,G**).

A

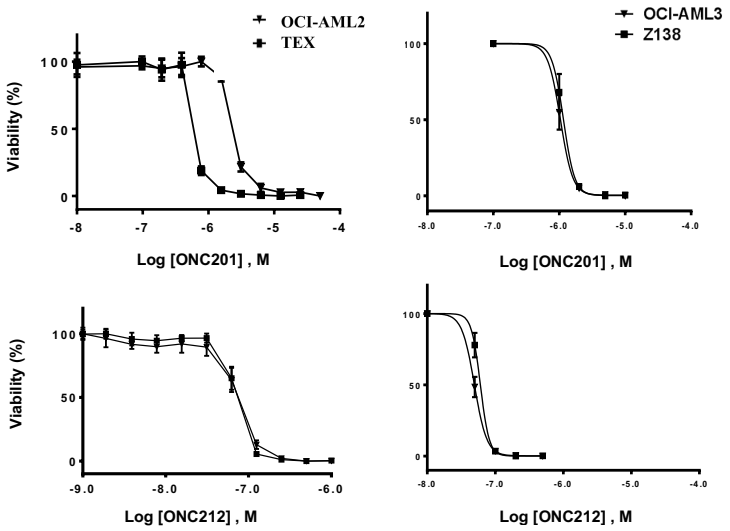
OCI-AML2
TEX
OCI-AML3
Z138
Viability (%)
Log [ONC201] , M
Log [ONC212] , M

B

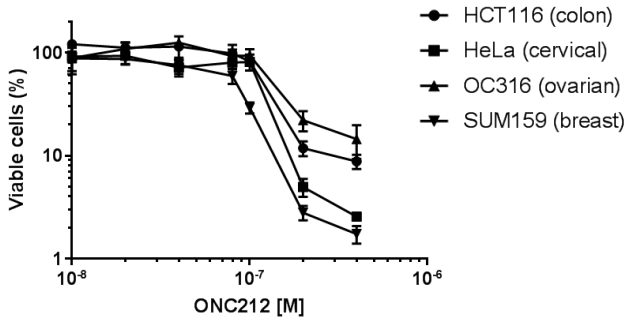
HCT116 (colon)
HeLa (cervical)
OC316 (ovarian)
SUM159 (breast)
Viable cells (%)
ONC212 [M]

C

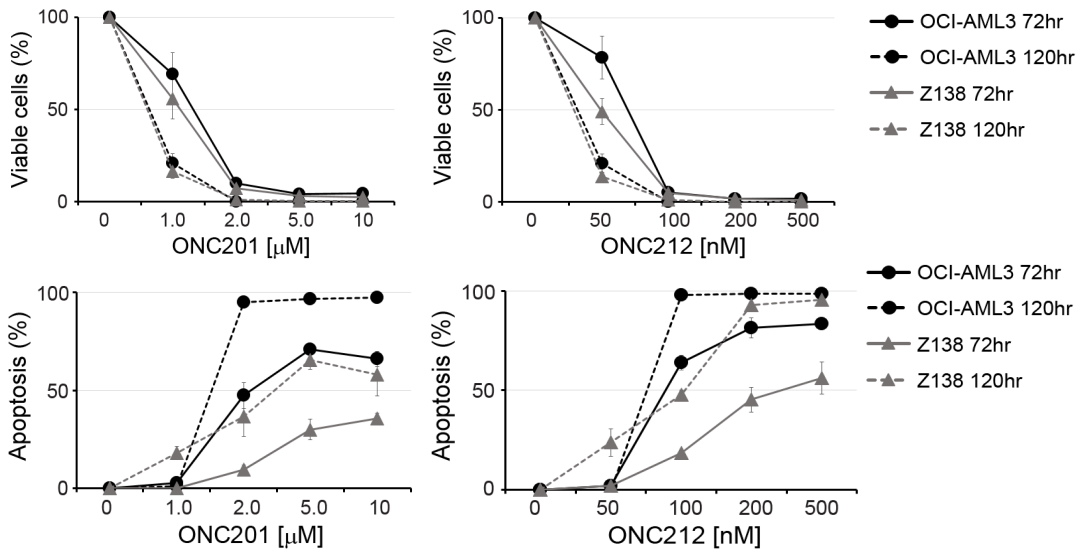
OCI-AML3 72hr
OCI-AML3 120hr
Z138 72hr
Z138 120hr
Viable cells (%)
Apoptosis (%)
ONC201 [μM]
ONC212 [nM]

D

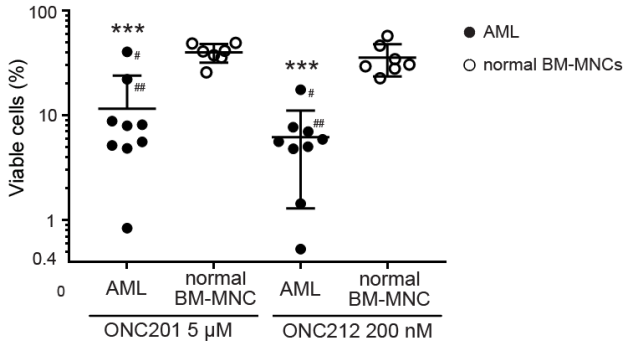
Viable cells (%)
100
10
1
0.4
0
***
#
##
AML
normal BM-MNCs
AML
normal BM-MNCs
ONC201 5 µM
ONC212 200 nM

E

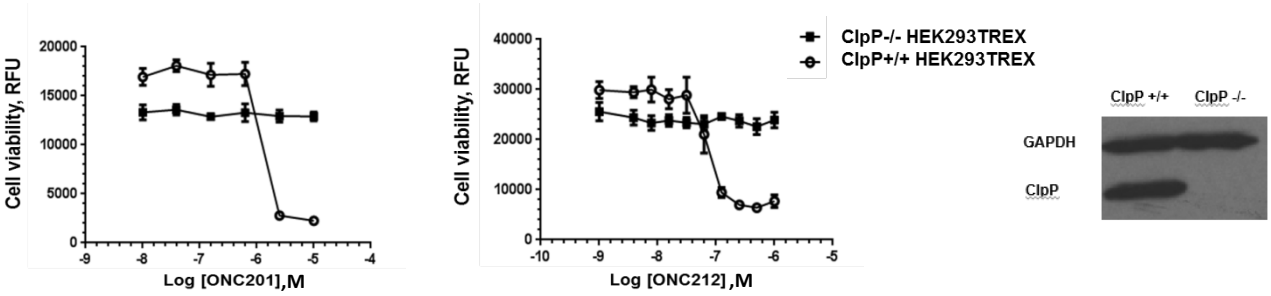
Cell viability, RFU
Log [ONC201],M
Cell viability, RFU
Log [ONC212],M
ClpP-/- HEK293TREX
ClpP+/+ HEK293TREX
ClpP +/+
ClpP -/-
GAPDH
ClpP

F

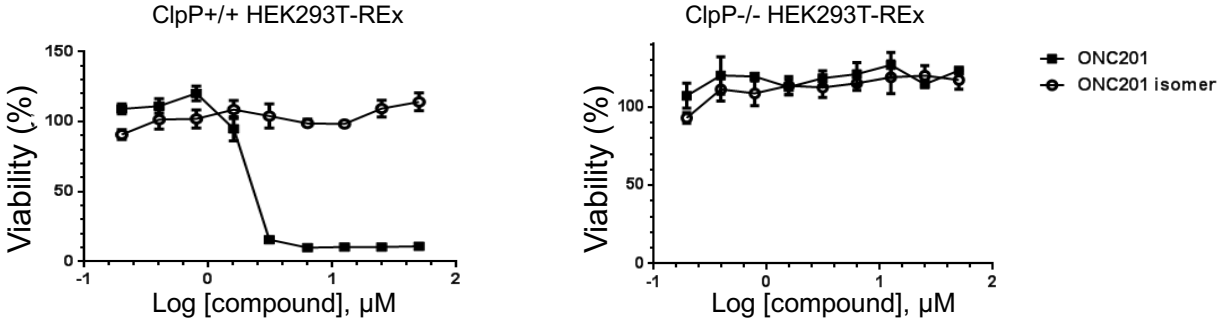
ClpP+/+ HEK293T-REx
ClpP-/- HEK293T-REx
Viability (%)
Log [compound], µM
ONC201
ONC201 isomer

G

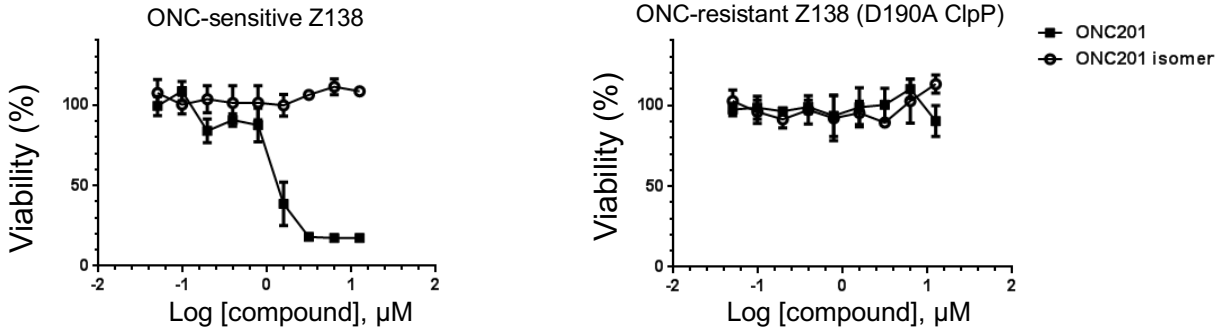
ONC-sensitive Z138
ONC-resistant Z138 (D190A ClpP)
Viability (%)
Log [compound], µM
ONC201
ONC201 isomer

Figure 3-5. Cytotoxicity of imipridones ONC201 & ONC212 is ClpP dependent.

(A) Effects of ONC201 and ONC212 on viability of OCI-AML2, TEX, OCI-AML3 and Z138 cells. Data represent percent mean ± SD viable or apoptotic cells measured by alamar blue assay in OCI-AML2, TEX cells, or by annexin V assay in OCI-AML3 and Z138 cells after a 72-hr period of exposure to the drugs.

(B) Effects of ONC212 on viability of HCT-116, HeLa, OC316 and SUM159 cells. Data Data represent percent mean ± SD viable cells measured by annexin V assay after a 72-hour period of exposure to ONC212.

(C) Apoptosis in Z138 and OCI-AML3 cells treated with ONC201 and ONC212. Cells were treated with ONC201 or ONC212 at indicated concentrations for 72 or 120 hours. Annexin V- and PI-negative cells were counted as live cells (upper panels), and Annexin V+ cells were counted as apoptotic cells (lower panels), normalized to untreated samples.

(D) Changes in live cell number by ONC201 and ONC212 compared to untreated controls in primary AML and normal bone marrow mononuclear cells (BM-MNC). Cells were treated with ONC201 and ONC212 at indicated concentrations for 72 hr. Annexin V- and DAPI-negative cells were measured by flow cytometry and normalized to that in untreated controls. #, ##: samples which were relatively resistant to ONC201 (Table 3-1).

(E) Effects of ONC201 and ONC212 on viability in ClpP / & ClpP -/- T-REx HEK293 cells. Data represent percent mean ± SD viable cells measured by alamar blue assay after a 72-hr period of exposure to the drugs.

(F & G) Effects of ONC201 & its inactive isomer on viability in ClpP +/+ or ClpP -/- T-REx HEK293 (F) and ONC201-sensitive or ONC201-resistant Z138 (G) cells. Data represent percent mean ± SD viable cells measured by alamar blue assay after a 72-hour period of exposure to the compounds.

Table 3-1. Clinical information of samples used for Figure 3-5D

Sample No.	Gender	Age	Organ	WBC ($10^3/mm^3$)	Blast (%)	Gene mutations	Cytogenetics	Disease Status
1	M	68	PB	98.7	91	FLT3-ITD, CEBPA, WT1	intermediate	Refractory
2 (#)	M	74	PB	8.9	66	ASXL1, DNMT3A, IDH2, SRSF2, TP53	High risk (complex)	Refractory
3 (##)	F	36	PB	46.5	90	DNMT3A, FLT3-ITD, NPM1, IDH2	High risk (complex)	Relapsed/Refractory
4	F	41	BM	-	77	PHF6	High risk (complex)	Relapsed/Refractory
5	F	51	PB	49.9	49	NRAS, TET	Intermediate	Relapsed/Refractory
6	M	72	PB	63.1	98	FLT3, IDH1, NPM1, PRPF40B, SRSF2	Intermediate (diploid)	Newly Diagnosed
7	F	62	BM	-	87	KRAS, NRAS	Intermediate	Newly Diagnosed
8	M	63	BM	-	77	ASXL1, CSF3R, NF1	High risk (monosomy 7)	Refractory
9	M	72	BM	-	90	IDH2, NPM1, SRSF2	intermediate (diploid)	Newly Diagnosed

3.4.6 Levels of ClpP are associated with response to ClpP activators in primary AML cells

To identify whether ClpP expression level in primary AML sample predicts their response to ClpP activators, we measured pretreatment ClpP levels in 11 primary AML samples and assessed their response to ONC201 treatment. Sensitivity to ONC201 correlated with pretreatment ClpP expression in these samples ($r = -0.82$, $p = 0.003$) (**Figure 3-6A,B and Table 3-2**). Primary AML patient samples with higher ClpP expression were significantly more sensitive to the ClpP activator compared with samples with pretreatment ClpP values that were 1 SD below average ($p = 0.0003$). Thus, ClpP activators preferentially induce cell death and apoptosis in primary AML over normal cells and ClpP expression might serve as a biomarker for patients that respond to ClpP activators, including ONC201 and ONC212.

A

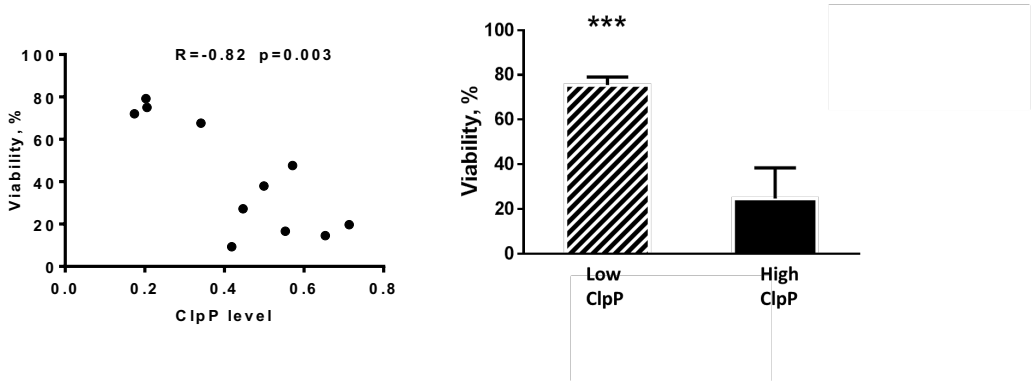
R=-0.82 p=0.003
Viability, %
ClpP level
***
Low ClpP
High ClpP

B

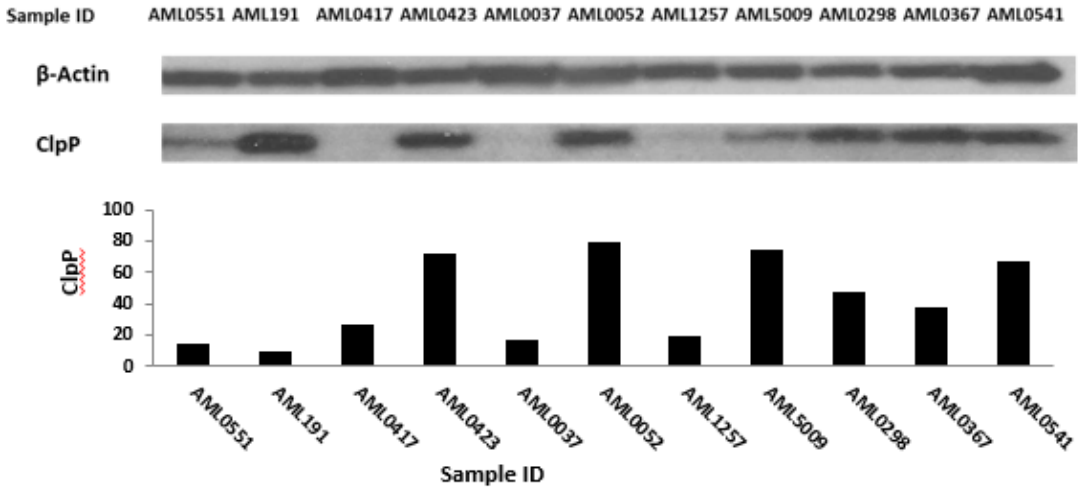
Sample ID
AML0551 AML191 AML0417 AML0423 AML0037 AML0052 AML1257 AML5009 AML0298 AML0367 AML0541
β-Actin
ClpP
ClpP
Sample ID

Figure 3-6. ClpP expression level in primary AML sample predicts their response to ClpP activators.

(A) Correlation between pretreatment expression level of ClpP and the effects of ONC201 on viability of primary AML samples measured by annexin V assay after a 72-hr period of exposure to the drug. ClpP levels were quantified by immunoblot analysis of untreated samples. Low ClpP = samples with ClpP levels that were 1SD below average. High ClpP= all other samples.

(B) Effect of ONC201 on viability of primary AML samples measured by annexin V assay after a 72 hour period of exposure. ClpP expression level in each sample was measured by immunoblot analysis of untreated samples.

Table 3-2. Clinical information of samples used for Figure 3-6 A&B

ID	Age	Gender	Source	Disease Status	WBC (x10e9/L)	PB Blasts (x10e9/L)	BM Blasts (%)	NPM1
AML0367	42	M	PB	Diagnosis	313	291.09	90	-
AML0551	32	M	PB	Diagnosis	145	101.5	85	not done
AML1257	58	M	PB	Diagnosis	189	111	70	Positive
AML0052	73	F	PB	Diagnosis/ Secondary to CMML	60.7	0	20	not done
AML0298	54	M	PB	Diagnosis	97.7	89.88	97	Positive
AML5009	73	F	PB	Diagnosis/ Secondary to MPN	31.3	15.96	48	Negative
AML0541	51	F	PB	Diagnosis	166	151.3	86	Positive
AML0037	24	F	PB	Diagnosis	43.3	12.99	not done	not done
AML191	39	M	BM	Diagnosis	168	159.6	90	not done

3.4.7 Inactivating mutations in ClpP render cells resistant to imipridones

To further evaluate the importance of ClpP for ONC201 and ONC212 mediated cell death and identify potential mechanisms of resistance to ClpP activators, we treated Z138 cells with increasing concentrations of ONC201 and selected a population of cells resistant to the drug (ONC-R Z138). ONC-R Z138 cells were also cross-resistant to ONC212 (**Figure 3-7A)**, but retained similar sensitivity to Adriamycin and Vincristine (**Figure 3-7B**).

To identify the mechanism of resistance of these cells to ONC201 and ONC212, we performed RNA sequencing (RNA-seq) and unbiased analysis identified D190A mutation in ClpP (**Figure 3-7C**) with an allele frequency of 47% in the ONC-R Z138 population of cells. To confirm the heterozygosity of the mutation, resistant clones were isolated and 7 clones were randomly selected for analysis. All 7 clones retained resistance to ONC201 and ONC212 (**Figure 3-7D, E)**, and a heterozygous mutation in *CLPP* (D190A) was detected by Sanger sequencing of genomic DNA in every clone (**Figure 3-7F)**.

To assess how the D190A mutation affects ClpP function, we generated and purified recombinant D190A ClpP and measured its enzymatic activity and response to ONC201 and ONC212. D190A ClpP had minimal proteolytic activity and could not degrade the fluorogenic peptide AC-WLA-AMC or FITC-casein under basal conditions **(Figure 3-7G)**. Moreover, ONC201 and ONC212 could not activate proteolytic activity of D190A ClpP for either peptide or protein substrates **(Figure 3-7H)**. However, ONC201 continued to bind recombinant D190A ClpP protease, as its binding site is a distance away from the mutation site, but the binding affinity was moderately reduced (**Figure 3-7I**).

To understand how the D190A mutation might affect ClpP activity and structure, we compared the crystal structures of human mitochondrial ClpP (Kang et al., 2004) and its ClpP-ONC201 complex**.** In the former, Asp-190 is located at the dimer interface and is

important as a compensating charge to an unusual stacked arginine pair that consists of Arg-226 residues from two neighboring peptide chains (**Figure 3-7J**). Asp-190 is also only 6.4 Å from Asp-227 of the catalytic triad of ClpP (**Figure 3-7K**). However, in the ClpP-ONC201 complex structure this region undergoes a major conformational change and displays high mobility with Asp-190 in close proximity to Asp-93 in most subunits. Loss of negative charge in D190A mutant can therefore have deleterious effects on the active site through impacting the mobility and sidechain interactions of the 178-193 loop.

In order to determine whether the D190A mutation was functionally important for resistance to ONC201 and ONC212, we over-expressed wild type ClpP in D190A ClpP-mutant (ONC-R Z138) cells and D190A mutant ClpP in parental (wild-type ClpP) Z138 and OCI-AML3 cells. Over-expression of wild type ClpP restored the sensitivity of the ONC-R Z138 cells to ONC201 and ONC212 (**Figure 3-7J, L**) while over-expression of D190A ClpP in parental Z138 and OCI-AML3 cells reproduced resistance to ONC201 and ONC212 (**Figure 3-7M,N**), suggesting dominant-negative inhibition of endogenous wild-type CLPP by the D190A mutant ClpP. Resistance to ONC201 was also induced in HCT116 cells by overexpression of D190A ClpP (**Figure 3-7O**). Of note, over-expression of wild-type ClpP in parental Z138 and OCI-AML3 cell lines increased sensitivity to ONC201 and ONC212 (**Figure 3-7P**). Thus, these data indicate that activation of ClpP is functionally important for cell death induced by ONC201 and ONC212 and identify a mechanism of resistance to ClpP activators.

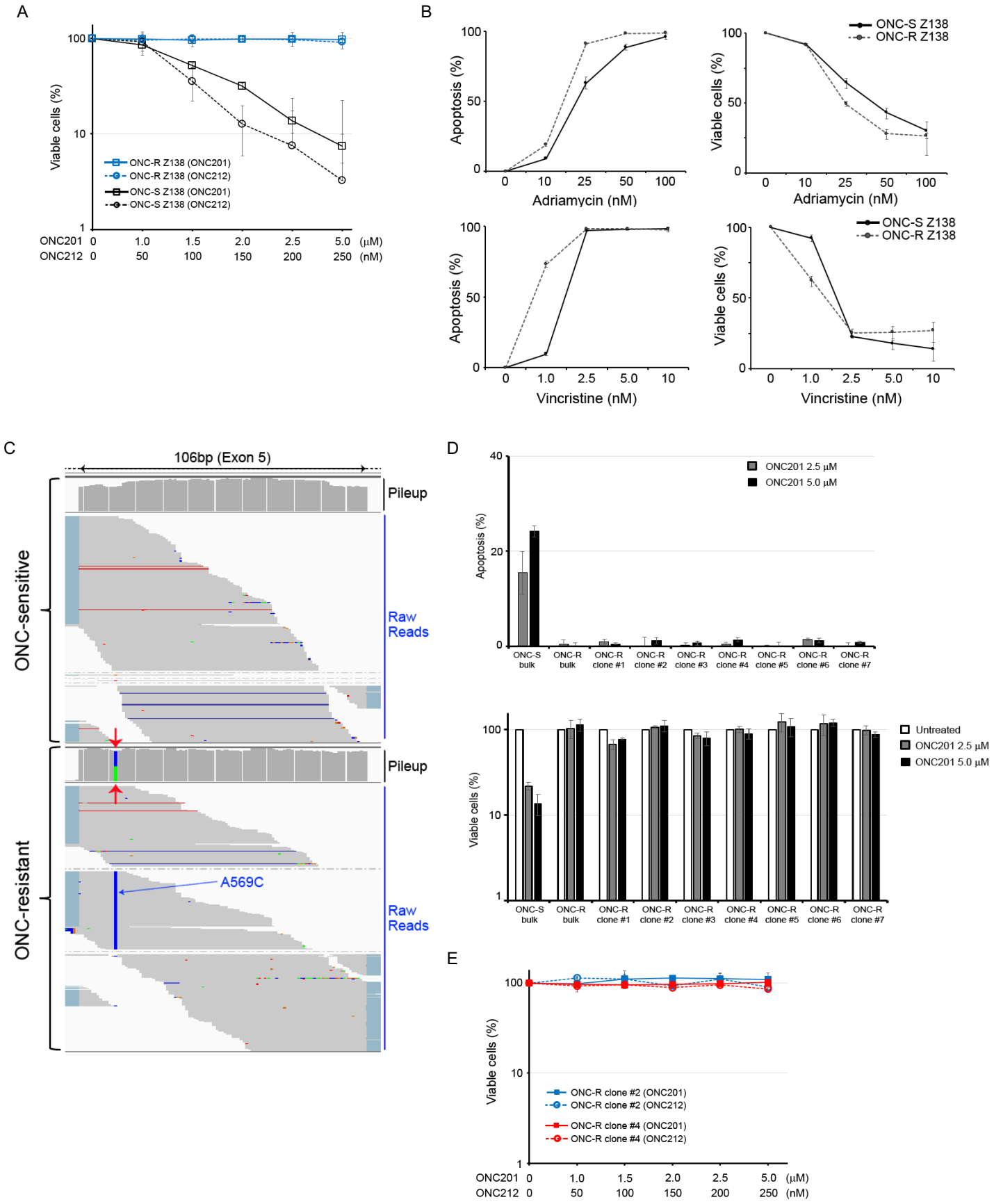
A
Viable cells (%)
ONC-R Z138 (ONC201)
ONC-R Z138 (ONC212)
ONC-S Z138 (ONC201)
ONC-S Z138 (ONC212)
ONC201 0 1.0 1.5 2.0 2.5 5.0 (μM)
ONC212 0 50 100 150 200 250 (nM)
B
Apoptosis (%)
Adriamycin (nM)
Viable cells (%)
ONC-S Z138
ONC-R Z138
Vincristine (nM)
C
106bp (Exon 5)
Pileup
Raw Reads
ONC-sensitive
ONC-resistant
A569C
D
Apoptosis (%)
ONC201 2.5 μM
ONC201 5.0 μM
ONC-S bulk
ONC-R bulk
ONC-R clone #1
ONC-R clone #2
ONC-R clone #3
ONC-R clone #4
ONC-R clone #5
ONC-R clone #6
ONC-R clone #7
Viable cells (%)
Untreated
E
ONC-R clone #2 (ONC201)
ONC-R clone #2 (ONC212)
ONC-R clone #4 (ONC201)
ONC-R clone #4 (ONC212)

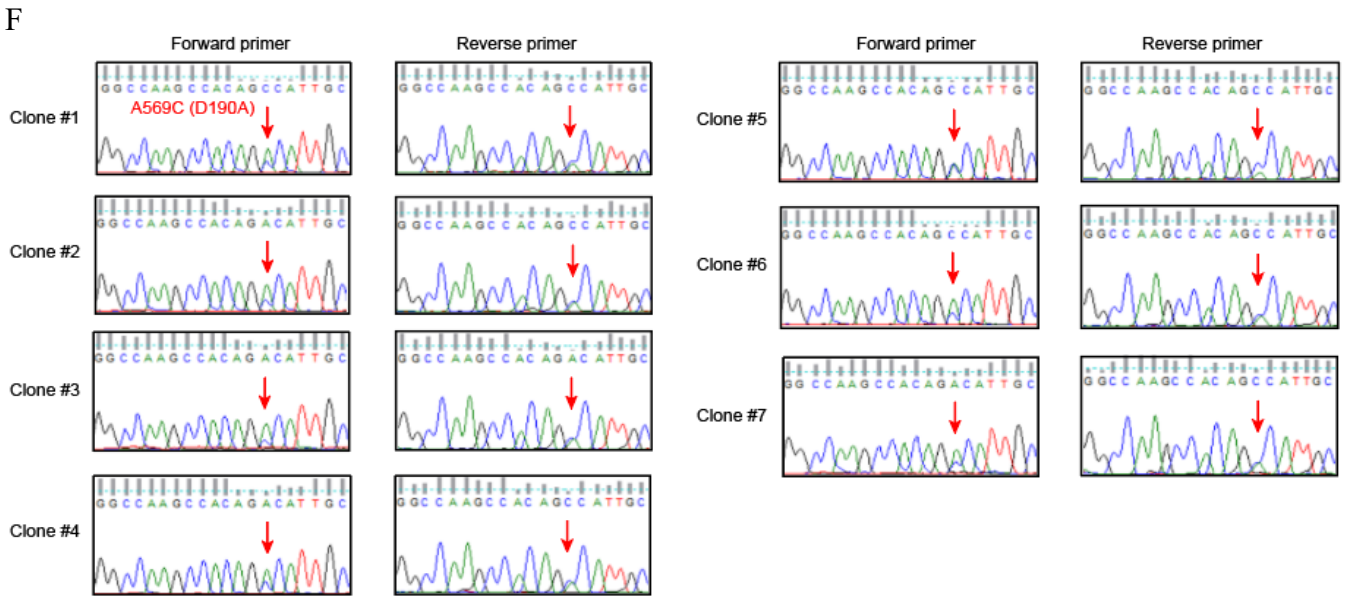
F
Forward primer
Reverse primer
Clone #1
A569C (D190A)
Clone #2
Clone #3
Clone #4
Clone #5
Clone #6
Clone #7

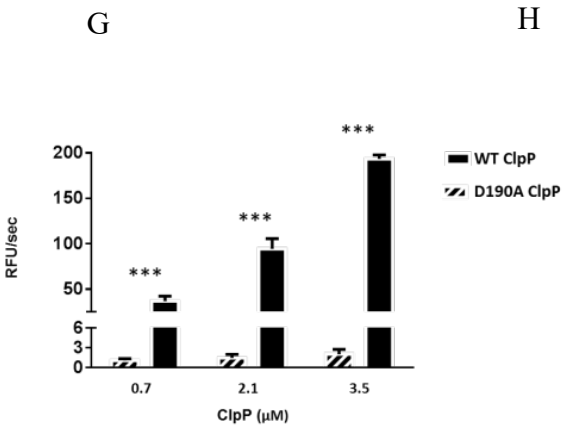
G
RFU/sec
ClpP (μM)
WT ClpP
D190A ClpP
***

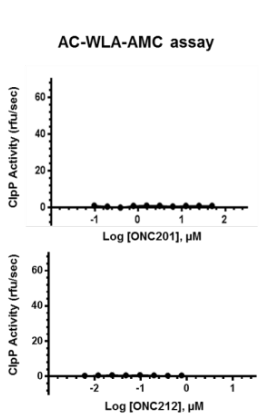
H
AC-WLA-AMC assay
ClpP Activity (rfu/sec)
Log [ONC201], μM
Log [ONC212], μM

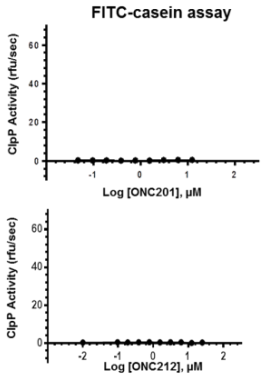
FITC-casein assay
ClpP Activity (rfu/sec)
Log [ONC201], μM
Log [ONC212], μM

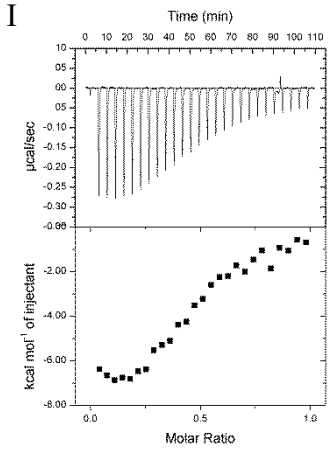
I
Time (min)
μcal/sec
kcal mol⁻¹ of injectant
Molar Ratio

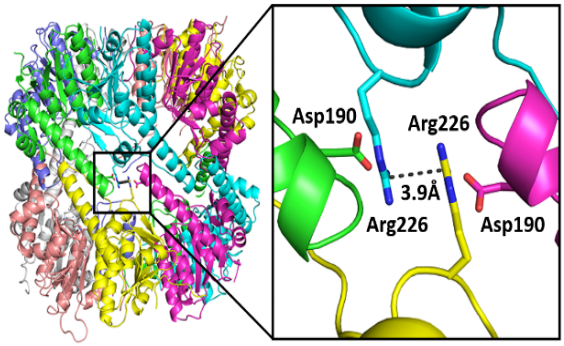
J
Asp190
Arg226
3.9Å
Arg226
Asp190

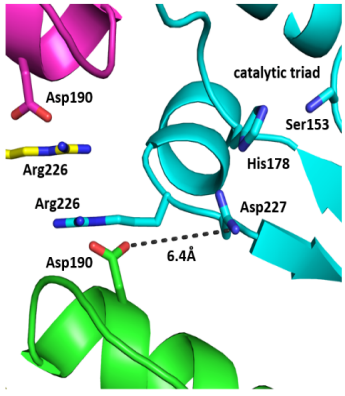
K
catalytic triad
Asp190
Ser153
Arg226
His178
Arg226
Asp227
6.4Å
Asp190

L

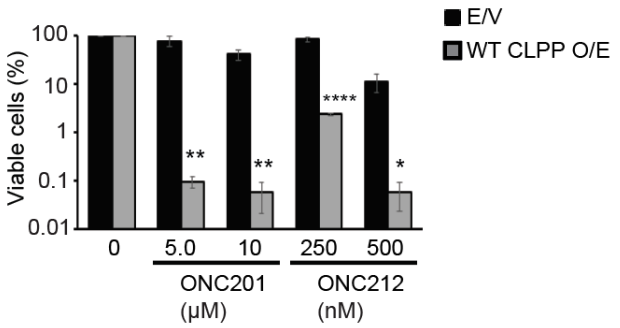
E/V
WT CLPP O/E
Viable cells (%)
100
10
1
0.1
0.01
**
**
****
*
0
5.0
10
250
500
ONC201 (μM)
ONC212 (nM)

M

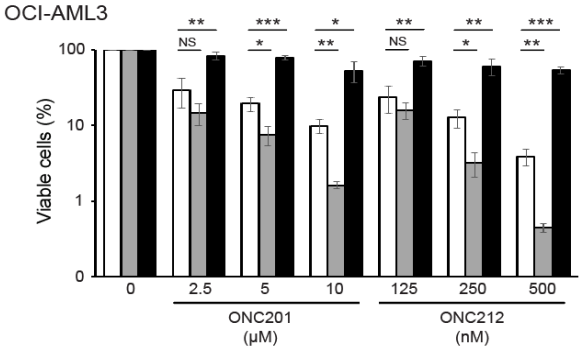
OCI-AML3
Viable cells (%)
100
10
1
0
NS
*
**
NS
*
**
0
2.5
5
10
125
250
500
ONC201 (μM)
ONC212 (nM)

N

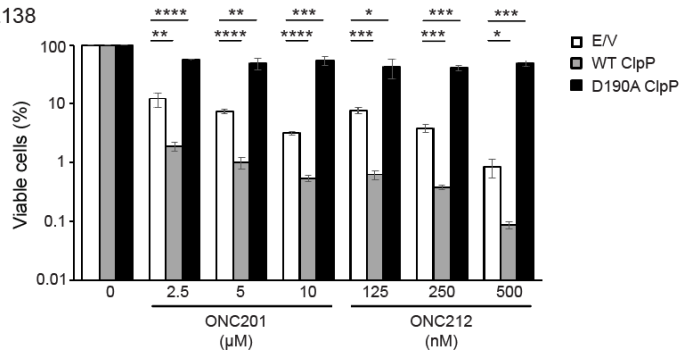
Z138
Viable cells (%)
100
10
1
0.1
0.01
E/V
WT ClpP
D190A ClpP
0
2.5
5
10
125
250
500
ONC201 (μM)
ONC212 (nM)

O

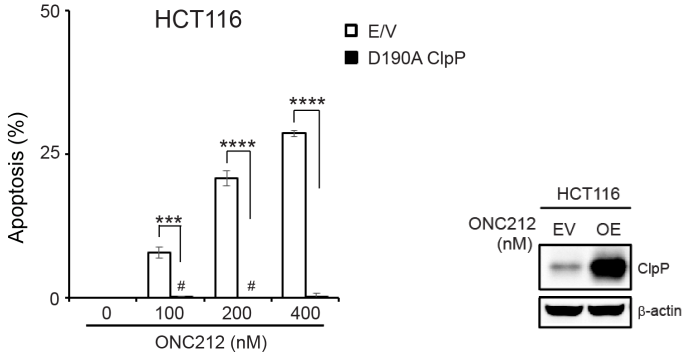
HCT116
Apoptosis (%)
50
25
0
E/V
D190A ClpP
***
****
****
#
#
0
100
200
400
ONC212 (nM)
HCT116
ONC212 (nM)
EV
OE
ClpP
β-actin

P

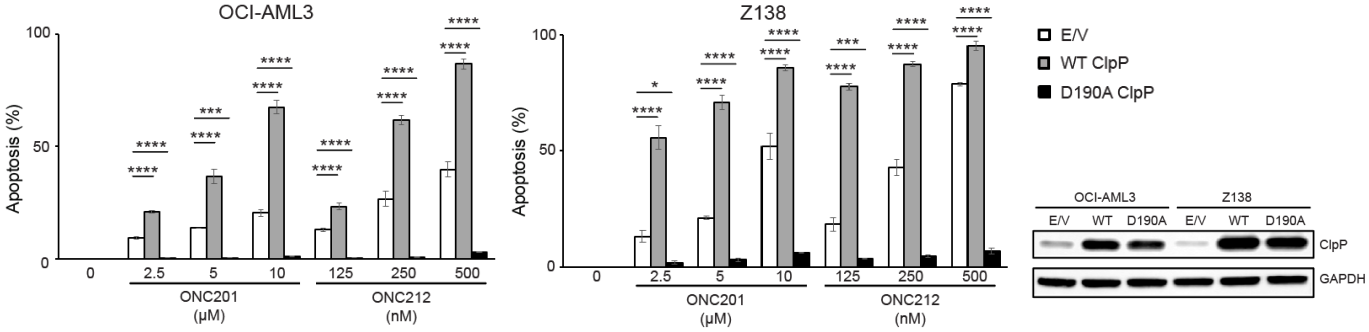
OCI-AML3
Z138
Apoptosis (%)
100
50
0
E/V
WT ClpP
D190A ClpP
0
2.5
5
10
125
250
500
ONC201 (μM)
ONC212 (nM)
OCI-AML3
Z138
E/V
WT
D190A
E/V
WT
D190A
ClpP
GAPDH

Figure 3-7. Inactivating ClpP mutation renders cells resistant to imipridones.

(A) Sensitivity of ONC201-naïve and ONC201-resistant Z138 to ONC201 and ONC212 was assessed by Annexin V assays. Data represent percent mean ± SD viable (annexin V and PI double negative) cells.

(B) Sensitivity of ONC201-resistant cells to standard chemo-agents. ONC201-resistant Z138 cells (clone #2) were treated with Adriamycin (upper panels) and Vincristine (lower panels) at indicated concentrations for 72 hours. Annexin V-positive cells (left) and Annexin V/PI double negative cells (right) were measured by flow cytometry.

(C) Result of RNA sequencing of parental (ONC-sensitive) and ONC-resistant Z138 cells. Individual reads are visualized below for each cell line, and above bar graphs indicate the number of reads ("pileup") at each nucleotide of the genomic exon sequence. Red arrows indicate the position of wild-type A569 (green) and A569C mutation (blue).

(D) Sensitivity of single cell clones of ONC201-resistant Z138 cells to ONC201. Single cell clones derived from ONC201-resistant Z138 cells were treated with ONC201 at indicated concentrations for 72 hours. Apoptotic cells (annexin V-positive) cells (upper) and live (Annexin V- and PI-double negative) cells (lower) were measured by flow cytometry.

(E) Sensitivity of single-cell clones #2 and #4 derived from ONC201-resistant Z138 cells to ONC201 and ONC212 was assessed by Annexin V assays. Data represent percent mean ± SD viable (annexin V and PI double negative) cells.

(F) Sanger sequence of genomic DNA. A D190A heterozygous mutation was detected in all the tested 7 single- cell clones.

(G) Effects of wild-type and D190A-ClpP on degradation of fluorogenic AC-WLA-AMC. Mean ± SD.
(H) Effects of ONC201 and ONC212 on degradation of fluorogenic substrates (AC-WLA-AMC) (left) and FITC-casein (right)) by D190A ClpP. Mean ± SD.
(I) ITC data for ONC201 (100μM) titrated into D190A-ClpP (20μM; concentration of ClpP monomer).
(J) The location of D190 and R226 at the interface of two heptamer rings in an apparently closed conformation of human mitochondrial ClpP.
(K) The location of D190 and Asp227 in the 3-D structure of an apparently closed conformation of human mitochondrial ClpP. D227 (Asp227) is 6.4 angstroms away from D190 and part of the catalytic triad of ClpP.

(L) Overexpression (O/E) of wild-type ClpP in ONC201-resistant (ONC-R) Z138 cells carrying D190A mutant ClpP. Cells were treated with ONC201 and ONC212 at indicated concentrations for 72 hr. Data represent percent mean ± SD apoptotic (annexin V-positive) cells. E/V; empty vector as control. Protein expression levels of ClpP was assessed by immunoblotting. **P < 0.01, ***P < 0.001, ****P < 0.0001

(M,N) Changes in live cell number by ONC201 and ONC212 on ClpP-overexpressed OCI-AML3 (M) and Z138 (N) cells. Viable cells were measured by flow cytometry. Data represent percent mean ± SD viable (annexin V and PI double negative) cells. (P) WT ClpP over-expressing ONC201-resistant Z138 cells. (Q) WT or D190A ClpP over-expressing OCI-AML3 and Z138 cells. * P < 0.05, **P < 0.01, ***P < 0.001, ****P < 0.0001.

(O) Overexpression of D190A-ClpP in HCT116 cells. Cells were treated with ONC201 and ONC212 at indicated concentrations for 72 hours. Data represent percent mean ± SD apoptotic (annexin V-positive) cells. Protein expression levels of ClpP were assessed by immunoblotting. EV; empty vector, OE; overexpression. #; invisible bars because of low numerical values. ***P < 0.001, ****P < 0.0001.

(P) Overexpression of wild-type or D190A-ClpP in parental (ONC201-sensitive) Z138 and OCI-AML3 cells. Cells were treated with ONC201 and ONC212 at indicated concentrations

for 72 hr. Data represent percent mean ± SD apoptotic (annexin V-positive) cells. Protein expression levels of ClpP were assessed by immunoblotting. **P < 0.01, ***P < 0.001, ****P < 0.0001.

3.4.8 ClpP activation leads to reduction in respiratory chain complex subunits and impaired oxidative phosphorylation

We next used BioID(Roux et al., 2012) to identify interacting partners of ClpP after chemical or genetic activation. To chemically hyperactivate the protease, T-REx HEK293 cells expressing FlagBirA-ClpP(WT) were treated with 0.6 μM ONC201 for 48 hour. As a genetic approach, we expressed FlagBirA-ClpP (Y118A). We compared the interactome of activated ClpP to non-stimulated WT ClpP. Proteins that interacted with unstimulated WT ClpP in the BioID assay, but whose spectral counts decreased when ClpP was activated were postulated to represent potential substrates of hyperactivated ClpP.

Over 200 mitochondrial proteins were identified as high confidence ClpP interacting partners. Of these polypeptides 90 displayed a ≥ 4-fold decrease in spectral counts ($p \leq 0.001$) following ONC201 treatment. Amongst the proteins displaying the most robust decrease were components of the electron transport chain (and in particular, subunits of respiratory chain complex I) and polypeptides involved in mitochondrial translation **(Figure 3-8A &Table 3-3)**. Expression of the constitutively active Y118A ClpP mutant yielded a depletion of an overlapping set of interacting partners, but the degree of reduction in peptide counts was smaller than that observed in response to ONC201, likely reflecting the weaker activation of the protease by the mutation (**Table 3-3)**.

Previously, we and others identified respiratory chain subunits SDHA and SDHB as putative ClpP substrates and inhibition of ClpP led to the accumulation of degraded or misfolded subunits (Cole et al., 2015). To investigate the effects of ClpP activation on the levels of protein identified as interacting partners in our BioID assay, we treated Z138 with increasing concentrations of ONC201. Treatment with ONC201 decreased levels of respiratory chain complex proteins such as SDHA and SDHB and reductions in respiratory chain I subunits were most pronounced (**Figure 3-8B**). In contrast, levels of these proteins did not significantly change after treating resistant Z138 carrying D190A mutant ClpP with ONC201 (**Figure 3-8B**). Over-expressing wild type ClpP in these cells restored sensitivity to ONC201 with depletion of respiratory chain complex

proteins (**Figure 3-8B**). Finally, over-expressing D190A ClpP mutant protein in wild type Z138 cells rendered them resistant to ONC201 with no significant reductions in respiratory chain proteins (**Figure 3-8C**). ONC212 also reduced the level of the identified ClpP interactors in a dose dependent manner (**Figure 3-8F,G**). The reduction in NDUFA12 and SDHB by ONC212 was also observed in HCT116, HeLa, OC316 and SUM159 cells (**Figure 3-8H**). The reduction of NDUFA12 and SDHB in HCT116 cells was blocked by overexpression of the inactivating mutant D190A ClpP (**Figure 3-8I**), as observed in Z138 cells (**Figure 3-8C**). While we observed reductions in respiratory chain proteins, levels of mRNA encoding mitochondrial respiratory chain substrates were either unchanged or increased (**Figure 3-8J**). Furthermore, the addition of recombinant ClpP and ONC201 to lysates of mitochondria isolated from ClpP -/- HEK293T-REx and OCI-AML2 cells decreased levels of the complex I subunit NDUFB8 and complex III subunit UQCRC2, indicating that ClpP activation can increase the degradation of selective ClpP substrates, independent of cytoplasmic or nuclear pathways (**Figure 7-8K**).

Likewise, we examined the effects of induction of the Y118A ClpP activating mutant on respiratory chain subunits in Z138 cells. Similar to the results with the chemical ClpP activators, induction of the Y118A ClpP mutant led to reductions in SDHA, SDHB and NDUFA12 in a dose-dependent manner (**Figure 3-8D**). In contrast, another respiratory complex subunit, ATP5A, was not reduced by Y118A ClpP overexpression, ONC201 or ONC212 (**Figure 3-8D,F**), reflecting selective degradation of particular subunits by ClpP activation.

We also tested the effects of ONC201 and ONC212 on levels of respiratory chain proteins in primary AML cells. Similar to the effects on cell lines, we observed a reduction in respiratory chain proteins in primary cells treated with the imipridones (**Figure 3-8E**). Interestingly, similar reductions in respiratory chain proteins were also observed in normal hematopoietic cells (**Figure 3-8E**). Thus, greater sensitivity of AML cells to ClpP activation likely reflects their increased reliance on oxidative phosphorylation and lower spare reserve capacity in their respiratory chain (Sriskanthadevan et al., 2015).

Next, we investigated the effects of ClpP activation on oxidative phosphorylation and mitochondrial function. Z138 cells carrying WT and D190A ClpP were treated with increasing concentrations of ONC201. Treatment with ONC201 decreased basal OCR and spare reserve capacity in Z138 cells with WT ClpP, while no change was observed in Z138 cells with D190A ClpP (**Figure 3-8M)**. Likewise, ClpP activation decreased the enzymatic activity of respiratory chain complexes I, II, and IV, with complex I being the most sensitive (**Figure 3-8N).** Finally, ClpP activation increased the production of mitochondrial ROS in Z138 cells with WT ClpP, but no change was seen in Z138 cells with D190A ClpP (**Figure 3-8O)**. Consistently, mitochondria were morphologically damaged by ONC201 treatment, as assessed by electron microscopy, demonstrating particular damages of matrix and cristae structures (**Figure 3-8P**).

We previously published that ONC201 induces atypical integrated stress response (ISR) where ATF4 protein increase is induced irrespectively of phosphorylation status of eIF2α, unlike classical ISRs(Ishizawa et al., 2016). Indeed, overexpression of Y118A ClpP in Z138 cells showed increase in ATF4 protein without increasing phosphorylation of eIF2α (**Figure 3-8Q**).

A

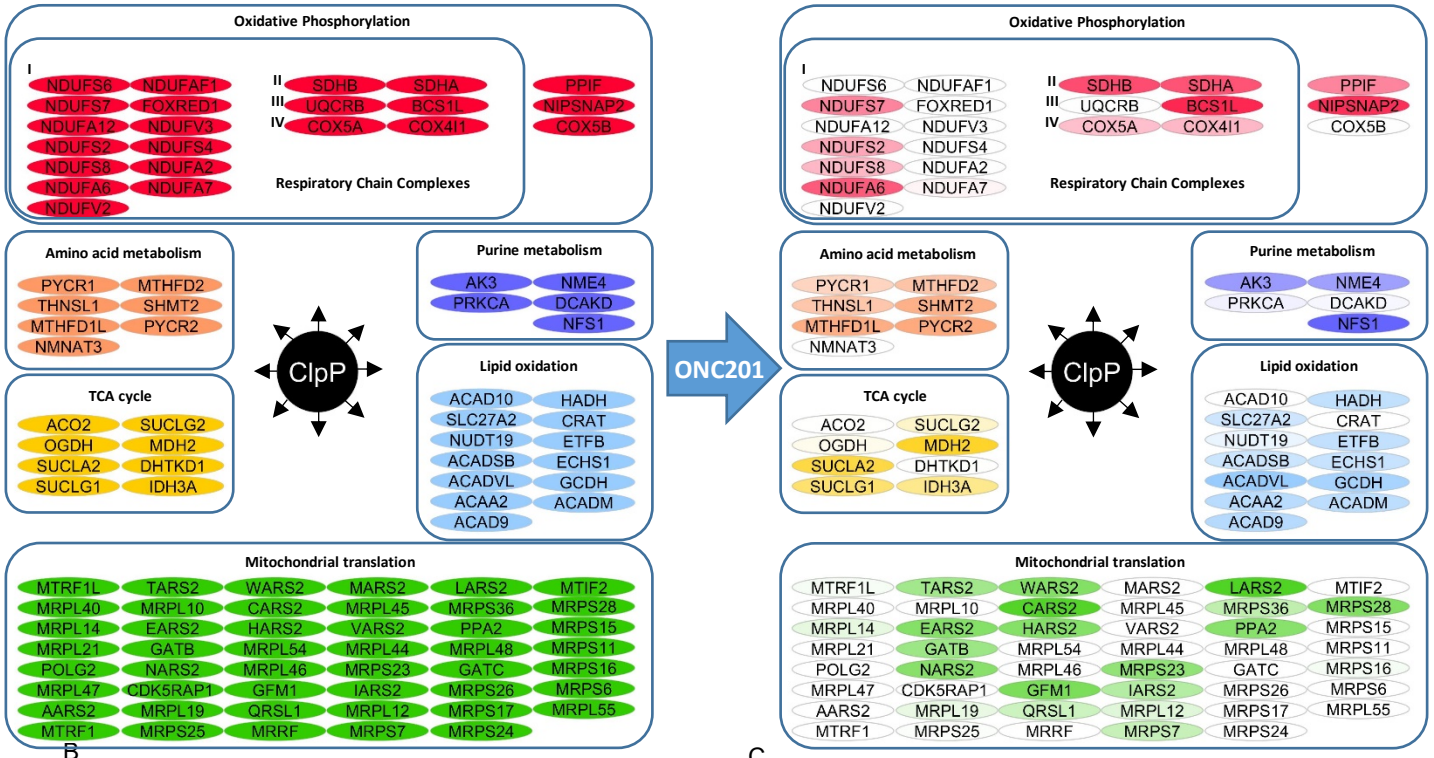
Oxidative Phosphorylation
I
NDUFS6 NDUFAF1
NDUFS7 FOXRED1
NDUFA12 NDUFV3
NDUFS2 NDUFS4
NDUFS8 NDUFA2
NDUFA6 NDUFA7
NDUFV2
II SDHB SDHA
III UQCRB BCS1L
IV COX5A COX4I1
Respiratory Chain Complexes
PPIF
NIPSNAP2
COX5B
Amino acid metabolism
PYCR1 MTHFD2
THNSL1 SHMT2
MTHFD1L PYCR2
NMNAT3
ClpP
Purine metabolism
AK3 NME4
PRKCA DCAKD
NFS1
Lipid oxidation
ACAD10 HADH
SLC27A2 CRAT
NUDT19 ETFB
ACADSB ECHS1
ACADVL GCDH
ACAA2 ACADM
ACAD9
TCA cycle
ACO2 SUCLG2
OGDH MDH2
SUCLA2 DHTKD1
SUCLG1 IDH3A
ONC201
Mitochondrial translation
MTRF1L TARS2 WARS2 MARS2 LARS2 MTIF2
MRPL40 MRPL10 CARS2 MRPL45 MRPS36 MRPS28
MRPL14 EARS2 HARS2 VARS2 PPA2 MRPS15
MRPL21 GATB MRPL54 MRPL44 MRPL48 MRPS11
POLG2 NARS2 MRPL46 MRPS23 GATC MRPS16
MRPL47 CDK5RAP1 GFM1 IARS2 MRPS26 MRPS6
AARS2 MRPL19 QRSL1 MRPL12 MRPS17 MRPL55
MTRF1 MRPS25 MRRF MRPS7 MRPS24

B

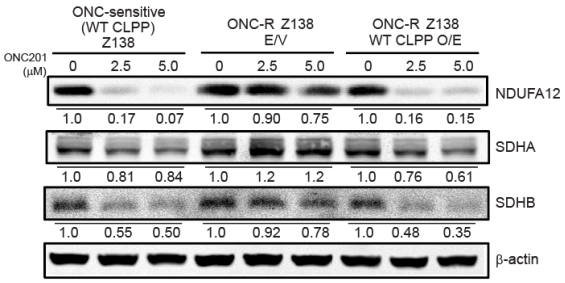
ONC-sensitive (WT CLPP) Z138
ONC-R Z138 E/V
ONC-R Z138 WT CLPP O/E
ONC201 (μM) 0 2.5 5.0 0 2.5 5.0 0 2.5 5.0
NDUFA12 1.0 0.17 0.07 1.0 0.90 0.75 1.0 0.16 0.15
SDHA 1.0 0.81 0.84 1.0 1.2 1.2 1.0 0.76 0.61
SDHB 1.0 0.55 0.50 1.0 0.92 0.78 1.0 0.48 0.35
β-actin

C

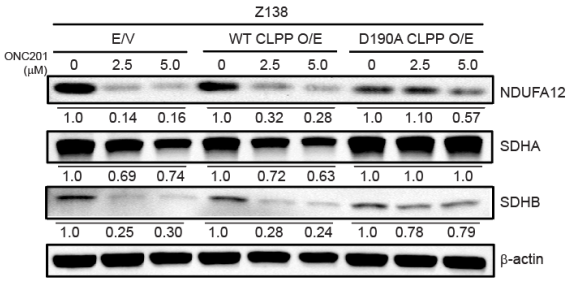
Z138
E/V
WT CLPP O/E
D190A CLPP O/E
ONC201 (μM) 0 2.5 5.0 0 2.5 5.0 0 2.5 5.0
NDUFA12 1.0 0.14 0.16 1.0 0.32 0.28 1.0 1.10 0.57
SDHA 1.0 0.69 0.74 1.0 0.72 0.63 1.0 1.0 1.0
SDHB 1.0 0.25 0.30 1.0 0.28 0.24 1.0 0.78 0.79
β-actin

D

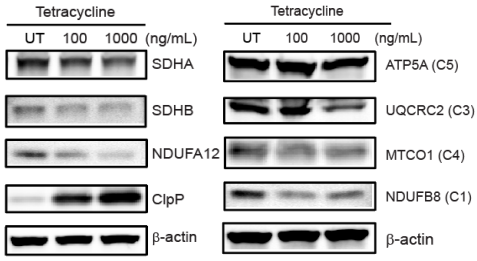
Tetracycline
UT 100 1000 (ng/mL)
SDHA
SDHB
NDUFA12
ClpP
β-actin
Tetracycline
UT 100 1000 (ng/mL)
ATP5A (C5)
UQCRC2 (C3)
MTCO1 (C4)
NDUFB8 (C1)
β-actin

E

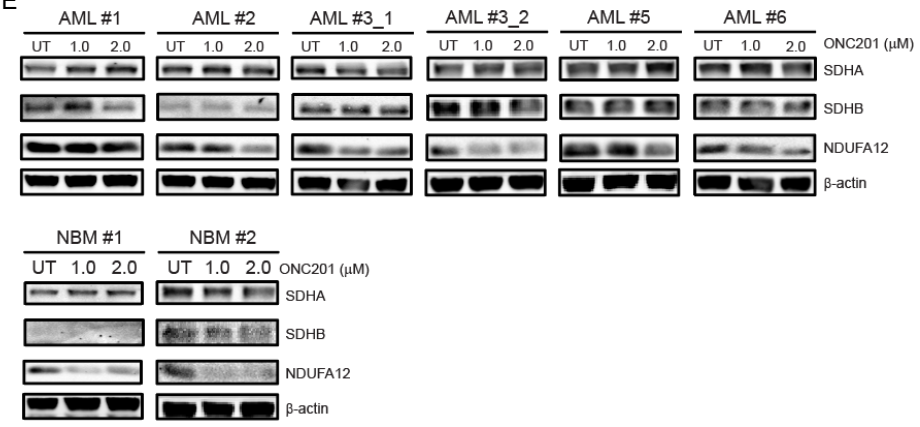
AML #1
AML #2
AML #3_1
AML #3_2
AML #5
AML #6
UT 1.0 2.0
ONC201 (μM)
SDHA
SDHB
NDUFA12
β-actin
NBM #1
NBM #2
UT 1.0 2.0
ONC201 (μM)
SDHA
SDHB
NDUFA12
β-actin

F

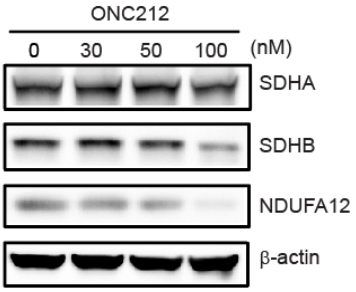
ONC212
0
30
50
100
(nM)
SDHA
SDHB
NDUFA12
β-actin

G

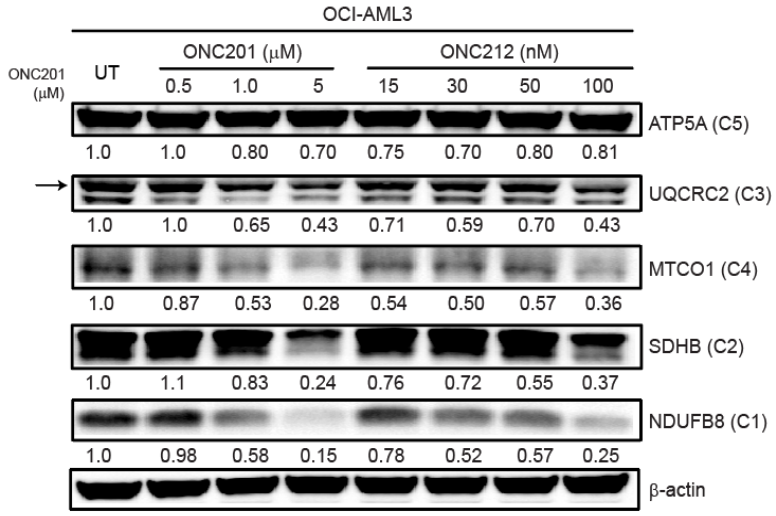
OCI-AML3
ONC201 (μM)
UT
ONC201 (μM)
0.5
1.0
5
ONC212 (nM)
15
30
50
100
ATP5A (C5)
1.0 1.0 0.80 0.70 0.75 0.70 0.80 0.81
UQCRC2 (C3)
1.0 1.0 0.65 0.43 0.71 0.59 0.70 0.43
MTCO1 (C4)
1.0 0.87 0.53 0.28 0.54 0.50 0.57 0.36
SDHB (C2)
1.0 1.1 0.83 0.24 0.76 0.72 0.55 0.37
NDUFB8 (C1)
1.0 0.98 0.58 0.15 0.78 0.52 0.57 0.25
β-actin

H

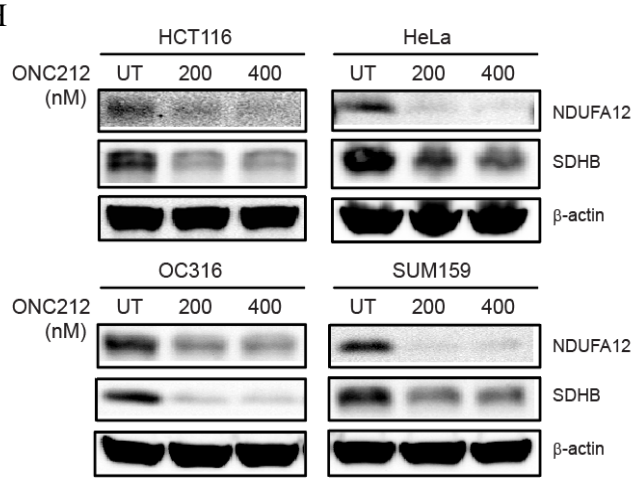
HCT116
HeLa
ONC212 (nM)
UT
200
400
NDUFA12
SDHB
β-actin
OC316
SUM159

I

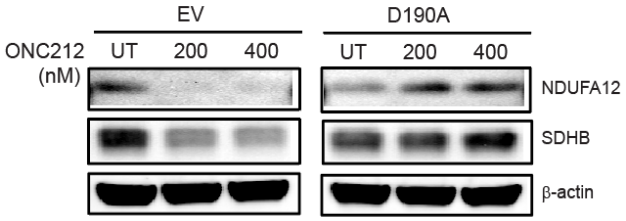
EV
D190A
ONC212 (nM)
UT
200
400
NDUFA12
SDHB
β-actin

J

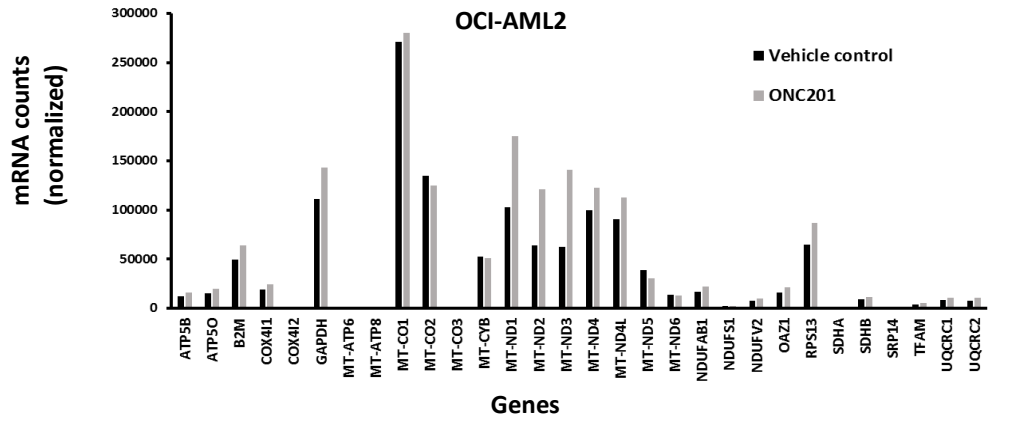
OCI-AML2
mRNA counts (normalized)
Vehicle control
ONC201
300000
250000
200000
150000
100000
50000
0
ATP5B ATP5O B2M COX4I1 COX4I2 GAPDH MT-ATP6 MT-ATP8 MT-CO1 MT-CO2 MT-CO3 MT-CYB MT-ND1 MT-ND2 MT-ND3 MT-ND4 MT-ND4L MT-ND5 MT-ND6 NDUFAB1 NDUFS1 NDUFV2 OAZ1 RPS13 SDHA SDHB SRP14 TFAM UQCRC1 UQCRC2
Genes

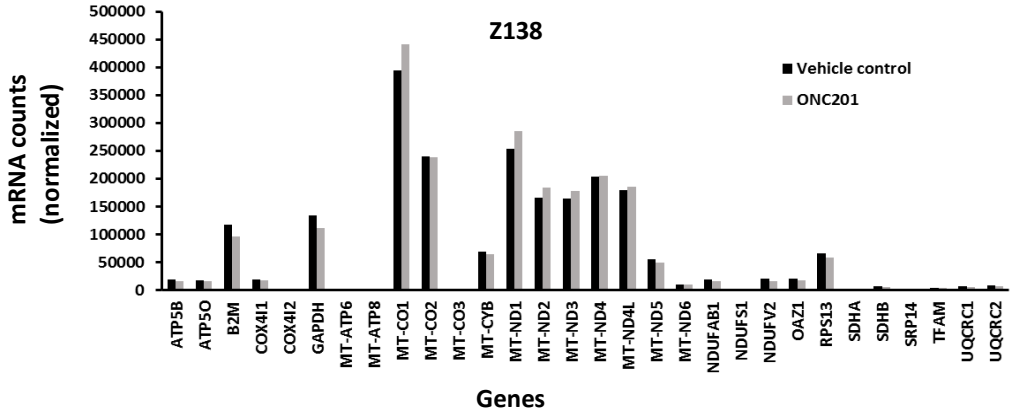
Z138
mRNA counts (normalized)
Vehicle control
ONC201
500000
450000
400000
350000
300000
250000
200000
150000
100000
50000
0
ATP5B ATP5O B2M COX4I1 COX4I2 GAPDH MT-ATP6 MT-ATP8 MT-CO1 MT-CO2 MT-CO3 MT-CYB MT-ND1 MT-ND2 MT-ND3 MT-ND4 MT-ND4L MT-ND5 MT-ND6 NDUFAB1 NDUFS1 NDUFV2 OAZ1 RPS13 SDHA SDHB SRP14 TFAM UQCRC1 UQCRC2
Genes

K

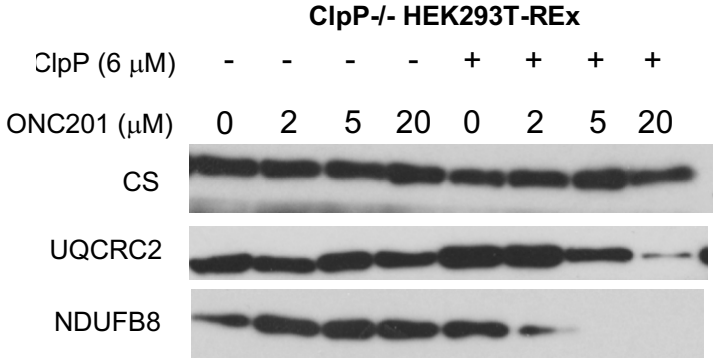
ClpP-/- HEK293T-REx
ClpP (6 μM) - - - - + + + +
ONC201 (μM) 0 2 5 20 0 2 5 20
CS
UQCRC2
NDUFB8

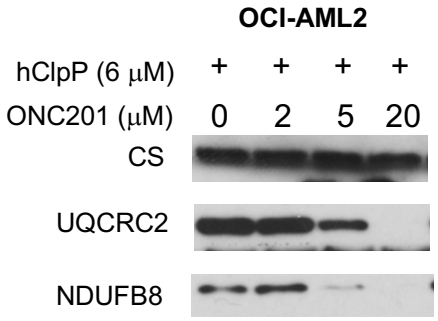
OCI-AML2
hClpP (6 μM) + + + +
ONC201 (μM) 0 2 5 20
CS
UQCRC2
NDUFB8

L

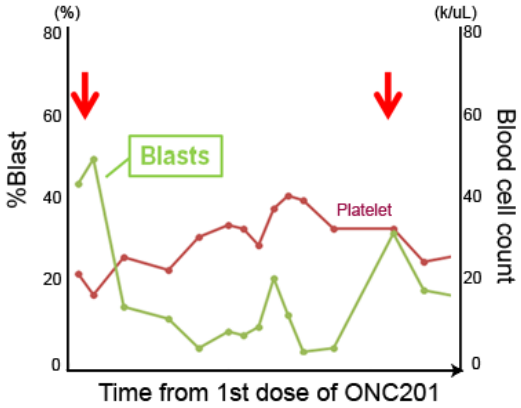
(%)
(k/uL)
80
60
40
20
0
%Blast
Blood cell count
Blasts
Platelet
Time from 1st dose of ONC201

M

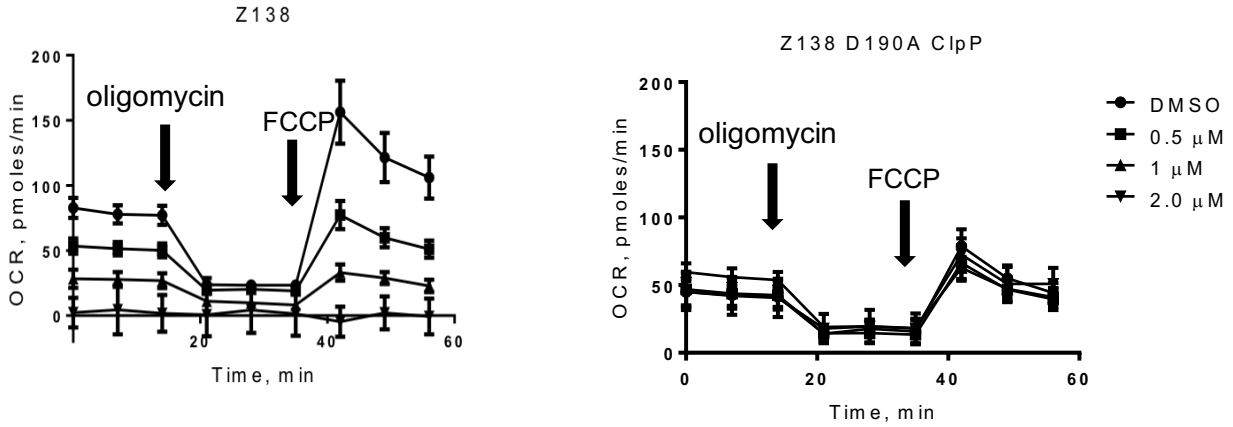
Z138
oligomycin
FCCP
OCR, pmoles/min
Time, min
Z138 D190A ClpP
oligomycin
FCCP
OCR, pmoles/min
Time, min
DMSO
0.5 μM
1 μM
2.0 μM

N

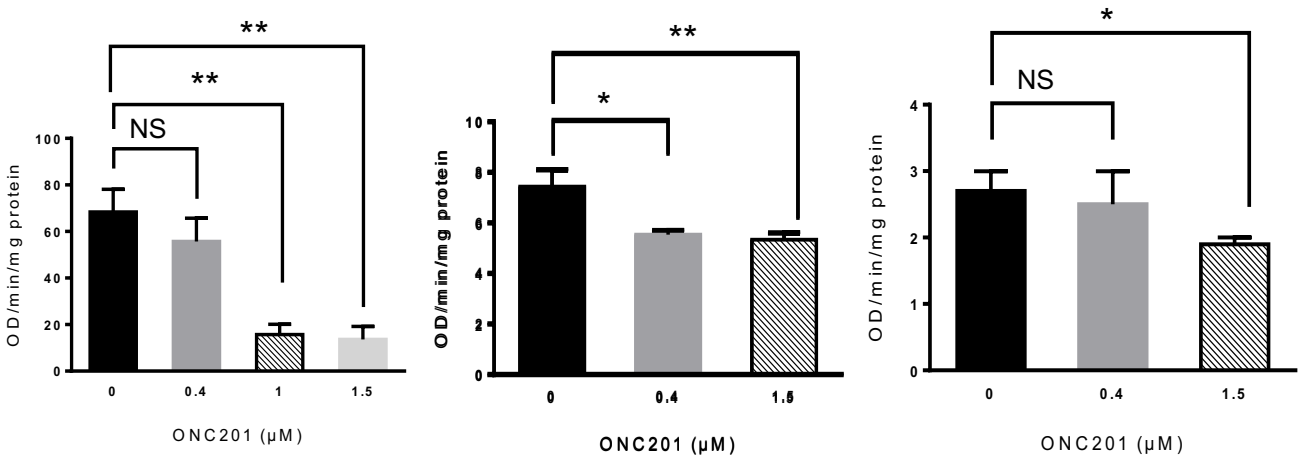
Complex I
Complex II
Complex IV
OD/min/mg protein
NS
ONC201 (μM)
OD/min/mg protein
ONC201 (μM)
OD/min/mg protein
NS
ONC201 (μM)

O

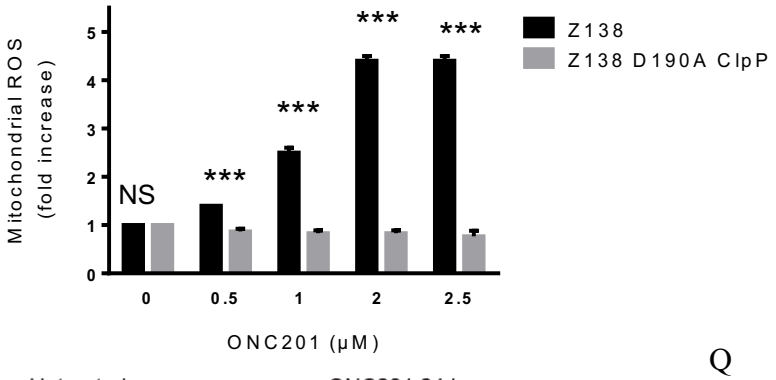
Mitochondrial ROS
(fold increase)
NS
ONC201 (μM)
Z138
Z138 D190A ClpP

P

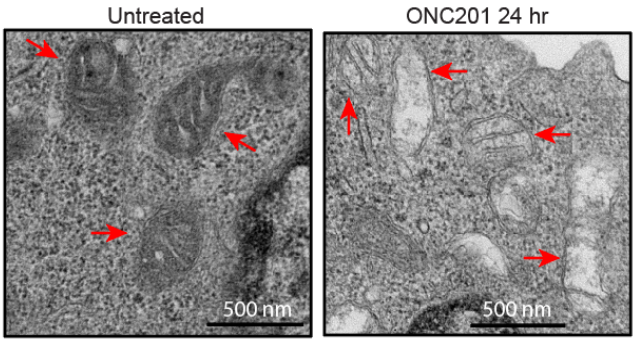
Untreated
ONC201 24 hr
500 nm
500 nm

Q

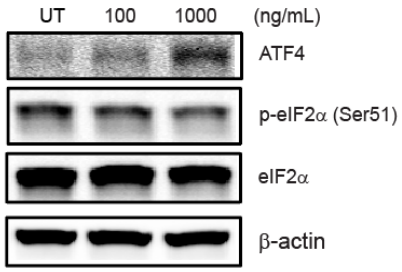
UT
100
1000
(ng/mL)
ATF4
p-eIF2α (Ser51)
eIF2α
β-actin

Figure 3-8. ClpP hyperactivation induces apoptosis following reduction of respiratory chain complex subunits.

(A) A subset of ClpP mitochondrial interactors was identified using BioID-MS and categorized according to selected gene ontology biological processes. Decreases in spectral counts following ONC201 treatment is illustrated and proportional to the decreases in color intensity.
(B-E) Immunoblot analysis of respiratory chain complex subunits in parental (ONC-sensitive) Z138 cells and ONC201-resistant Z138 cells (the single-clone #2 carrying D190A mutant ClpP) with over-expression of wild-type ClpP or an empty vector (B); in parental (ONC-naïve) Z138 cells with over-expression of wild-type ClpP, D190A mutant ClpP, or an empty vector (C); in tetracycline-inducible Y118A mutant ClpP in Z138 cells (D); in primary AML cells and normal bone marrow (NBM) cells (E). AML#3_1 and #3_2 are from the same patient but at different time points in relapse. Cells were treated with ONC201 at indicated concentrations for 24 hr.
(F) Immunoblot of SDHA, SDHB and NDUFA12 in OCI-AML3 cells treated with ON212 for 24 hours at indicated concentrations.
(G) Immunoblot of respiratory chain complex subunits. OCI-AML3 cells were treated with ONC201 or ONC212 at indicated concentrations for 24 hours.
(H) Immunoblot of SDHB and NDUFA12 in HCT-116, HeLa, OC316 and SUM159 cells treated with ON212 for 24 hours at indicated concentrations.
(I) Immunoblot analysis of respiratory chain complex subunits in HCT116 cells with over-expression of D190A mutant ClpP or an empty vector (EV).

(J) Effect of ONC201 (0.6 μM) on levels of mRNA encoding mitochondrial respiratory chain subunits in OCI-AML2 and Z138 cells.

(K) Immunoblots of citrate synthase (CS), UQCRC2 (complex III), and NDUFB8 (complex I) in mitochondrial lysates isolated from ClpP -/- HEK293T-REx and OCI-AML2 cells treated with increasing concentrations of ONC201 with or without recombinant ClpP (6 μM) after a brief (3 hr) period of incubation.
(L) A patient with AML refractory to decitabine, fludarabine, cyarabine and two investigational IDH2 inhibitors was enrolled in the Phase 1 trial of ONC201. Blasts (50% to 3%) and platelet transfusion requirements were reduced after oral administration of a single dose of ONC201 (250mg). Arrows indicate ONC201 administration.

(M) Effect of ONC201 on oxygen consumption in Z138 and Z138 D190A ClpP cells (measured by Seahorse Analyzer). 2 μM Oligomycin and 0.25 μM FCCP were used to derive parameters of mitochondrial respiration.
(N) Effects of ONC201 treatment on activity of respiratory chain complexes I, II, & IV in OCI-AML2 cells.
(O) Effect of ONC201 treatment on mitochondrial ROS production in Z138 and Z138 D190A ClpP cells. Percent mean ± SD from one of 3 representative experiment is shown.
(P) Effect of ONC201 treatment on mitochondrial morphology. Mitochondria were imaged by a transmission electron microscopy in OCI-AML3 cells treated with or without 5 mM ONC201 for 24 hr.
(Q) Immunoblot of ATF4, p-eIF2α and eIF2α in Y118A ClpP-overexpressed Z138 cells. Z138 cells with tetracycline-inducible Y118A ClpP were treated with tetracycline for 48 hr at indicated concentrations.

Table 3-3. Effect of ClpP activation after treatment with 0.6 μM ONC201 or expression of Y118A ClpP mutant on degradation of mitochondrial peptides in HEK293TREX cells detected by BioID mass spectrometry.

Gene Symbol	Gene Name	ClpP						ClpP+Drug								ClpP-Y118A							
		BioRep1		BioRep2		Total	SAINT	BioRep1		BioRep2		Total	SAINT	Log2 Fold change (vs	p-value	BioRep1		BioRep2		Total	SAINT	Log2 Fold change (vs	p-value
		Rep1	Rep2	Rep1	Rep2			Rep1	Rep2	Rep1	Rep2					Rep1	Rep2	Rep1	Rep2				
CLPP	*caseinolytic mitochondrial matrix peptidase proteolytic subuni*	1294	1247	1091	1083	4715	#N/A	1152	1143	1106	1036	4437	#N/A	#N/A	#N/A	922	884	790	722	3318	#N/A	#N/A	#N/A
VWA8	*malic enzyme 2*	16	17	18	18	69	1	58	62	50	53	223	1	1.69	0.00	42	41	29	28	140	1	1.02	0.00
NFS1	*NFS1, cysteine desulfurase*	40	39	33	39	151	1	56	51	58	56	221	1	0.55	0.00	46	48	47	39	180	1	0.25	0.03
HSPA1L	*heat shock protein family A (Hsp70) member 1 like*	102	108	112	104	426	1	147	138	161	157	603	1	0.50	0.00	137	0	0	123	260	0	-0.71	0.31
PNPT1	*polyribonucleotide nucleotidyltransferase 1*	52	48	53	51	204	1	65	59	66	64	254	1	0.32	0.00	50	57	46	41	194	1	-0.07	0.51
MGME1	*leucine rich pentatricopeptide repeat containing*	128	126	148	138	540	1	165	157	164	167	653	1	0.27	0.00	209	196	179	148	732	1	0.44	0.01
SSBP1	*single stranded DNA binding protein 1*	27	25	23	24	99	1	30	24	25	25	104	1	0.07	0.46	51	47	46	39	183	1	0.89	0.00
RNMTL1	*mitochondrial rRNA methyltransferase 3*	7	8	9	7	31	1	8	10	7	7	32	1	0.05	0.78	6	10	6	5	27	1	-0.20	0.44
HSD17B10	*hydroxysteroid 17-beta dehydrogenase 10*	104	98	94	93	389	1	108	89	99	97	393	1	0.01	0.84	181	167	153	140	641	1	0.72	0.00
LYRM4	*LYR motif containing 4*	10	9	9	9	37	1	9	9	11	8	37	1	0.00	1.00	14	14	12	13	53	1	0.52	0.00
MTPAP	*mitochondrial poly(A) polymerase*	9	7	9	6	31	1	7	8	6	8	29	1	-0.10	0.59	6	7	5	0	18	0.75	-0.78	0.11
PIN1	*peptidylprolyl cis/trans isomerase, NIMA-interacting 1*	6	5	9	8	28	1	6	6	8	6	26	1	-0.11	0.65	0	0	0	2	2	0	-3.81	0.00
SUPV3L1	*Suv3 like RNA helicase*	15	10	12	12	49	1	10	11	13	11	45	1	-0.12	0.44	22	24	16	10	72	1	0.56	0.13
AFG3L2	*AFG3 like matrix AAA peptidase subunit 2*	47	51	61	47	206	1	48	43	48	48	187	1	-0.14	0.23	82	77	61	57	277	1	0.43	0.04
ARG2	*arginase 2*	6	9	7	6	28	1	8	5	5	7	25	1	-0.16	0.49	13	15	9	11	48	1	0.78	0.01
ALDH2	*aldehyde dehydrogenase 2 family member*	25	23	26	26	100	1	21	23	24	21	89	1	-0.17	0.04	25	28	19	16	88	1	-0.18	0.33
BCS1L	*BCS1 homolog, ubiquinol-cytochrome c reductase complex cha*	50	52	50	46	198	1	44	38	45	49	176	1	-0.17	0.08	72	70	74	59	275	1	0.47	0.00
GCDH	*glutaryl-CoA dehydrogenase*	20	20	15	17	72	1	17	15	17	15	64	1	-0.17	0.19	38	34	38	34	144	1	1.00	0.00
CARS2	*cysteinyl-tRNA synthetase 2, mitochondrial*	60	52	51	47	210	1	48	43	47	44	182	1	-0.21	0.06	52	47	32	30	161	1	-0.38	0.09
PYCR2	*pyrroline-5-carboxylate reductase 2*	57	55	56	56	224	1	56	47	48	43	194	1	-0.21	0.03	74	75	61	59	269	1	0.26	0.04
MDH2	*malate dehydrogenase 2*	99	101	99	95	394	1	89	87	82	75	333	1	-0.24	0.00	103	94	96	94	387	1	-0.03	0.51
SLIRP	*SRA stem-loop interacting RNA binding protein*	8	7	9	8	32	1	7	8	6	6	27	1	-0.25	0.09	7	11	10	10	38	1	0.25	0.17
NIPSNAP2	*DNA polymerase delta interacting protein 2*	37	27	25	20	109	1	23	21	24	20	88	1	-0.31	0.20	47	46	40	33	166	1	0.61	0.03
HSPE1	*heat shock protein family E (Hsp10) member 1*	30	27	28	29	114	1	25	18	25	21	89	1	-0.36	0.01	50	61	52	53	216	1	0.92	0.00
MMAB	*methylmalonic aciduria (cobalamin deficiency) cblB type*	50	51	54	54	209	1	44	35	42	41	162	1	-0.37	0.00	57	55	59	54	225	1	0.11	0.04
MTHFD1L	*methylenetetrahydrofolate dehydrogenase (NADP+ dependen*	35	40	37	35	147	1	32	35	24	21	112	1	-0.39	0.05	53	46	38	38	175	1	0.25	0.12
ABCB7	*ATP binding cassette subfamily B member 7*	24	23	30	28	105	1	19	16	26	16	77	1	-0.45	0.05	15	20	18	14	67	1	-0.65	0.00
PTPMT1	*protein tyrosine phosphatase, mitochondrial 1*	9	9	11	10	39	1	8	7	5	8	28	1	-0.48	0.02	8	9	12	9	38	1	-0.04	0.81
CLIC4	*chloride intracellular channel 4*	13	10	6	6	35	1	8	8	3	6	25	1	-0.49	0.27	0	0	5	0	5	0	-2.81	0.01
SHMT2	*serine hydroxymethyltransferase 2*	375	411	336	325	1447	1	265	258	243	247	1013	1	-0.51	0.00	337	310	303	265	1215	1	-0.25	0.06
TIMM44	*translocase of inner mitochondrial membrane 44*	50	46	55	47	198	1	35	36	37	30	138	1	-0.52	0.00	47	42	52	41	182	1	-0.12	0.26
FASTKD2	*FAST kinase domains 2*	10	13	12	11	46	1	8	9	7	6	30	1	-0.62	0.00	19	21	20	15	75	1	0.71	0.00
NDUFAF5	*nicotinamide nucleotide transhydrogenase*	35	40	36	32	143	1	24	24	20	21	89	0.99	-0.68	0.00	26	26	23	28	103	1	-0.47	0.00
GLS	*glutaminase*	76	69	75	67	287	1	43	41	47	45	176	1	-0.71	0.00	89	85	83	75	332	1	0.21	0.02
SUCLA2	*succinate-CoA ligase ADP-forming beta subunit*	32	32	22	20	106	1	13	16	17	19	65	1	-0.71	0.02	24	29	25	24	102	1	-0.06	0.78
KIAA0564	*von Willebrand factor A domain containing 8*	46	39	53	48	186	1	27	31	29	27	114	1	-0.71	0.00	66	69	43	49	227	1	0.29	0.19
HSDL2	*hydroxysteroid dehydrogenase like 2*	19	19	22	22	82	1	16	10	12	12	50	0.85	-0.71	0.00	41	42	34	29	146	1	0.83	0.00
NDUFAF3	*NADH:ubiquinone oxidoreductase complex assembly factor 3*	15	10	16	12	53	1	7	9	8	8	32	1	-0.73	0.01	21	22	17	13	73	1	0.46	0.09
ACAD9	*acyl-CoA dehydrogenase family member 9*	19	21	16	15	71	1	14	13	7	8	42	1	-0.76	0.02	51	49	29	32	161	1	1.18	0.01
SDHB	*succinate dehydrogenase complex iron sulfur subunit B*	14	13	13	13	53	1	9	9	6	6	30	1	-0.82	0.001	9	9	8	9	35	1	-0.60	0.00
THEM4	*thioesterase superfamily member 4*	45	44	32	28	149	1	24	17	22	18	81	1	-0.88	0.01	35	35	29	33	132	1	-0.17	0.38
ACAA2	*acetyl-CoA acyltransferase 2*	16	17	19	18	70	1	10	9	10	9	38	1	-0.88	0.00	11	12	8	6	37	1	-0.92	0.00
LETM1	*leucine zipper and EF-hand containing transmembrane protein*	95	92	104	109	400	1	61	48	51	49	209	1	-0.94	0.00	253	232	186	162	833	1	1.06	0.00
SDHA	*succinate dehydrogenase complex flavoprotein subunit A*	30	25	21	24	100	1	14	12	15	11	52	1	-0.94	0.001	32	32	28	35	127	1	0.34	0.03
NUDT1	*nudix hydrolase 1*	4	4	6	4	18	1	3	0	4	2	9	0	-1.00	0.06	2	0	0	0	2	0	-3.17	0.00
IBA57	*IBA57, iron-sulfur cluster assembly*	29	31	36	34	130	1	20	14	17	12	63	1	-1.05	0.00	105	99	100	105	409	1	1.65	0.00
AK3	*adenylate kinase 3*	35	32	28	29	124	1	17	14	14	15	60	1	-1.05	0.00	25	27	26	24	102	1	-0.28	0.02
ACADM	*acyl-CoA dehydrogenase medium chain*	24	27	22	27	100	1	14	13	11	10	48	1	-1.06	0.00	17	22	19	18	76	1	-0.40	0.01
GFM1	*G elongation factor mitochondrial 1*	34	33	34	26	127	1	17	15	16	12	60	1	-1.08	0.00	29	27	27	23	106	1	-0.26	0.06
NDUFA6	*NADH:ubiquinone oxidoreductase subunit A6*	18	20	16	16	70	1	7	8	9	9	33	1	-1.08	0.00	24	23	22	26	95	1	0.44	0.00
NDUFAF4	*NADH:ubiquinone oxidoreductase complex assembly factor 4*	16	14	22	15	67	1	11	6	7	7	31	1	-1.11	0.01	34	42	31	33	140	1	1.06	0.00
NME4	*NME/NM23 nucleoside diphosphate kinase 4*	73	69	51	52	245	1	32	23	27	28	110	1	-1.16	0.00	40	53	46	44	183	1	-0.42	0.05
HINT2	*histidine triad nucleotide binding protein 2*	22	23	17	17	79	1	7	10	7	11	35	1	-1.17	0.00	21	16	27	20	84	1	0.09	0.67
C7orf55	*formation of mitochondrial complex V assembly factor 1 homo*	7	6	6	6	25	1	6	5	0	0	11	0	-1.18	0.07	5	5	0	5	15	0	-0.74	0.10
C8orf82	*chromosome 8 open reading frame 82*	15	14	19	18	66	1	10	11	8	0	29	0.75	-1.19	0.02	50	52	51	47	200	1	1.60	0.00
NIPSNAP1	*nipsnap homolog 1*	38	35	17	15	105	1	12	10	11	13	46	0.99	-1.19	0.05	32	24	33	24	113	1	0.11	0.77
C20orf7	*NADH:ubiquinone oxidoreductase complex assembly factor 5*	33	30	17	17	97	1	11	11	9	11	42	1	-1.21	0.02	26	18	27	22	93	1	-0.06	0.84
PMPCA	*peptidase, mitochondrial processing alpha subunit*	9	12	7	9	37	1	5	3	4	4	16	1	-1.21	0.00	14	11	9	7	41	1	0.15	0.60
MRPS28	*mitochondrial ribosomal protein S28*	18	17	20	18	73	1	10	7	6	8	31	1	-1.24	0.00	17	16	6	13	52	1	-0.49	0.09
SPRYD4	*SPRY domain containing 4*	20	24	19	21	84	1	9	7	9	10	35	1	-1.26	0.00	24	25	24	25	98	1	0.22	0.02
WARS2	*tryptophanyl tRNA synthetase 2, mitochondrial*	24	26	20	19	89	1	8	8	10	11	37	1	-1.27	0.00	35	25	25	21	106	1	0.25	0.26
EARS2	*glutamyl-tRNA synthetase 2, mitochondrial*	16	10	9	9	44	1	6	4	3	5	18	1	-1.29	0.01	12	16	5	6	39	1	-0.17	0.70
HADH	*hydroxyacyl-CoA dehydrogenase*	5	8	7	7	27	1	4	3	2	2	11	0.97	-1.30	0.00	12	16	8	11	47	1	0.80	0.03
HARS2	*histidyl-tRNA synthetase 2, mitochondrial*	22	24	26	29	101	1	12	11	9	9	41	1	-1.30	0.00	18	19	17	18	72	1	-0.49	0.00
RG9MTD1	*tRNA methyltransferase 10C, mitochondrial RNase P subunit*	57	54	59	57	227	1	26	28	18	20	92	0.97	-1.30	0.00	77	86	80	71	314	1	0.47	0.00
ETFB	*electron transfer flavoprotein beta subunit*	28	22	30	32	112	1	13	13	9	9	44	0	-1.35	0.00	43	41	33	31	148	1	0.40	0.05
NARS2	*asparaginyl-tRNA synthetase 2, mitochondrial*	35	32	29	32	128	1	15	10	13	12	50	1	-1.36	0.00	30	30	34	22	116	1	-0.14	0.32
PPA2	*pyrophosphatase (inorganic) 2*	30	28	39	36	133	1	15	8	16	12	51	1	-1.38	0.00	33	38	32	32	135	1	0.02	0.87
LYRM7	*LYR motif containing 7*	12	12	12	11	47	1	6	4	4	4	18	1	-1.38	0.00	16	12	15	12	55	1	0.23	0.11
MTHFD2	*methylenetetrahydrofolate dehydrogenase (NADP+ dependen*	15	12	15	12	54	1	5	4	5	6	20	1	-1.43	0.00	15	15	18	15	63	1	0.22	0.10
SUCLG1	*succinate-CoA ligase alpha subunit*	16	12	15	14	57	1	6	4	5	6	21	1	-1.44	0.00	10	14	11	12	47	1	-0.28	0.08
ECHS1	*enoyl-CoA hydratase, short chain 1*	91	84	88	83	346	1	27	33	31	32	123	1	-1.49	0.00	76	86	54	59	275	1	-0.33	0.06
RTN4IP1	*reticulon 4 interacting protein 1*	36	35	30	32	133	1	15	10	12	10	47	1	-1.50	0.00	25	27	22	19	93	1	-0.52	0.00
ABHD10	*abhydrolase domain containing 10*	45	41	33	37	156	1	13	12	16	13	54	1	-1.53	0.00	35	30	40	35	140	1	-0.16	0.27
THNSL1	*threonine synthase like 1*	11	12	15	9	47	1	6	4	3	3	16	0.99	-1.55	0.00	11	15	12	10	48	1	0.03	0.88
HIBCH	*3-hydroxyisobutyryl-CoA hydrolase*	17	10	14	6	47	1	4	5	4	3	16	1	-1.55	0.02	14	15	15	16	60	1	0.35	0.23
FECH	*ferrochelatase*	13	15	13	12	53	1	7	3	4	4	18	1	-1.56	0.00	8	10	7	8	33	1	-0.68	0.00
TFAM	*transcription factor A, mitochondrial*	13	11	15	10	49	1	7	3	2	4	16	0.98	-1.61	0.00	27	21	12	16	76	1	0.63	0.10
MRM3	*NADH:ubiquinone oxidoreductase core subunit S3*	84	78	70	70	302	1	27	26	19	26	98	0.76	-1.62	0.00	93	88	78	73	332	1	0.14	0.24
CLYBL	*citrate lyase beta like*	28	27	28	25	108	1	9	9	9	8	35	1	-1.63	0.00	4	2	3	3	12	0.98	-3.17	0.00
GLUD1	*glutamate dehydrogenase 1*	91	95	86	80	352	1	31	31	26	26	114	0	-1.63	0.00	68	67	70	63	268	1	-0.39	0.00
XPNPEP3	*X-prolyl aminopeptidase 3*	7	9	8	7	31	1	3	3	0	4	10	0	-1.63	0.00	12	9	0	4	25	0	-0.31	0.60
ACADSB	*acyl-CoA dehydrogenase short/branched chain*	19	23	13	16	71	1	7	4	6	4	21	1	-1.76	0.00	14	12	20	16	62	1	-0.20	0.44
NDUFS7	*NADH:ubiquinone oxidoreductase core subunit S7*	23	25	28	22	98	1	6	5	11	6	28	0.9	-1.81	0.00	24	23	22	24	93	1	-0.08	0.41
PPIF	*peptidylprolyl isomerase F*	36	43	39	36	154	1	14	12	8	10	44	1	-1.81	0.00	43	41	41	39	164	1	0.09	0.22
GATB	*argininosuccinate synthase 1*	28	34	31	36	129	1	12	11	8	5	36	0	-1.84	0.00	0	2	10	3	15	0	-3.10	0.00
NDUFAF7	*electron transfer flavoprotein alpha subunit*	53	56	62	51	222	1	14	14	15	17	60	0	-1.89	0.00	68	57	53	50	228	1	0.04	0.76
ADCK3	*coenzyme Q8A*	18	17	25	19	79	1	5	6	5	5	21	0	-1.91	0.00	20	19	14	11	64	0.95	-0.30	0.23
IDE	*insulin degrading enzyme*	12	10	15	14	51	1	4	2	3	4	13	0.98	-1.97	0.00	12	14	9	11	46	1	-0.15	0.44
IDH3A	*isocitrate dehydrogenase 3 (NAD(+)) alpha*	5	7	5	7	24	1	2	0	4	0	6	0	-2.00	0.01	9	10	4	0	23	0	-0.06	0.92
NADKD1	*NAD kinase 2, mitochondrial*	10	10	11	6	37	1	0	4	2	3	9	0	-2.04	0.00	5	6	3	4	18	1	-1.04	0.01
PYCR1	*pyrroline-5-carboxylate reductase 1*	32	27	36	35	130	1	7	6	7	9	29	1	-2.16	0.00	71	68	67	68	274	1	1.08	0.00
ATPAF1	*ATP synthase mitochondrial F1 complex assembly factor 1*	43	38	42	44	167	1	11	13	9	4	37	1	-2.17	0.00	70	72	52	57	251	1	0.59	0.01
ALDH4A1	*aldehyde dehydrogenase 4 family member A1*	39	39	52	50	180	1	10	12	8	9	39	1	-2.21	0.00	25	32	23	23	103	1	-0.81	0.00
IARS2	*isoleucyl-tRNA synthetase 2, mitochondrial*	111	116	107	108	442	1	23	20	21	21	85	1	-2.38	0.00	151	162	146	136	595	1	0.43	0.00
C2orf56	*NADH:ubiquinone oxidoreductase complex assembly factor 7*	25	22	20	20	87	1	4	5	3	4	16	1	-2.44	0.00	25	23	24	27	99	1	0.19	0.09
NDUFS2	*NADH:ubiquinone oxidoreductase core subunit S2*	122	122	90	74	408	1	22	18	21	14	75	1	-2.44	0.00	127	112	112	87	438	1	0.10	0.63
OXCT1	*3-oxoacid CoA-transferase 1*	34	22	28	24	108	1	7	0	5	6	18	0.75	-2.58	0.00	14	18	12	12	56	1	-0.95	0.00
ATPAF2	*ATP synthase mitochondrial F1 complex assembly factor 2*	9	9	6	6	30	1	3	2	0	0	5	0	-2.58	0.00	5	7	2	2	16	0.97	-0.91	0.06
GTPBP3	*GTP binding protein 3, mitochondrial*	5	8	5	6	24	1	2	0	0	2	4	0	-2.58	0.00	8	4	2	3	17	0.98	-0.50	0.29
MRPS36	*mitochondrial ribosomal protein S36*	27	26	24	25	102	1	6	4	3	4	17	1	-2.58	0.00	29	28	27	26	110	1	0.11	0.07
NDUFS8	*NADH:ubiquinone oxidoreductase core subunit S8*	23	24	31	28	106	1	5	4	3	4	16	1	-2.73	0.00	33	33	27	28	121	1	0.19	0.18

GBAS	*nipsnap homolog 2*	30	29	13	11	83	1	5	4	3	0	12	0	-2.79	0.01	20	17	14	13	64	1	-0.38	0.41
COX5A	*cytochrome c oxidase subunit 5A*	20	20	18	15	73	1	5	2	0	3	10	0	-2.87	0.00	30	27	23	20	100	1	0.45	0.04
QRSL1	*glutaminyl-tRNA synthase (glutamine-hydrolyzing)-like 1*	42	39	40	36	157	1	6	7	2	6	21	0.99	-2.90	0.00	42	41	36	37	156	1	-0.01	0.90
POLRMT	*RNA polymerase mitochondrial*	14	12	16	12	54	1	0	7	0	0	7	0	-2.95	0.00	21	26	19	14	80	1	0.57	0.05
OXA1L	*OXA1L, mitochondrial inner membrane protein*	4	6	8	6	24	1	3	0	0	0	3	0	-3.00	0.00	2	3	4	3	12	0.99	-1.00	0.02
PET112	*glutamyl-tRNA amidotransferase subunit B*	36	32	34	37	139	1	5	6	4	2	17	0.98	-3.03	0.00	33	30	24	26	113	1	-0.30	0.03
SUCLG2	*succinate-CoA ligase GDP-forming beta subunit*	22	19	16	19	76	1	2	0	3	4	9	0	-3.08	0.00	14	15	14	11	54	1	-0.49	0.01
NUDT19	*nudix hydrolase 19*	15	13	17	15	60	1	0	3	2	2	7	0	-3.10	0.00	8	12	11	9	40	1	-0.58	0.01
MRPL12	*mitochondrial ribosomal protein L12*	13	12	13	12	50	1	3	0	2	0	5	0	-3.32	0.00	15	16	14	13	58	1	0.21	0.03
ZADH2	*zinc binding alcohol dehydrogenase domain containing 2*	7	5	5	5	22	1	2	0	0	0	2	0	-3.46	0.00	3	3	2	0	8	0	-1.46	0.01
C20orf72	*mitochondrial genome maintenance exonuclease 1*	12	11	10	13	46	1	2	0	2	0	4	0	-3.52	0.00	11	11	15	13	50	1	0.12	0.42
OGDH	*oxoglutarate dehydrogenase*	5	7	5	9	26	1	2	0	0	0	2	0	-3.70	0.00	24	25	20	14	83	1	1.67	0.00
C12orf10	*chromosome 12 open reading frame 10*	8	8	6	5	27	1	0	0	2	0	2	0	-3.75	0.00	2	0	0	0	2	0	-3.75	0.00
DCAKD	*dephospho-CoA kinase domain containing*	9	6	7	5	27	1	0	0	0	2	2	0	-3.75	0.00	0	0	0	2	2	0	-3.75	0.00
NDUFA7	*NADH:ubiquinone oxidoreductase subunit A7*	3	4	3	4	14	1	0	0	0	0	1	0	-3.81	0.00	0	3	0	0	3	0	-2.22	0.01
SDHAF3	*NADH:ubiquinone oxidoreductase subunit A9*	87	78	98	91	354	1	5	6	8	6	25	0	-3.82	0.00	99	96	80	71	346	1	-0.03	0.81
CRAT	*carnitine O-acetyltransferase*	5	4	4	3	16	1	0	0	0	0	1	0	-4.00	0.00	2	0	0	0	2	0	-3.00	0.00
MRPL54	*mitochondrial ribosomal protein L54*	5	4	4	3	16	1	0	0	0	0	1	0	-4.00	0.00	2	0	0	0	2	0	-3.00	0.00
GUF1	*GUF1 homolog, GTPase*	9	11	5	8	33	1	0	0	2	0	2	0	-4.04	0.00	12	12	10	9	43	1	0.38	0.14
ACAD10	*acyl-CoA dehydrogenase family member 10*	4	5	3	5	17	1	0	0	0	0	1	0	-4.09	0.00	0	0	0	0	1	0	-4.09	0.00
FOXRED1	*FAD dependent oxidoreductase domain containing 1*	5	5	3	4	17	1	0	0	0	0	1	0	-4.09	0.00	0	0	0	0	1	0	-4.09	0.00
NUBPL	*nucleotide binding protein like*	4	5	6	3	18	1	0	0	0	0	1	0	-4.17	0.00	0	3	0	0	3	0	-2.58	0.01
CDK5RAP1	*CDK5 regulatory subunit associated protein 1*	4	5	5	4	18	1	0	0	0	0	1	0	-4.17	0.00	4	4	5	2	15	0.98	-0.26	0.32
MRPL48	*mitochondrial ribosomal protein L48*	4	4	6	4	18	1	0	0	0	0	1	0	-4.17	0.00	6	8	6	0	20	0.75	0.15	0.79
NADK2	*mitochondrial ribosomal protein S31*	42	35	37	37	151	1	4	2	2	0	8	0	-4.24	0.00	47	48	30	32	157	1	0.06	0.77
MTRF1	*mitochondrial translation release factor 1*	3	4	5	7	19	1	0	0	0	0	1	0	-4.25	0.00	3	2	0	2	7	0	-1.44	0.03
MRPS17	*mitochondrial ribosomal protein S17*	4	5	5	5	19	1	0	0	0	0	1	0	-4.25	0.00	3	6	0	4	13	0	-0.55	0.28
MRPS11	*mitochondrial ribosomal protein S11*	6	5	4	4	19	1	0	0	0	0	1	0	-4.25	0.00	7	2	3	3	15	0.98	-0.34	0.44
PITRM1	*pitrilysin metallopeptidase 1*	13	10	8	7	38	1	0	0	0	2	2	0	-4.25	0.00	10	11	7	6	34	1	-0.16	0.59
MICU2	*NADH:ubiquinone oxidoreductase core subunit V1*	46	44	47	42	179	1	4	5	0	0	9	0	-4.31	0.00	43	43	37	35	158	1	-0.18	0.07
NDUFAF1	*NADH:ubiquinone oxidoreductase complex assembly factor 1*	6	6	4	4	20	1	0	0	0	0	1	0	-4.32	0.00	0	0	0	0	1	0	-4.32	0.00
NFU1	*NFU1 iron-sulfur cluster scaffold*	6	6	4	4	20	1	0	0	0	0	1	0	-4.32	0.00	5	5	4	2	16	0.98	-0.32	0.32
POLG	*DNA polymerase gamma, catalytic subunit*	5	6	5	4	20	1	0	0	0	0	1	0	-4.32	0.00	8	9	3	4	24	1	0.26	0.54
BCKDHA	*branched chain keto acid dehydrogenase E1, alpha polypeptid*	5	3	7	5	20	1	0	0	0	0	1	0	-4.32	0.00	20	18	14	12	64	1	1.68	0.00
ACSS1	*acyl-CoA synthetase short chain family member 1*	4	8	5	5	22	1	0	0	0	0	1	0	-4.46	0.00	6	0	0	2	8	0	-1.46	0.08
MPST	*mercaptopyruvate sulfurtransferase*	6	9	4	3	22	1	0	0	0	0	1	0	-4.46	0.01	0	3	4	2	9	0	-1.29	0.08
MRPL10	*mitochondrial ribosomal protein L10*	4	7	7	4	22	1	0	0	0	0	1	0	-4.46	0.00	6	6	4	3	19	1	-0.21	0.54
MRPL21	*mitochondrial ribosomal protein L21*	5	4	7	7	23	1	0	0	0	0	1	0	-4.52	0.00	8	6	0	0	14	0	-0.72	0.34
MRPS6	*mitochondrial ribosomal protein S6*	4	9	5	5	23	1	0	0	0	0	1	0	-4.52	0.00	5	4	3	3	15	1	-0.62	0.15
MARS2	*methionyl-tRNA synthetase 2, mitochondrial*	8	5	6	4	23	1	0	0	0	0	1	0	-4.52	0.00	7	9	3	8	27	1	0.23	0.55
UQCRB	*ubiquinol-cytochrome c reductase binding protein*	8	7	6	5	26	1	0	0	0	0	1	0	-4.70	0.00	0	0	3	2	5	0	-2.38	0.00
COQ8A	*NADH:ubiquinone oxidoreductase core subunit S1*	156	152	180	178	666	1	7	7	6	5	25	0	-4.74	0.00	121	118	92	87	418	1	-0.67	0.00
MRPS24	*mitochondrial ribosomal protein S24*	8	5	9	6	28	1	0	0	0	0	1	0	-4.81	0.00	15	15	17	14	61	1	1.12	0.00
TACO1	*translational activator of cytochrome c oxidase I*	61	57	51	57	226	1	2	3	0	3	8	0	-4.82	0.00	71	64	53	49	237	1	0.07	0.63
MRPS15	*mitochondrial ribosomal protein S15*	6	8	7	9	30	1	0	0	0	0	1	0	-4.91	0.00	0	6	0	0	6	0	-2.32	0.01
GTPBP10	*GTP binding protein 10*	8	12	5	5	30	1	0	0	0	0	1	0	-4.91	0.00	6	4	3	3	16	1	-0.91	0.10
BCKDHB	*branched chain keto acid dehydrogenase E1 subunit beta*	5	8	9	8	30	1	0	0	0	0	1	0	-4.91	0.00	14	16	11	11	52	1	0.79	0.01
PDPR	*pyruvate dehydrogenase phosphatase regulatory subunit*	8	9	6	8	31	1	0	0	0	0	1	0	-4.95	0.00	8	11	8	6	33	1	0.09	0.69
COX5B	*cytochrome c oxidase subunit 5B*	7	8	9	8	32	1	0	0	0	0	1	0	-5.00	0.00	12	11	13	8	44	1	0.46	0.03
MRPL44	*mitochondrial ribosomal protein L44*	6	9	8	10	33	1	0	0	0	0	1	0	-5.04	0.00	19	19	19	15	72	1	1.13	0.00
MRPL40	*mitochondrial ribosomal protein L40*	8	8	10	8	34	1	0	0	0	0	1	0	-5.09	0.00	11	11	13	9	44	1	0.37	0.04
GLRX5	*glutaredoxin 5*	11	11	7	8	37	1	0	0	0	0	1	0	-5.21	0.00	7	8	9	7	31	1	-0.26	0.24
MRPL55	*mitochondrial ribosomal protein L55*	10	9	11	8	38	1	0	0	0	0	1	0	-5.25	0.00	11	9	6	7	33	1	-0.20	0.37
DHTKD1	*dehydrogenase E1 and transketolase domain containing 1*	8	13	9	8	38	1	0	0	0	0	1	0	-5.25	0.00	9	8	9	9	35	1	-0.12	0.56
POLG2	*DNA polymerase gamma 2, accessory subunit*	7	10	11	11	39	1	0	0	0	0	1	0	-5.29	0.00	6	7	3	5	21	1	-0.89	0.01
PCK2	*phosphoenolpyruvate carboxykinase 2, mitochondrial*	8	8	12	12	40	1	0	0	0	0	1	0	-5.32	0.00	6	7	8	7	28	1	-0.51	0.05
ECSIT	*ECSIT signalling integrator*	10	5	14	12	41	1	0	0	0	0	1	0	-5.36	0.00	6	6	4	4	20	1	-1.04	0.04
ACN9	*succinate dehydrogenase complex assembly factor 3*	13	13	10	8	44	1	0	0	0	0	1	0	-5.46	0.00	3	3	4	0	10	0	-2.14	0.00
ACO2	*aconitase 2*	13	11	9	11	44	1	0	0	0	0	1	0	-5.46	0.00	12	6	11	7	36	1	-0.29	0.28
MRRF	*mitochondrial ribosome recycling factor*	10	10	12	13	45	1	0	0	0	0	1	0	-5.49	0.00	12	10	10	10	42	1	-0.10	0.44
GRPEL1	*GrpE like 1, mitochondrial*	9	13	12	12	46	1	0	0	0	0	1	0	-5.52	0.00	15	15	7	9	46	1	0.00	1.00
VARS2	*valyl-tRNA synthetase 2, mitochondrial*	13	12	11	10	46	1	0	0	0	0	1	0	-5.52	0.00	21	24	16	17	78	1	0.76	0.01
TST	*thiosulfate sulfurtransferase*	17	15	7	8	47	1	0	0	0	0	1	0	-5.55	0.00	7	8	7	11	33	1	-0.51	0.24
MTIF2	*mitochondrial translational initiation factor 2*	14	12	11	10	47	1	0	0	0	0	1	0	-5.55	0.00	18	19	10	11	58	1	0.30	0.31
AARS2	*alanyl-tRNA synthetase 2, mitochondrial*	11	13	15	14	53	1	0	0	0	0	1	0	-5.73	0.00	13	17	8	10	48	1	-0.14	0.58
PDE12	*phosphodiesterase 12*	14	14	15	12	55	1	0	0	0	0	1	0	-5.78	0.00	18	21	11	6	56	1	0.03	0.94
PAM16	*presequence translocase associated motor 16*	17	17	12	14	60	1	0	0	0	0	1	0	-5.91	0.00	16	16	0	13	45	0.75	-0.42	0.39
NDUFS4	*NADH:ubiquinone oxidoreductase subunit S4*	13	14	17	17	61	1	0	0	0	0	1	0	-5.93	0.00	9	12	10	10	41	1	-0.57	0.01
NDUFV2	*NADH:ubiquinone oxidoreductase core subunit V2*	62	61	60	66	249	1	0	2	2	0	4	0	-5.96	0.00	52	41	41	46	180	1	-0.47	0.00
GATC	*glutamyl-tRNA amidotransferase subunit C*	15	17	18	13	63	1	0	0	0	0	1	0	-5.98	0.00	18	16	13	14	61	1	-0.05	0.76
ALDH1L2	*aldehyde dehydrogenase 1 family member L2*	16	18	16	16	66	1	0	0	0	0	1	0	-6.04	0.00	10	7	12	12	41	1	-0.69	0.00
MRPL46	*mitochondrial ribosomal protein L46*	14	16	18	20	68	1	0	0	0	0	1	0	-6.09	0.00	17	18	10	11	56	1	-0.28	0.26
ERAL1	*Era like 12S mitochondrial rRNA chaperone 1*	20	18	19	16	73	1	0	0	0	0	1	0	-6.19	0.00	9	7	7	6	29	1	-1.33	0.00
NDUFS6	*NADH:ubiquinone oxidoreductase subunit S6*	24	19	19	18	80	1	0	0	0	0	1	0	-6.32	0.00	15	18	16	18	67	1	-0.26	0.08
NDUFA2	*NADH:ubiquinone oxidoreductase subunit A2*	22	20	19	19	80	1	0	0	0	0	1	0	-6.32	0.00	20	17	16	15	68	1	-0.23	0.06
GRSF1	*G-rich RNA sequence binding factor 1*	21	18	21	21	81	1	0	0	0	0	1	0	-6.34	0.00	84	91	69	61	305	1	1.91	0.00
MRPS26	*mitochondrial ribosomal protein S26*	20	21	21	21	83	1	0	0	0	0	1	0	-6.38	0.00	16	20	8	14	58	1	-0.52	0.05
FMC1	*pentatricopeptide repeat domain 3*	32	27	28	29	116	1	0	0	0	0	1	0	-6.86	0.00	49	45	34	26	154	1	0.41	0.13
NDUFA12	*NADH:ubiquinone oxidoreductase subunit A12*	47	45	48	48	188	1	0	0	0	0	1	0	-7.55	0.00	29	26	22	16	93	1	-1.02	0.00
NDUFAF2	*NADH:ubiquinone oxidoreductase complex assembly factor 2*	64	58	63	61	246	1	0	0	0	0	1	0	-7.94	0.00	58	55	55	54	222	1	-0.15	0.01
NDUFV3	*NADH:ubiquinone oxidoreductase subunit V3*	72	72	70	76	290	1	0	0	0	0	1	0	-8.18	0.00	80	75	78	67	300	1	0.05	0.45
RPS15A	*ribosomal protein S15a*	80	85	62	58	285	0.99	50	43	44	40	177	0	-0.69	0.01	53	49	53	54	209	0	-0.45	0.03
SLC27A2	*solute carrier family 27 member 2*	3	4	3	4	14	0.99	4	0	0	0	4	0	-1.81	0.05	0	0	0	0	1	0	-3.81	0.00
MRPS7	*mitochondrial ribosomal protein S7*	10	9	11	11	41	0.99	4	2	0	0	6	0	-2.77	0.00	19	17	13	18	67	1	0.71	0.00
MRPL14	*mitochondrial ribosomal protein L14*	3	2	3	3	11	0.99	0	0	0	0	1	0	-3.46	0.00	2	2	4	3	11	0.98	0.00	1.00
METTL17	*methyltransferase like 17*	2	3	4	3	12	0.99	0	0	0	0	1	0	-3.58	0.00	0	0	0	0	1	0	-3.58	#####
ALDH6A1	*aldehyde dehydrogenase 6 family member A1*	5	3	3	3	14	0.99	0	0	0	0	1	0	-3.81	0.00	3	3	0	0	6	0	-1.22	0.09
MRPS16	*mitochondrial ribosomal protein S16*	4	3	3	4	14	0.99	0	0	0	0	1	0	-3.81	0.00	6	9	0	0	15	0	0.10	0.92
MTRF1L	*mitochondrial translational release factor 1 like*	5	3	3	3	14	0.99	0	0	0	0	1	0	-3.81	0.00	5	8	4	3	20	1	0.51	0.25
MRPS25	*mitochondrial ribosomal protein S25*	3	3	3	6	15	0.99	0	0	0	0	1	0	-3.91	0.00	6	7	6	4	23	1	0.62	0.09
NMNAT3	*nicotinamide nucleotide adenylyltransferase 3*	6	4	3	3	16	0.99	0	0	0	0	1	0	-4.00	0.00	0	0	0	0	1	0	-4.00	0.00
MRPL45	*mitochondrial ribosomal protein L45*	23	22	21	21	87	0.99	0	0	0	0	1	0	-6.44	0.00	20	19	18	14	71	0.98	-0.29	0.03
LARS2	*leucyl-tRNA synthetase 2, mitochondrial*	8	11	14	11	44	0.98	10	11	10	9	40	0.98	-0.14	0.47	13	15	12	7	47	0.98	0.10	0.73
IDI1	*isopentenyl-diphosphate delta isomerase 1*	5	4	2	3	14	0.98	3	2	3	4	12	0.98	-0.22	0.54	6	8	9	11	34	1	1.28	0.01
CPOX	*coproporphyrinogen oxidase*	5	3	3	2	13	0.98	0	3	0	0	3	0	-2.12	0.04	5	4	6	9	24	1	0.88	0.07
ABAT	*4-aminobutyrate aminotransferase*	4	3	3	2	12	0.98	2	0	0	0	2	0	-2.58	0.01	0	0	0	0	1	0	-3.58	0.00
CHCHD3	*coiled-coil-helix-coiled-coil-helix domain containing 3*	2	3	3	3	11	0.98	0	0	0	0	1	0	-3.46	0.00	0	0	0	2	2	0	-2.46	0.01
PRKCA	*protein kinase C alpha*	3	2	3	4	12	0.98	0	0	0	0	1	0	-3.58	0.00	0	0	0	0	1	0	-3.58	0.00
GPT2	*glutamic--pyruvic transaminase 2*	4	3	2	4	13	0.98	0	0	0	0	1	0	-3.70	0.00	4	5	4	2	15	0.98	0.21	0.55
COQ6	*coenzyme Q6, monooxygenase*	3	2	5	3	13	0.98	0	0	0	0	1	0	-3.70	0.00	6	5	3	6	20	1	0.62	0.11
PDIA3	*protein disulfide isomerase family A member 3*	26	26	23	26	101	0.97	29	24	27	23	103	0.96	0.03	0.76	21	17	20	18	76	0	-0.41	0.00
HSD17B8	*hydroxysteroid 17-beta dehydrogenase 8*	2	2	5	3	12	0.97	0	3	0	2	5	0	-1.26	0.14	2	0	0	0	2	0	-2.58	0.03
DHRS4	*dehydrogenase/reductase 4*	2	2	2	4	10	0.96	2	0	0	0	2	0	-2.32	0.03	5	2	2	2	11	0.96	0.14	0.79
TARS2	*threonyl-tRNA synthetase 2, mitochondrial*	16	17	17	12	62	0.94	6	4	3	3	16	0	-1.95	0.00	18	16	9	9	52	0.87	-0.25	0.38
SFXN4	*sideroflexin 4*	7	7	8	8	30	0.93	8	4	3	5	20	0	-0.58	0.07	6	7	6	4	23	0.79	-0.38	0.04
AIFM1	*apoptosis inducing factor mitochondria associated 1*	12	14	10	9	45	0.93	4	4	4	3	15	0	-1.58	0.00	4	3	0	2	9	0	-2.32	0.00
ACADVL	*acyl-CoA dehydrogenase very long chain*	17	11	15	13	56	0.92	19	22	19	22	82	0.99	0.55	0.01	17	20	16	15	68	0.97	0.28	0.12
MRPS23	*mitochondrial ribosomal protein S23*	11	10	10	11	42	0.92	4	6	4	0	14	0	-1.58	0.00	8	7	9	12	36	0.86	-0.22	0.23
MRPL19	*mitochondrial ribosomal protein L19*	18	17	11	11	57	0.92	3	0	0	2	5	0	-3.51	0.00	7	8	8	6	29	0	-0.97	0.01
TBRG4	*transforming growth factor beta regulator 4*	7	8	7	6	28	0.9	9	9	9	7	34	0.96	0.28	0.06	8	14	6	6	34	0.91	0.28	0.47
ACAT1	*acetyl-CoA acetyltransferase 1*	35	38	39	37	149	0.82	28	27	20	24	99	0	-0.59	0.00	39	40	35	34	148	0	-0.01	0.89
PDK3	*pyruvate dehydrogenase kinase 3*	11	15	8	13	47	0.82	4	7	3	2	16	0	-1.55	0.01	21	23	13	14	71	1	0.60	0.08
COX4I1	*cytochrome c oxidase subunit 4I1*	11	9	9	11	40	0.8	3	3	0	0	6	0	-2.74	0.00	9	13	12	11	45	0.86	0.17	0.27
MRPL47	*mitochondrial ribosomal protein L47*	6	7	5	5	23	0.8	0	0	0	0	1	0	-4.52	0.00	0	3	3	0	6	0	-1.94	0.01
ABCB10	*ATP binding cassette subfamily B member 10*	14	12	12	7	45	0.78	13	10	8	7	38	0	-0.24	0.41	4	7	4	3	18	0	-1.32	0.01
EFHA1	*mitochondrial calcium uptake 2*	7	6	0	5	18	0.75	8	0	5	0	13	0	-0.47	0.64	0	0	0	0	1	0	-4.17	0.03
FASTKD5	*FAST kinase domains 5*	7	10	6	7	30	0.75	0	0	0	0	1	0	-4.91	0.00	17	18	18	9	62	0.96	1.05	0.01

3.4.9 ClpP activation by imipridones exerts anti-tumor effects in vivo

To test if ClpP activation by ONC212 induces anti-tumor effects in vivo, we established xenograft mouse models using Z138 cells with WT or D190A ClpP overexpression, and treated the mice with oral gavage of ONC212. The Z138 cells were luciferase-labeled, and systemic tumor burden was followed by measuring luciferase activity with IVIS imaging. Consistent with our in vitro findings, tumor burden was significantly reduced by ONC212 treatment in the WT ClpP group, whereas there was no discernable anti-tumor activity in the D190A ClpP group (**Figure 3-9A, B)**. The resultant survival was significantly prolonged in the ONC212-treated WT ClpP group, but not in the D190A mutant group (median survival: WT; 49 vs 55 days, $p = 0.008$, D190A mutant; 53 vs 54 days, $p = 0.40$) (**Figure 3-9C**). The result indicated that in vivo efficacy of ONC212 is ClpP-dependent. We also validated the in vivo anti-tumor effects of ONC201 in a xenograft model of OCI-AML2 cells. Oral ONC201 significantly reduced the leukemic burden in mice compared to the control group (**Figure 3-9D**). Collectively, imipridones are effective in vivo in lymphoma and AML mouse models. To further evaluate the effects of ONC212 on leukemia-initiating cells (LICs), we treated patient-derived xenograft AML cells from secondarily engrafted mice (i.e., LICs enriched) with ONC212 and then injected the cells into recipient NSG mice. Survival of the mice was significantly prolonged (median survival: 36 vs 82 days, $p < 0.0001$) (**Figure 3-9E**), suggesting that ClpP activation inhibits the engraftment capacity of LICs. In an ongoing clinical trial in patients with relapsed/refractory AML, decrease in circulating blasts and subsequent increase in platelet counts was observed (**Figure 3-8L**) following a single dose of ONC201 (250 mg orally).

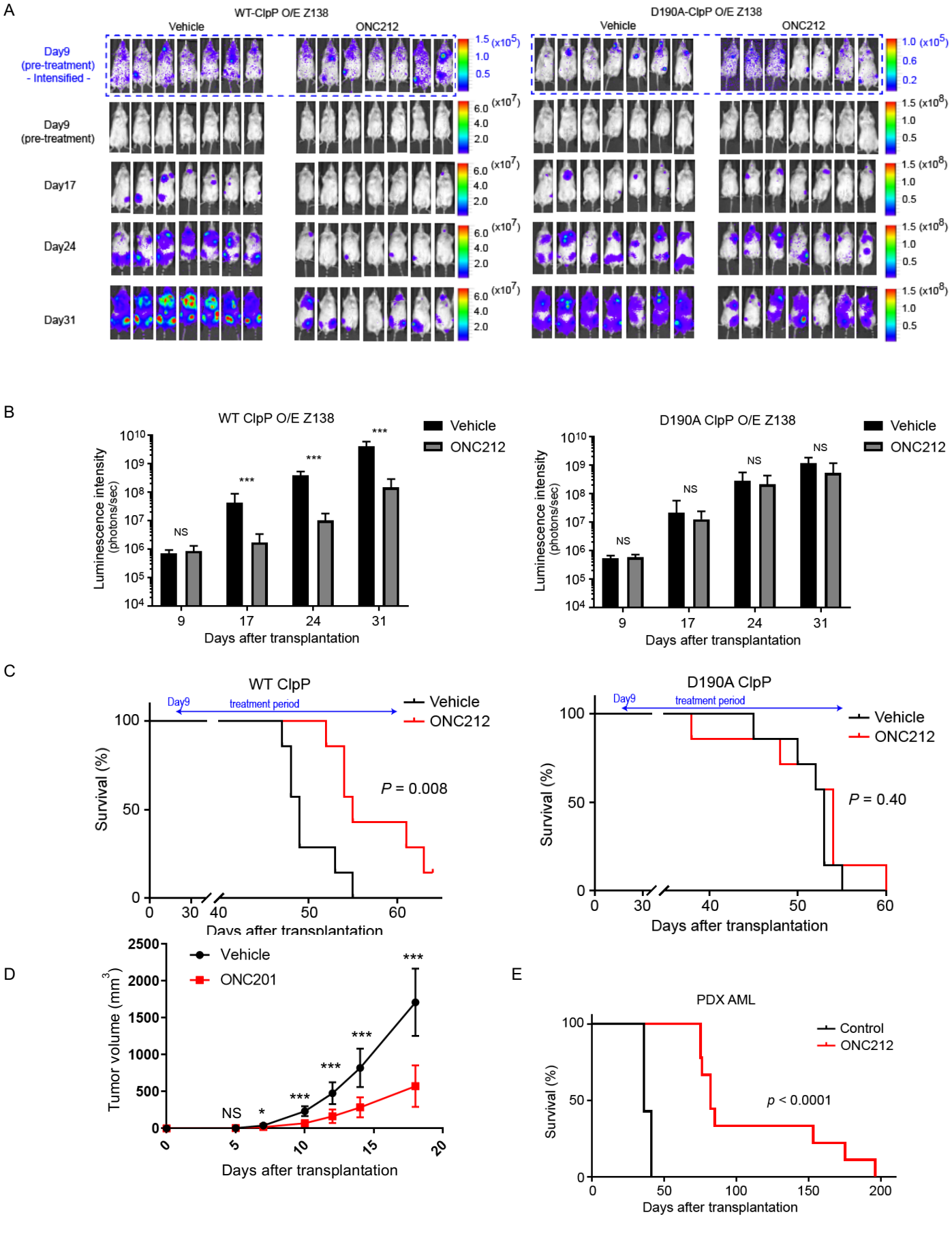
A
WT-ClpP O/E Z138
D190A-ClpP O/E Z138
Vehicle
ONC212
Day9 (pre-treatment) - Intensified -
Day9 (pre-treatment)
Day17
Day24
Day31
B
WT ClpP O/E Z138
D190A ClpP O/E Z138
Luminescence intensity (photons/sec)
Days after transplantation
NS
***
C
WT ClpP
D190A ClpP
Day9
treatment period
Survival (%)
P = 0.008
P = 0.40
D
ONC201
Tumor volume (mm3)
E
PDX AML
Control
p < 0.0001

Figure 3-9. ClpP activation exerts anti-tumor effects in vivo.

(A) Tumor burden measured by luciferase activity using IVIS imaging in xenograft mice with wild-type or D190A-mutant ClpP overexpressing Z138 cells treated with or without ONC212. Mice (n = 7 each) were treated with ONC212 (50 mg/kg every other day, oral gavage) or vehicle after confirming engraftment.
(B) Intensities of luminescence detected by IVIS imaging in the mice in Figure 3-9A.
(C) Survivals of xenograft mice using Z138 cells over-expressed with WT or D190A ClpP.
(D) Tumor volumes of xenograft mice using OCI-AML2 cells. Mice (n = 10 each) were treated with ONC201 (100 mg/kg twice daily, oral gavage) or vehicle from 5 days after transplantation for 13 days.

(E) Survivals of Pdx AML mice. Pdx cells [t(9;11)(p22; q23), CEBPA and ATM mutants] were treated with or without 250 nM ONC212 for 36 hr, then injected into NSG mice (n = 10 each). * $p<0.01$, *** $p<0.0001$

3.5 Discussion

Despite newly developed targeted agents, the majority of hematologic malignancies and solid tumors is incurable. This includes essentially all patients with *TP53* mutations. Therefore, anti-tumor agents with novel mechanisms of action are urgently needed. Accumulating evidence demonstrates that mitochondrial function is critical for maintenance and therapy resistance of leukemias (Cole et al., 2015; Farge et al., 2017; Kuntz et al., 2017; Moschoi et al., 2016; Samudio et al., 2010; Skrtic et al., 2011) and certain solid tumors (Birsoy et al., 2014; Kotschy et al., 2016; Viale et al., 2014), and therapeutic strategies to effectively disrupt the integrity of mitochondria have been investigated (Birsoy et al., 2014; Cole et al., 2015; Konopleva et al., 2006; Konopleva et al., 2016; Kotschy et al., 2016; Kuntz et al., 2017; Pan et al., 2014; Pan et al., 2017; Skrtic et al., 2011; Viale et al., 2014). Here we found that ClpP hyperactivation induces lethality in leukemias and lymphomas, due to selective proteolysis in subsets of the mitochondrial proteome which are involved in mitochondrial respiration and oxidative phosphorylation. In contrast, normal hematopoietic cells display resistance to ClpP hyperactivation, likely reflecting their decreased reliance on oxidative phosphorylation and greater spare reserve capacity in their respiratory chain, compared to AML cells (Sriskanthadevan et al., 2015).

We recently identified ClpP interacting proteins (Cole et al., 2015), but we had not performed a comprehensive assessment of ClpP substrates. In the present study, by chemical and genetic activation of ClpP in the BioID assay, we report a comprehensive list of interacting partners of mitochondrial ClpP in living cells. We demonstrate that a subset of mitochondrial enzymes, including subunits of the respiratory chain complexes, are selectively sensitive to ClpP-mediated degradation. Top hits in the BioID assays were complex I subunits. Indeed, ClpP activation functionally inhibited complex I most effectively, compared to complex II and IV which were also inhibited but to a lesser degree. As a result, ClpP activation damaged mitochondria morphologically and functionally through structural disruption of cristae, inhibition of oxidative phosphorylation and accumulation of mitochondrial ROS, resulting in anti-tumor effects. Considering several recent reports showing that cancer stem and chemo-resistant cells rely highly on oxidative phosphorylation (Farge et al., 2017; Kuntz et al., 2017; Lagadinou et al., 2013; Marin-Valencia et al., 2012; Viale et al., 2014), we speculate that this therapeutic approach may also have potential to eliminate chemo-resistant populations of malignant cells and prevent relapse of the disease, which is an important direction to be addressed in future studies.

Deletions or mutations of ClpP have never been reported in primary AML, suggesting that ClpP could be an effective target across the spectrum of molecular and cytogenetic subsets of AML. However, our data indicate that patient samples with the lowest levels of ClpP are less sensitive to ClpP hyperactivation. Thus, levels of ClpP could serve as a biomarker to select AML patients most and least likely to respond to this therapy. Further studies with larger numbers of patients would be required to establish thresholds of ClpP expression that best predict response.

We established genetic systems to activate and inactivate human ClpP by identifying certain point mutations. We demonstrated that Y118A mutation in human ClpP leads to constitutive hyperactivation of the protease. The D190A mutation which we discovered in ONC201-resistant cells has never been reported. We demonstrated this to be an inactivating mutation both *in vitro* and in cellular assays. Thus, we identified a potential mechanism of resistance to ClpP activators and established a system with which to study the biological role of ClpP and its activators.

Our drug screen identified agonists of mitochondrial ClpP that are more potent than the antibiotic agents ADEPs. The most potent activator imipridones (ONC201 and ONC212) are a class of anti-cancer compounds which effectively kill cancer cells but are much less toxic to normal cells (Allen et al., 2013; Ishizawa et al., 2016). Their efficacy is independent of *TP53* mutation status (Allen et al., 2013; Ishizawa et al., 2016). While the preclinical efficacy of these compounds has been established in numerous cancers, the direct target was elusive. The dopamine receptor DRD2 has been suggested as a putative target of ONC201 (Kline et al., 2016; Kline et al., 2018), based on homology modeling and a cellular β-arrestin assay but not based on evidence of direct binding. Also, DRD2 KO cells can be sensitive to ONC201(Kline et al., 2018), suggesting that it may not be the functionally critical mechanism of action. Our crystal structure of the ClpP-ONC201 complex confirmed ClpP as a direct target for ONC201 and identified its binding pocket. It also showed that ONC201-mediated activation of ClpP has global structural effects that go beyond those of ADEP-mediated activation (Gersch et al., 2015; Lee et al., 2010). Drug binding not only widened the axial entrance pore but also opened up channel-like pores on the "side wall" of the assembled protease. The mechanism of peptide products' escape from the ClpP reaction chamber has been debated in the literature (Sprangers et al., 2005). The new opening, together with the increased dynamics of this region, suggests that these pores could provide a convenient escape route for cleaved peptide products and could help the ClpP machinery to prevent peptide accumulation in the

degradation chamber. ONC201-binding not only increases the dynamics of the ClpP N-terminal residues, a region well known as a major regulatory site crucial for ClpX-mediated activation (Kang et al., 2004), but also induces major conformational changes at the heptamer-heptamer interface with direct effects on the active site region. ADEPs structural effects of activation of bacterial ClpP are most pronounced in the apical region of the protein with the heptamer-heptamer interface largely undisturbed (Gersch et al., 2015; Lee et al., 2010). Collectively, our findings provide an explanation for the recent report demonstrating that ONC201 reduces oxidative phosphorylation (Greer et al., 2018). A refined model of the ClpP-ONC212 complex suggests that its trifluoromethyl substituent enhances ONC212's potency through increased binding affinity and improved structural complementarity to ClpP. We demonstrated that genetic ClpP activation results in ATF4 increase in Z138 cells without increase of phosphorylated eIF2α, validating our recent finding that ONC201 induces atypical integrated stress response (ISR), characterized by eIF2α-independent induction of ATF4 unlike eIF2α-dependent classical ISRs (Ishizawa et al., 2016). This is also consistent with another recent report of eIF2α-independent ATF4 induction being downstream of mitochondrial unfolded stress response (UPR^{mt}) (Munch and Harper, 2016), and reflecting that activation of human ClpP phenocopies UPR^{mt}. Unlike ClpP functionality reported in *C. elegans* (Haynes et al., 2007; Quiros et al., 2016), several reports suggest that ClpP may not be a master regulator of UPR^{mt} in mammals (Bezawork-Geleta et al., 2015; Jin and Youle, 2013; Seiferling et al., 2016). Also, several reports indicate that UPR^{mt} may increase ClpP expression (Houtkooper et al., 2013; Zhao et al., 2002). However, it remains unknown how hyperactivating ClpP will affect UPR^{mt} signaling.

ONC201 is currently in early phase clinical trials against AML and other cancers (Arrillaga-Romany et al., 2017; Kline et al., 2016; Stein et al., 2017), to determine safety and optimal dosing schedule. An early example of blast reduction in a patient with AML is shown in Figure S10, but these trials are still ongoing. In some solid tumors, in particular in gliomas, the trials have demonstrated promising clinical responses without serious adverse events. Thus, our findings related to ONC201 as a ClpP activator can immediately be validated in ongoing clinical trials in patients, and potentially also be tested in future clinical trials of its improved analogues which include ONC206 (Wagner et al., 2017) and ONC212. Of note, ample evidence suggests lethality in *TP53* wild-type and mutant tumors (Allen et al., 2013; Ishizawa et al., 2016; Kline et al., 2016). Moreover, in conjunction with previous reports showing that ADEPs are promising antibiotics and that ADEP-resistant strains of

staphylococcal isolates are rare (Conlon et al., 2013), imipridones may even exert effective antibiotic properties.

Of note, neither Perrault Syndrome patients, who carry inactivating mutations of ClpP, nor ClpP-deficient mice develop tumors. Previously, we demonstrated that inhibiting ClpP in leukemic cells leads to the accumulation of misfolded or damaged respiratory chain complex subunits that impair respiratory chain activity and causes cell death. In contrast, in our present study we showed that hyperactivating ClpP in cancer cells increases degradation of respiratory chain complex subunits leading to impaired respiratory chain activity. Thus, ClpP needs to be tightly regulated in malignancies as both inhibition and hyperactivation of ClpP impairs respiratory chain activity and causes cell death, although through different mechanisms.

In conclusion, hyperactivation of ClpP is a therapeutic strategy against hematologic and solid tumors, which induces selective proteolysis of particular subsets of mitochondrial matrix proteins, resulting in prominent anti-tumor effects. Currently the most potent ClpP activators, imipridones, are being evaluated in clinical trials, and apart from imipridones, other activators of ClpP could be developed in the future.

3.6 References

Adams, P.D., Afonine, P.V., Bunkoczi, G., Chen, V.B., Davis, I.W., Echols, N., Headd, J.J., Hung, L.W., Kapral, G.J., Grosse-Kunstleve, R.W*., et al.* (2010). PHENIX: a comprehensive Python-based system for macromolecular structure solution. Acta crystallographica Section D, Biological crystallography *66*, 213-221.

Afonine, P.V., and Adams, P.D. (2012). On the contribution of hydrogen atoms to X-ray scattering. Computational Crystallography Newsletter *3*, 18-21.

Allen, J.E., Kline, C.L., Prabhu, V.V., Wagner, J., Ishizawa, J., Madhukar, N., Lev, A., Baumeister, M., Zhou, L., Lulla, A*., et al.* (2016). Discovery and clinical introduction of first-in-class imipridone ONC201. Oncotarget *7*, 74380-74392.

Allen, J.E., Krigsfeld, G., Mayes, P.A., Patel, L., Dicker, D.T., Patel, A.S., Dolloff, N.G., Messaris, E., Scata, K.A., Wang, W*., et al.* (2013). Dual inactivation of Akt and ERK by TIC10 signals Foxo3a nuclear translocation, TRAIL gene induction, and potent antitumor effects. Science translational medicine *5*, 171ra117.

Arrillaga-Romany, I., Chi, A.S., Allen, J.E., Oster, W., Wen, P.Y., and Batchelor, T.T. (2017). A phase 2 study of the first imipridone ONC201, a selective DRD2 antagonist for oncology, administered every three weeks in recurrent glioblastoma. Oncotarget *8*, 79298-79304.

Bezawork-Geleta, A., Brodie, E.J., Dougan, D.A., and Truscott, K.N. (2015). LON is the master protease that protects against protein aggregation in human mitochondria through direct degradation of misfolded proteins. Scientific reports *5*, 17397.

Birsoy, K., Possemato, R., Lorbeer, F.K., Bayraktar, E.C., Thiru, P., Yucel, B., Wang, T., Chen, W.W., Clish, C.B., and Sabatini, D.M. (2014). Metabolic determinants of cancer cell sensitivity to glucose limitation and biguanides. Nature *508*, 108-112.

Brotz-Oesterhelt, H., Beyer, D., Kroll, H.P., Endermann, R., Ladel, C., Schroeder, W., Hinzen, B., Raddatz, S., Paulsen, H., Henninger, K.*, et al.* (2005). Dysregulation of bacterial proteolytic machinery by a new class of antibiotics. Nature medicine *11*, 1082-1087.

Cole, A., Wang, Z., Coyaud, E., Voisin, V., Gronda, M., Jitkova, Y., Mattson, R., Hurren, R., Babovic, S., Maclean, N.*, et al.* (2015). Inhibition of the Mitochondrial Protease ClpP as a Therapeutic Strategy for Human Acute Myeloid Leukemia. Cancer cell *27*, 864-876.

Conlon, B.P., Nakayasu, E.S., Fleck, L.E., LaFleur, M.D., Isabella, V.M., Coleman, K., Leonard, S.N., Smith, R.D., Adkins, J.N., and Lewis, K. (2013). Activated ClpP kills persisters and eradicates a chronic biofilm infection. Nature *503*, 365-370.

Corydon, T.J., Bross, P., Holst, H.U., Neve, S., Kristiansen, K., Gregersen, N., and Bolund, L. (1998). A human homologue of Escherichia coli ClpP caseinolytic protease: recombinant expression, intracellular processing and subcellular localization. The Biochemical journal *331 (Pt 1)*, 309-316.

Craig, R., and Beavis, R.C. (2004). TANDEM: matching proteins with tandem mass spectra. Bioinform *20*, 1466-1467.

de Sagarra, M.R., Mayo, I., Marco, S., Rodriguez-Vilarino, S., Oliva, J., Carrascosa, J.L., and Casta n, J.G. (1999). Mitochondrial localization and oligomeric structure of HClpP, the human homologue of E. coli ClpP. Journal of molecular biology *292*, 819-825.

DeLano, W.L. (2002). The PyMOL. Mol Graph Syst, DeLano Scientific, Palo Alto.
Emsley, P., and Cowtan, K. (2004). Coot: model-building tools for molecular graphics. Acta crystallographica Section D, Biological crystallography *60*, 2126-2132.

Emsley, P., Lohkamp, B., Scott, W.G., and Cowtan, K. (2010). Features and development of Coot. Acta Crystallogr D Biol Crystallogr *66*, 486-501.

Eng, J.K., Jahan, T.A., and Hoopmann, M.R. (2013). Comet: an open-source MS/MS sequence database search tool. Proteomics *13*, 22-24.

Farge, T., Saland, E., de Toni, F., Aroua, N., Hosseini, M., Perry, R., Bosc, C., Sugita, M., Stuani, L., Fraisse, M.*, et al.* (2017). Chemotherapy-Resistant Human Acute Myeloid Leukemia Cells Are Not Enriched for Leukemic Stem Cells but Require Oxidative Metabolism. Cancer discovery *7*, 716-735.

Frolova, O., Samudio, I., Benito, J.M., Jacamo, R., Kornblau, S.M., Markovic, A., Schober, W., Lu, H., Qiu, Y.H., Buglio, D.*, et al.* (2012). Regulation of HIF-1alpha signaling and chemoresistance in acute lymphocytic leukemia under hypoxic conditions of the bone marrow microenvironment. Cancer biology & therapy *13*, 858-870.

Gersch, M., Famulla, K., Dahmen, M., Gobl, C., Malik, I., Richter, K., Korotkov, V.S., Sass, P., Rubsamen-Schaeff, H., Madl, T.*, et al.* (2015). AAA chaperones and acyldepsipeptides activate the ClpP protease via conformational control. Nature communications *6*, 6320.

Gersch, M., Stahl, M., Poreba, M., Dahmen, M., Dziedzic, A., Drag, M., and Sieber, S.A. (2016). Barrel-shaped ClpP Proteases Display Attenuated Cleavage Specificities. ACS chemical biology *11*, 389-399.

Greer, Y.E., Porat-Shliom, N., Nagashima, K., Stuelten, C., Crooks, D., Koparde, V.N., Gilbert, S.F., Islam, C., Ubaldini, A., Ji, Y.*, et al.* (2018). ONC201 kills breast cancer cells in vitro by targeting mitochondria. Oncotarget *9*, 18454-18479.

Haynes, C.M., Petrova, K., Benedetti, C., Yang, Y., and Ron, D. (2007). ClpP mediates activation of a mitochondrial unfolded protein response in C. elegans. Developmental cell *13*, 467-480.

Houtkooper, R.H., Mouchiroud, L., Ryu, D., Moullan, N., Katsyuba, E., Knott, G., Williams, R.W., and Auwerx, J. (2013). Mitonuclear protein imbalance as a conserved longevity mechanism. Nature *497*, 451-457.

Ishizawa, J., Kojima, K., Chachad, D., Ruvolo, P., Ruvolo, V., Jacamo, R.O., Borthakur, G., Mu, H., Zeng, Z., Tabe, Y.*, et al.* (2016). ATF4 induction through an atypical integrated stress

response to ONC201 triggers p53-independent apoptosis in hematological malignancies. Science signaling *9*, ra17.

Jafari, R., Almqvist, H., Axelsson, H., Ignatushchenko, M., Lundback, T., Nordlund, P., and Martinez Molina, D. (2014). The cellular thermal shift assay for evaluating drug target interactions in cells. Nature protocols *9*, 2100-2122.

Jin, S.M., and Youle, R.J. (2013). The accumulation of misfolded proteins in the mitochondrial matrix is sensed by PINK1 to induce PARK2/Parkin-mediated mitophagy of polarized mitochondria. Autophagy *9*, 1750-1757.

Kabsch, W. (2010). XDS. Acta Crystallogr Sect D: Biol Crystallogr *66*, 125-132.
Kang, S.G., Dimitrova, M.N., Ortega, J., Ginsburg, A., and Maurizi, M.R. (2005). Human mitochondrial ClpP is a stable heptamer that assembles into a tetradecamer in the presence of ClpX. The Journal of biological chemistry *280*, 35424-35432.

Kang, S.G., Maurizi, M.R., Thompson, M., Mueser, T., and Ahvazi, B. (2004). Crystallography and mutagenesis point to an essential role for the N-terminus of human mitochondrial ClpP. Journal of structural biology *148*, 338-352.

Kessner, D., Chambers, M., Burke, R., Agus, D., and Mallick, P. (2008). ProteoWizard: open source software for rapid proteomics tools development. Bioinformatics *24*, 2534-2536.
Kimber, M.S., Yu, A.Y., Borg, M., Leung, E., Chan, H.S., and Houry, W.A. (2010). Structural and theoretical studies indicate that the cylindrical protease ClpP samples extended and compact conformations. Structure *18*, 798-808.

Kline, C.L., Van den Heuvel, A.P., Allen, J.E., Prabhu, V.V., Dicker, D.T., and El-Deiry, W.S. (2016). ONC201 kills solid tumor cells by triggering an integrated stress response dependent on ATF4 activation by specific eIF2alpha kinases. Science signaling *9*, ra18.

Kline, C.L.B., Ralff, M.D., Lulla, A.R., Wagner, J.M., Abbosh, P.H., Dicker, D.T., Allen, J.E., and El-Deiry, W.S. (2018). Role of Dopamine Receptors in the Anticancer Activity of ONC201. Neoplasia *20*, 80-91.

Konopleva, M., Contractor, R., Tsao, T., Samudio, I., Ruvolo, P.P., Kitada, S., Deng, X., Zhai, D., Shi, Y.X., Sneed, T.*, et al.* (2006). Mechanisms of apoptosis sensitivity and resistance to the BH3 mimetic ABT-737 in acute myeloid leukemia. Cancer cell *10*, 375-388.

Konopleva, M., Pollyea, D.A., Potluri, J., Chyla, B., Hogdal, L., Busman, T., McKeegan, E., Salem, A.H., Zhu, M., Ricker, J.L.*, et al.* (2016). Efficacy and Biological Correlates of Response in a Phase II Study of Venetoclax Monotherapy in Patients with Acute Myelogenous Leukemia. Cancer discovery *6*, 1106-1117.

Kotschy, A., Szlavik, Z., Murray, J., Davidson, J., Maragno, A.L., Le Toumelin-Braizat, G., Chanrion, M., Kelly, G.L., Gong, J.N., Moujalled, D.M.*, et al.* (2016). The MCL1 inhibitor S63845 is tolerable and effective in diverse cancer models. Nature *538*, 477-482.

Kuntz, E.M., Baquero, P., Michie, A.M., Dunn, K., Tardito, S., Holyoake, T.L., Helgason, G.V., and Gottlieb, E. (2017). Targeting mitochondrial oxidative phosphorylation eradicates therapy-resistant chronic myeloid leukemia stem cells. Nature medicine *23*, 1234-1240.

Lagadinou, E.D., Sach, A., Callahan, K., Rossi, R.M., Neering, S.J., Minhajuddin, M., Ashton, J.M., Pei, S., Grose, V., O'Dwyer, K.M.*, et al.* (2013). BCL-2 inhibition targets oxidative phosphorylation and selectively eradicates quiescent human leukemia stem cells. Cell stem cell *12*, 329-341.

Lee, B.G., Park, E.Y., Lee, K.E., Jeon, H., Sung, K.H., Paulsen, H., Rubsamen-Schaeff, H., Brotz-Oesterhelt, H., and Song, H.K. (2010). Structures of ClpP in complex with acyldepsipeptide antibiotics reveal its activation mechanism. Nature structural & molecular biology *17*, 471-478.

Lee, C.D., Sun, H.C., Hu, S.M., Chiu, C.F., Homhuan, A., Liang, S.M., Leng, C.H., and Wang, T.F. (2008). An improved SUMO fusion protein system for effective production of native proteins. Protein science : a publication of the Protein Society *17*, 1241-1248.

Leung, E., Datti, A., Cossette, M., Goodreid, J., McCaw, S.E., Mah, M., Nakhamchik, A., Ogata, K., El Bakkouri, M., Cheng, Y.Q.*, et al.* (2011). Activators of cylindrical proteases as antimicrobials: identification and development of small molecule activators of ClpP protease. Chemistry & biology *18*, 1167-1178.

Lev, A., Lulla, A.R., Wagner, J., Ralff, M.D., Kiehl, J.B., Zhou, Y., Benes, C.H., Prabhu, V.V., Oster, W., Astsaturov, I.*, et al.* (2017). Anti-pancreatic cancer activity of ONC212 involves the unfolded protein response (UPR) and is reduced by IGF1-R and GRP78/BIP. Oncotarget *8*, 81776-81793.

Marin-Valencia, I., Yang, C., Mashimo, T., Cho, S., Baek, H., Yang, X.L., Rajagopalan, K.N., Maddie, M., Vemireddy, V., Zhao, Z.*, et al.* (2012). Analysis of tumor metabolism reveals mitochondrial glucose oxidation in genetically diverse human glioblastomas in the mouse brain in vivo. Cell metabolism *15*, 827-837.

McCoy, A.J., Grosse-Kunstleve, R.W., Adams, P.D., Winn, M.D., Storoni, L.C., and Read, R.J. (2007). Phaser crystallographic software. Journal of applied crystallography *40*, 658-674.

Moschoi, R., Imbert, V., Nebout, M., Chiche, J., Mary, D., Prebet, T., Saland, E., Castellano, R., Pouyet, L., Collette, Y.*, et al.* (2016). Protective mitochondrial transfer from bone marrow stromal cells to acute myeloid leukemic cells during chemotherapy. Blood *128*, 253-264.

Muller, K., Faeh, C., and Diederich, F. (2007). Fluorine in pharmaceuticals: looking beyond intuition. Science *317*, 1881-1886.

Munch, C., and Harper, J.W. (2016). Mitochondrial unfolded protein response controls matrix pre-RNA processing and translation. Nature *534*, 710-713.

Ni, T., Ye, F., Liu, X., Zhang, J., Liu, H., Li, J., Zhang, Y., Sun, Y., Wang, M., Luo, C.*, et al.* (2016). Characterization of Gain-of-Function Mutant Provides New Insights into ClpP Structure. ACS chemical biology *11*, 1964-1972.

Pan, R., Hogdal, L.J., Benito, J.M., Bucci, D., Han, L., Borthakur, G., Cortes, J., DeAngelo, D.J., Debose, L., Mu, H.*, et al.* (2014). Selective BCL-2 inhibition by ABT-199 causes on-target cell death in acute myeloid leukemia. Cancer discovery *4*, 362-375.

Pan, R., Ruvolo, V., Mu, H., Leverson, J.D., Nichols, G., Reed, J.C., Konopleva, M., and Andreeff, M. (2017). Synthetic Lethality of Combined Bcl-2 Inhibition and p53 Activation in AML: Mechanisms and Superior Antileukemic Efficacy. Cancer cell *32*, 748-760 e746.

Quiros, P.M., Mottis, A., and Auwerx, J. (2016). Mitonuclear communication in homeostasis and stress. Nature reviews Molecular cell biology *17*, 213-226.
Roux, K.J., Kim, D.I., Raida, M., and Burke, B. (2012). A promiscuous biotin ligase fusion protein identifies proximal and interacting proteins in mammalian cells. The Journal of cell biology *196*, 801-810.

Samudio, I., Harmancey, R., Fiegl, M., Ka2ntarjian, H., Konopleva, M., Korchin, B., Kaluarachchi, K., Bornmann, W., Duvvuri, S., Taegtmeyer, H.*, et al.* (2010). Pharmacologic inhibition of fatty acid oxidation sensitizes human leukemia cells to apoptosis induction. The Journal of clinical investigation *120*, 142-156.

Seiferling, D., Szczepanowska, K., Becker, C., Senft, K., Hermans, S., Maiti, P., Konig, T., Kukat, A., and Trifunovic, A. (2016). Loss of CLPP alleviates mitochondrial cardiomyopathy without affecting the mammalian UPRmt. EMBO reports *17*, 953-964.

Skrtic, M., Sriskanthadevan, S., Jhas, B., Gebbia, M., Wang, X., Wang, Z., Hurren, R., Jitkova, Y., Gronda, M., Maclean, N.*, et al.* (2011). Inhibition of mitochondrial translation as a therapeutic strategy for human acute myeloid leukemia. Cancer cell *20*, 674-688.

Sprangers, R., Gribun, A., Hwang, P.M., Houry, W.A., and Kay, L.E. (2005). Quantitative NMR spectroscopy of supramolecular complexes: dynamic side pores in ClpP are important for product release. Proceedings of the National Academy of Sciences of the United States of America *102*, 16678-16683.

Sriskanthadevan, S., Jeyaraju, D.V., Chung, T.E., Prabha, S., Xu, W., Skrtic, M., Jhas, B., Hurren, R., Gronda, M., Wang, X.*, et al.* (2015). AML cells have low spare reserve capacity in their respiratory chain that renders them susceptible to oxidative metabolic stress. Blood *125*, 2120-2130.

Stein, M.N., Bertino, J.R., Kaufman, H.L., Mayer, T., Moss, R., Silk, A., Chan, N., Malhotra, J., Rodriguez, L., Aisner, J.*, et al.* (2017). First-in-Human Clinical Trial of Oral ONC201 in Patients with Refractory Solid Tumors. Clinical cancer research : an official journal of the American Association for Cancer Research *23*, 4163-4169.

Tu, Y.S., He, J., Liu, H., Lee, H.C., Wang, H., Ishizawa, J., Allen, J.E., Andreeff, M., Orlowski, R.Z., Davis, R.E.*, et al.* (2017). The Imipridone ONC201 Induces Apoptosis and Overcomes Chemotherapy Resistance by Up-Regulation of Bim in Multiple Myeloma. Neoplasia *19*, 772-780.

Viale, A., Pettazzoni, P., Lyssiotis, C.A., Ying, H., Sanchez, N., Marchesini, M., Carugo, A., Green, T., Seth, S., Giuliani, V.*, et al.* (2014). Oncogene ablation-resistant pancreatic cancer cells depend on mitochondrial function. Nature *514*, 628-632.

Wagner, J., Kline, C.L., Ralff, M.D., Lev, A., Lulla, A., Zhou, L., Olson, G.L., Nallaganchu, B.R., Benes, C.H., Allen, J.E.*, et al.* (2017). Preclinical evaluation of the imipridone family, analogs of clinical stage anti-cancer small molecule ONC201, reveals potent anti-cancer effects of ONC212. Cell cycle *16*, 1790-1799.

Wang, K., Li, M., and Hakonarson, H. (2010). ANNOVAR: functional annotation of genetic variants from high-throughput sequencing data. Nucleic acids research *38*, e164.

Warner, J.K., Wang, J.C., Takenaka, K., Doulatov, S., McKenzie, J.L., Harrington, L., and Dick, J.E. (2005). Direct evidence for cooperating genetic events in the leukemic transformation of normal human hematopoietic cells. Leukemia *19*, 1794-1805.

Winn, M.D., Ballard, C.C., Cowtan, K.D., Dodson, E.J., Emsley, P., Evans, P.R., Keegan, R.M., Krissinel, E.B., Leslie, A.G., McCoy, A.*, et al.* (2011). Overview of the CCP4 suite and

current developments. Acta crystallographica Section D, Biological crystallography *67*, 235-242.

Wong, K.S., Mabanglo, M.F., Seraphim, T.V., Mollical, A., Mao, Y., Rizzolo, K., Leung, E., Moutaoufik, M.T., Hoell, L., S., P.*, et al.* (2018). Acyldepsipeptide analogs dysregulate human mitochondrial ClpP protease activity and cause apoptotic cell death. Cell Chem Biol *25*, 1017-1030.

Zhao, Q., Wang, J., Levichkin, I.V., Stasinopoulos, S., Ryan, M.T., and Hoogenraad, N.J. (2002). A mitochondrial specific stress response in mammalian cells. The EMBO journal *21*, 4411-4419.

Chapter 4

4 Summary and Future Directions

4.1 Summary

The goal of this project was to investigate the clinical outcome of patients with refractory AML following treatment with a third induction course with currently available chemotherapeutic options and to evaluate ClpP hyperactivation as a novel therapeutic strategy for AML in preclinical models.

4.1.1 Clinical outcome of AML in the setting of primary induction failure

Despite ongoing efforts for development of novel therapeutic strategies in AML, only few new agents have been approved for management of AML in the past decades and the overall outcome of AML patients remains poor. The outcome is worse for patients who do not achieve remissions with first line therapies. For examples, in a retrospectyive analysis, Brandwein et al. reported an overall response rate of approximately 50% with reinduction for patients with AML who did not achieve CR with their first line induction chemotherapy (Brandwein et al, 2008). For patients who achieved CR following the second induction but their remissions were not consolidated with SCT, the median relapse free survival was 9.1 months. The relapse free survival was even shorter (6.8 months) for patients with high-risk cytogenetics.

Among AML patients, the prognosis of patients who do not achieve remission after two courses of induction chemotherapy (primary non-responders) is dismal. Depending on the institutional approaches and patients' preferences, various therapeutic plans have been offered to primary non-responders with AML including additional induction courses, SCT, experimental therapies, or palliation. However, the optimal approach for treatment of AML in this setting remains unclear.

SCT with or without preceding attempts to achieve CR with further inductions offers the highest chance of cure to primary non-responders with AML (Araki et al, 2016; Fung et al, 2003). However, for patients who have not attained CR, SCT is associated with higher

mortality rates and more frequent post-transplant relapses (Araki et al, 2016). In addition, depending on the patients' comorbidities, availability of a suitable donor, and based on institutional policies, SCT might not be available as a therapeutic option for primary non responders with AML who have not achieved CR. Thus, understanding the utility of a third course of induction in this context will provide important insight.

Here, we performed a retrospective chart review to investigate the outcome of primary non-responders with AML who received a third course of induction at Princess Margaret Cancer Center. Our data indicates that for primary non responders with AML who are not eligible for curative therapies a third course of induction does not appear to improve the survival outcome compared with palliative strategies. In addition a third induction course may increase the length of hospital admissions and thereby have a negative impact on the quality of life and the clinical outcome of these patients.

A third induction course, however, was associated with 21% (3 out of 14 patients) rate of CR in our retrospective cohort. Of these patients, only 1 patient was eligible for SCT and remains alive 4.6 years post CR. The other 2 patients were not eligible for SCT and received consolidation therapy following the third induction. The CR duration for these 2 patients were short (2.3 and 4.7 months). These data suggest that for AML patients with primary induction failure, the CR duration following a third course of induction is short if the induction therapy is not consolidated by SCT.

In summary, our data indicate that overall, in the setting of primary induction failure, the survival outcome of AML patients does not differ between those who do and do not receive a third induction. Remission rates are low in this clinical setting and for those who achieve CR following a third course of induction, the durations of remission are brief. Thus, for primary non-responders with AML, third inductions should only be considered for highly selected patients who are eligible for SCT and for whom a well-defined and rapid SCT strategy is in place.

4.1.2 ClpP activation as a novel therapeutic strategy in AML

Despite recent advancements in development of novel targeted agents, the prognosis of most patients with AML is poor. Given the biological complexities of this disease, efforts in development of novel antileukemic agents have not been very successful and only few targeted agents have been approved for treatment of this disease over the past decades. Therefore, anti-leukemic agents with novel mechanisms of action are urgently needed.

Recent evidence suggest a crucial role for mitochondrial metabolism and function in maintenance and progression of leukemias and certain solid tumors. Therefore, disruption of mitochondrial integrity has gained specific attention in recent years as a novel angel through which cancer cell lethality could be induced.

In search for novel therapeutic targets in AML, Cole et al. recently identified the mitochondrial caseinolytic protease P (ClpP) as an essential mitochondrial protease that plays a critical role in survival of AML cells. ClpP functions as a protein quality control mediator. It primarily interacts with enzymes that are involved in mitochondrial metabolism and is thought to have a central role in maintaining the integrity of mitochondrial function. Here we found that ClpP hyperactivation lead to selective proteolysis in subsets of the mitochondrial enzymes that are involved in mitochondrial respiration and oxidative phosphorylation. The resultant disruption of mitochondrial metabolism induces lethality in leukemias and lymphomas. In contrast, normal hematopoietic cells that are less reliant on oxidative phosphorylation and have greater spare reserve capacity in their respiratory chain display resistance to ClpP hyperactivation (Sriskanthadevan et al., 2015).

We performed a drug screen to identify activators of mitochondrial ClpP that are more potent than ADEP antibiotics which are currently available ClpP activators. We identified imipridones (ONC201 and ONC212) – a novel class of anti-cancer compounds - as potent ClpP activators. Imipridones effectively kill cancer cells but are much less toxic to normal cells (Allen et al., 2013; Ishizawa et al., 2016). These compounds have shown significant preclinical efficacy in numerous cancers. However, their direct target was elusive. Based on a

cellular β-arrestin assay and homology modeling the dopamine receptor DRD2 has been suggested as a putative target of ONC201 (Kline et al., 2016; Kline et al., 2018). However, functional assays have shown that DRD2 KO cells maintain their sensitivity to ONC201(Kline et al., 2018). Our crystal structure of the ClpP-ONC201 complex confirmed ClpP as a direct target for ONC201 and identified its binding pocket. Based on this structure, ONC201 binds ClpP non-covalently outside of the active site of the protease, stabilizes the ClpP 14-mer, and activates the protease by expanding the axial pores of the enzyme, and inducing structural changes in the residues surrounding and including the catalytic triad. Taken together, our structural data indicates that ONC201-mediated activation of ClpP has global effects on structure of the protease that go beyond those that are seen with ADEP-mediated ClpP activation (Gersch et al., 2015; Lee et al., 2010) and likely result in more efficient activation of the protease.

To investigate the functional consequences of ClpP activation in cells away from the potential toxic and off target effects of the imipridone compounds, we established genetic systems to activate and inactivate human ClpP by identifying certain point mutations. We identified Y118A mutation in human ClpP as a hyperactivating mutation based on sequence homology to previously reported constitutively active S. aureus ClpP mutants. We showed that Y118A leads to constitutive hyperactivation of the protease. We also identified the D190A mutation in ONC201-resistant cells. We demonstrated that D190A mutation inactivates ClpP both *in vitro* and in cellular assays. We used these ClpP mutants to establish a system to study the biological effects of ClpP activation and to investigate the functional effects of ClpP inactivation. In this system, D190A can also be used to investigate a potential mechanism of resistance to ClpP activators.

Using imipridone compounds as well as the ClpP activating Y118A mutant, we performed a comprehensive assessment of potential ClpP substrates in living cells. With BioID assays, we demonstrate that a subset of mitochondrial enzymes, including subunits of the respiratory chain complexes, are selectively sensitive to ClpP-mediated degradation. Top hits in the BioID assays were complex I subunits. Our functional assays validated this data and showed that ClpP activation decreased the activity of respiratory chain complexes I, II and IV and complex I was inhibited most effectively, compared to complex II and IV.

Inhibition of oxidative phosphorylation following ClpP activation resulted in accumulation of mitochondrial ROS and damaged mitochondria morphologically and functionally through structural disruption of cristae, and was lethal to cancer cells. Based on these observations, we speculate that this therapeutic approach may also have potential to eliminate chemo-resistant populations of malignant cells and prevent relapse given that cancer stem and chemo-resistant cells are particularly dependent on oxidative phosphorylation (Farge et al., 2017; Kuntz et al., 2017; Lagadinou et al., 2013; Marin-Valencia et al., 2012; Viale et al., 2014). Of note, ample evidence suggests the antitumor effects of imipridones are independent of *TP53* mutation status (Allen et al., 2013; Ishizawa et al., 2016; Kline et al., 2016).

In xenograft models, imipridones significantly reduced the tumor burden in lymphoma and AML mouse models and their in vivo efficacy was ClpP dependent. Furthermore, ClpP activation by imipridones inhibited the engraftment capacity of leukemia-initiating cells (LICs).

ONC201 is currently in early phase clinical trials against AML and other cancers (Arrillaga-Romany et al., 2017; Kline et al., 2016; Stein et al., 2017), to determine safety and optimal dosing schedule. Our data indicate that samples with highest levels of ClpP are most sensitive to imipridones. Thus, ClpP levels could be used as potential biomarkers to identify patients that will most benefit from these compounds. Importantly, imipridones have demonstrated promising clinical responses without serious adverse events in some clinical trials in solid tumors, in particular in gliomas. Thus, our findings related to ONC201 as a ClpP activator can immediately be validated in ongoing clinical trials in patients, and potentially also be tested in future clinical trials of its improved analogues which include ONC206 (Wagner et al., 2017) and ONC212. Furthermore, considering previous reports of promising antibiotic activity of ADEPs including their efficacy against resistant strains of staphylococcal isolates (Conlon et al., 2013), we postulate that imipridones could also exert significant antimicrobial effects.

In conclusion, we describe ClpP activation as a novel therapeutic strategy against hematologic malignancies and solid tumors. ClpP activation by imipridones induces selective proteolysis of particular subsets of mitochondrial matrix proteins, impairs mitochondrial function, and abrogates its structure. Currently the most potent ClpP activators, imipridones, display

prominent anti-tumor effects and are being evaluated in clinical trials. In addition to imipridonse, other activators of ClpP could be developed in the future.

4.2 Future directions

Next steps that will follow our investigations can be summarized in three major categories. a) further development of ClpP activators, b) clinical studies evaluating the effects of ClpP activation in AML patients using imipridones, c) biological studies to assess the mechanism of ClpP hyperactivation and cellular pathways that are triggered in this process.

Our crystal structure provides structural framework for development of new generations of imipridones that can fit better into the hydrophobic pockets of the protease, have optimal half life, and stay on target more efficiently and for longer durations. Other classes of ClpP activators can also be developed. In addition, to further develop ClpP activators and imipridones that are less toxic and more target specific, the off-target effects of imipridone should be studied more extensively and potential enzymes that can bind these molecules in cells should be identified using methods such as cellular target engagement assays.

ONC201 is currently being tested in a phase I clinical trial in patients with relapsed and refractory AML. In this trial, the safety and recommended Phase II dose of ONC201 in these patients will be determined. In addition, the pharmacokinetics of ONC201 in these patients will also be assessed and the rates of clinical response to ONC201 in AML will be defined.

To determine the biological effects of ClpP activation with ONC201 in patients with relapsed and refractory AML, correlative studies will be performed on peripheral blood and marrow samples taken from patients in the clinical trial to determine whether ONC201 activates ClpP in patients with AML. In this context, ClpP enzymatic activity and levels of respiratory chain complex proteins will be measured in AML blasts as markers of ClpP activity pre and post treatment with ONC201. The study will test whether ONC201 can increase ClpP enzymatic activity and decrease levels of its substrates, and will relate these changes to plasma levels of ONC201 and clinical responses. These correlative studies will help explain the success or

failure of ONC201 in these patient.

To determine the mechanisms of sensitivity and resistance to ONC201 in study patients, pre-treatment levels of ClpP will be measured to determine whether they can predict for clinical responses. For patients who respond to ONC201, but then relapse, the study will determine the mechanism of resistance. For example, it will investigate whether AML cells responsible for relapse have decreased levels of ClpP. In our preclinical studies, we identified acquired inactivating point mutations in ClpP that rendered cells resistant to the drug. Therefore, when patients respond but then relapse, samples should be tested for new ClpP mutations. If ClpP mutations are identified, biochemical studies will be conducted to determine the functional importance of the mutations.

ClpP is known to be overexpressed in a subset of solid tumors and hematologic malignancies. In our investigations, we showed that ClpP hyperactivation can be toxic in several solid tumor cell lines including colorectal, breast, ovarian and cervical cancer cells in addition to its toxicity in leukemia and lymphoma cell lines. Toxic effects of ClpP hyperactivation in these cancers should be studied more extensively including in vivo studies to assess whether ClpP activators can effectively penetrate solid tumor tissues and to assess their ability to inhibit metastatic processes.

ClpP activation can potentially induce intrinsic apoptotic pathways through activation of mtUPR. In this scenario, ClpP activation may show synergistic effects when combined with other cytotoxic agents that show their effects through induction of intrinsic apoptotic pathways such as Bcl2 inhibition. In vitro and in vivo effects of such combinations should be tested.

Lastly, the cellular biology of ClpP hyperactivation should be studied more extensively. As an example, to this date, the mitochondrial mechanisms of identifying and tagging misfolded proteins that are degraded by ClpP remain unknown. In addition, the compensatory cellular mechanisms following ClpP hyperactivation and the mechanisms through which malignant cells could escape the cytotoxicity of ClpP hyperactivation remain unknown and should be studied.

Appendix I

Key resources table (related to materials used in chapter 3)

REAGENT or RESOURCE	SOURCE	
Antibodies		
Antibody Cocktail	Abcam, Cambridge, UK	ab110413
Anti-SDHA	Abcam, Cambridge, UK	ab14715
Anti-ATF4	Cell Signaling, Danvers, MA	11815 D4B8
Anti-eIF2α	Cell Signaling, Danvers, MA	9722
Anti-phospho-eIF2a (S51)	Abcam, Cambridge, UK	ab32157, E90
Anti-ClpP	Abcam, Cambridge, UK	ab124822
Anti-β-actin	Millipore-Sigma, Darmstadt, Germany	A5316, AC-74
Anti-GAPDH	Cell Signaling, Danvers, MA	2118, 14C10

Total OXPHOS Rodent WB Antibody Cocktail	Abcam, Cambridge, UK	ab110413
Anti-SDHB	Abcam, Cambridge, UK	ab14714
Anti-NDUFA12	Abcam, Cambridge, UK	ab192617
Anti-NDUFB8	Abcam, Cambridge, UK	Ab152558, ab110242
Anti-UQCRC2 antibody	Abcam, Cambridge, UK	Ab14745
Anti-MTC01	Abcam, Cambridge, UK	Ab14705
Anti-CS	Abcam, Cambridge, UK	ab129095
Anti-ClpP	Millipore-Sigma, Darmstadt, Germany	HPA010649, ab 126102
Chemicals, Peptides, and Recombinant Proteins		
ONC201	Oncoceutics, Philadelphia, PA	NA

	MedChemExpress, Monmouth Junction, NJ	HY-15615A
ONC212	Oncoceutics, Philadelphia, PA	NA
ONC201 isomer (inactive analog)	MedChemExpress, Monmouth Junction, NJ	HY-15615
DMSO	Millipore-Sigma, Darmstadt, Germany	D2650
FCCP (Seahorse XFp Cell Energy Phenotype Test Kit)	Agilent Technologies, INC. Santa Clara, CA	103275-100
Penicillin-Streptomycin	ThermoFisher, Waltham, MA	15140122
complete™, Mini Protease Inhibitor Cocktail	Millipore-Sigma, Darmstadt, Germany	11836153001
Proteinase Inhibitors	ThermoFisher, Waltham, MA	78425
PBS	Corning, Corning, NY	21-040-CV

Antimycin A	Millipore-Sigma, Darmstadt, Germany	A8674
Hygromycin B	Bioshop Canada Inc., Burlington, ON	HYG005
Tryptone	BioShop Canada Inc,, Burlington, Canada	TRP402
Yeast Extract	BioShop Canada Inc,, Burlington, Canada	YEX555
Luria-Bertrani Broth	Wisent Bioproducts,ST-BRUNO, Quebec Canada	809-060-CL
Kanamycin	BioShop Canada Inc,, Burlington, Canada	KAN201
Isopropyl-1-thio-B-D-galactopyranoside (IPTG)	BioShop Canada Inc,, Burlington, Canada	IPT002
DL-Dithiothreitol (DTT)	BioShop Canada Inc,, Burlington, Canada	DTT002
HisPur™ Ni-NTA Res	ThermoFisher, Waltham, MA	88222

Triton X-100	BioShop Canada Inc,, Burlington, Canada	TRX777
Oligomycin (Seahorse XFp Cell Energy Phenotype Test Kit)	AGILENT TECHNOLOGIES, INC. Santa Clara, CA	103275-100
β-Mercaptoethanol	ThermoFisher, Waltham, MA	21985-023
Bromophenol Blue	Millipore-Sigma, Darmstadt, Germany	114391
Human Flt3-Ligand, premium grade	Il-Miltenyi Biotec, San Diego, CA	130-096-479
Human IL-7, premium grade	Miltenyi Biotec, San Diego, CA	130-095-363
Recombinant Human IL-3 Protein	R&D Systems, Minneapolis, MN	203-IL
Human IL-6, premium grade	Miltenyi Biotec, San Diego, CA	130-093-932
G-CSF (Neupogen)	Amgen Inc.	Thousand Oaks, CA
Human GM-CSF, premium grade	Miltenyi Biotec, San Diego, CA	130-093-866

Tetracycline	Millipore-Sigma, Darmstadt, Germany	D9891
Annexin V APC	ThermoFisher, Waltham, MA	A35110
Annexin V FITC	Beckman Colter, Brea, CA	IM3546
Propidium Iodide (PI)	Millipore-Sigma, Darmstadt, Germany	P4170
FBS	Millipore-Sigma, Darmstadt, Germany	F2442
RPMI 1640	Corning, Corning, NY	10-040-CV
IMDM	ThermoFisher, Waltham, MA	I6529
Luciferin	Gold biotechnology, St. Louis, MO	LUCK
Untagged human mitochondrial ClpP (ClpP)	(Wong et al, 2018)	N/A (produced in house)
Yeast SUMO protease	(Lee et al., 2008)	N/A (produced in house)

α-Casein	Millipore-Sigma, Darmstadt, Germany	C6780
Glycerol	Millipore-Sigma, Darmstadt, Germany	G5516
Glycerol Imidazole	BioShop Canada Inc,, Burlington, Canada	Cat#GLY002
Glycerol Imidazole NaCl	BioShop Canada Inc,, Burlington, Canada	IMD508
Glycerol Imidazole NaCl Tris Hydrochloride	BioShop Canada Inc,, Burlington, Canada	SOD001
Glycerol Imidazole	BioShop Canada Inc,, Burlington, Canada	TRS004

Glycerol	BioShop Canada Inc,, Burlington, Canada	HCL333
Imidazole		
NaCl	BioShop Canada Inc,, Burlington, Canada	BST666
KCl	BioShop Canada Inc,, Burlington, Canada	POC308
Sodium Acetate	BioShop Canada Inc,, Burlington, Canada	SAA555
MgCl2	Millipore-Sigma, Darmstadt, Germany	M1028
DMSO	Millipore-Sigma, Darmstadt, Germany	CAS 67-68-5
Creatine phosphate	Millipore-Sigma, Darmstadt, Germany	10621714001
Creatine kinase	Lee Biosolutions, Maryland Heights, USA	190-10
Tween 20	Millipore-Sigma, Darmstadt, Germany	P1379

PEG4000	Millipore-Sigma, Darmstadt, Germany	CAS 25322-68-3
Recombinant Human SCF Protein (TEX)	R&D Systems, Minneapolis, MN	255-sc/cf
L-Glutamine 200mM (TEX)	ThermoFisher Scientific	25030081
L-Glutamine	ThermoFisher, Waltham, MA	21051024
MitoSox Red	ThermoFisher, Waltham, MA	M36008
Ac-Trp-Leu-Ala-AMC (Ac-WLA-AMC)	Boston Biochem	S-330 lot 10066817
Ac-Phe-hArg-Leu-ACC	Life Technologies Inc.	PEP97MODMM
FITC-casein	Millipore-Sigma, Darmstadt, Germany	C0528
Clptide	Biomatik Corp., Cambridge, Canada	511266

Mca-Pro-Leu-Gly-Pro-D-Lys(Dnp)-OH	Bachem Americas, Inc, Torrance, USA	4027687
Seahorse Assay Medium	AGILENT TECHNOLOGIES, INC. Santa Clara, CA	102365-100
Sodium uccinate	Millipore-Sigma, Darmstadt, Germany	14160-100G
HEPES	Bioshop	HEP001.1
bovine serum albumin	Millipore-Sigma, Darmstadt, Germany	A3803-10G
rotenone	Millipore-Sigma, Darmstadt, Germany	R8875-1G
KCN	Millipore-Sigma, Darmstadt, Germany	60718-25G
2,6-dichloroindophenol	Millipore-Sigma, Darmstadt, Germany	D1878-5G
decylubiquinone	Millipore-Sigma, Darmstadt, Germany	D7911-10mg

ferricytochrome c	Millipore-Sigma, Darmstadt, Germany	C7752
dodecyl-D-maltoside	Millipore-Sigma, Darmstadt, Germany	D4641
L-ascorbic acid	Millipore-Sigma, Darmstadt, Germany	A5960-25G
Sodium Malonate	Millipore-Sigma, Darmstadt, Germany	63409-100G
Critical Commercial Assays		
Alamar-Blue Assay	ThermoFisher Sci	DAL1025
DNA Fingerprinting (Promega Powerplex 16 HS kit)	Promega, Madison, WI	DC2101
Complex I Enzyme Activity Microplate Assay Kit	Abcam, Cambridge, UK	ab109721
Deposited Data		
X-ray structure: human mitochondrial ClpP in complex with ONC201	This paper	PDB: 6DL7

X-ray structure: ClpP in complex with ADEP-28	(Wong et al., 2018)	PDB: 6BBA
Mass spectrometry analysis (related to Figure 5A)	MassIVE archive (massive.ucsd.edu)	MSV000082381
Sequence Read Archive (SRA)		ACNO SUB4176298
Experimental Models: Cell Lines		
Z138 Cells	ATCC, Manassas, VA	NA
OCI-AML2	Lab stock	NA
OCI-AML3	DSMZ, Braunschweig, Germany	NA
TEX Cells	Ontario Cancer Institute, Toronto, Canada	Gift
T-REx HEK293	CECAD Research Center, Cologne Grermany	Gift
HEK293T Cells	ATCC, Manassas, VA	NA
HCT116	Lab stock	NA

OC316	Lab stock	NA
SUM159	Lab stock	NA
Experimental Models: Organisms/Strains		
NSG Mice	The Jackson Laboratory, Bar Harbor, ME	NA
E. coli BL(DE3) *ΔclpP::cat* (SG1146)	(Kimber et al., 2010)	NA
Human Primary Cells	This paper	NA
Recombinant DNA		
pETSUMO	(Lee et al., 2008)	N/A
pETSUMO2-CLPP(-MTS)	(Wong et al., 2018)	N/A
Software and Algorithms		
GraphPad Prism 7	GraphPad , Inc. La Jolla, CA	NA
CCP4 Suite	(Winn et al., 2011)	http://www.ccp4.ac.uk/
PHENIX Software Package	(Adams et al., 2010)	https://www.phenix-online.org/

Phaser	(McCoy et al., 2007)	https://www.phenix-online.org/
Coot	(Emlsey and Cowtan, 2004)	https://www2.mrc-lmb.cam.ac.uk/personal/pemsley/coot/
PyMol	(DeLano, 2002)	https://pymol.org/2/
rnaseqmut		https://github.com/davidliwei/rnaseqmut
Origin7 MicroCal Analysis Software	Malvern, Malvern, UK	NA
ANNOVAR	(Wang et al, 2010)	
Proteowizard	ProteoWizard release: 3.0.10800 (2017-4-27)	http://proteowizard.sourceforge.net/
X!Tandem	X! TANDEM Jackhammer TPP (2013.06.15.1 - LabKey, Insilicos, ISB)	https://www.thegpm.org/tandem/
Comet	Comet version "2014.02 rev. 2"	http://comet-ms.sourceforge.net/
SAINT	SAINT Version:2.5.0, Express Version:exp3.6.1	http://prohitsms.com

Cytoscape	Cytoscape 3.6.0	http://www.cytoscape.org